Vol. 21 No. 02
July 2024

p-ISSN 1412-2960
e-ISSN 2579-521X

Indonesian Physics Communication

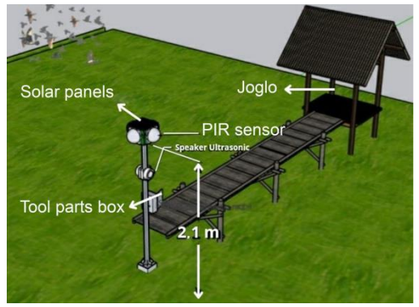

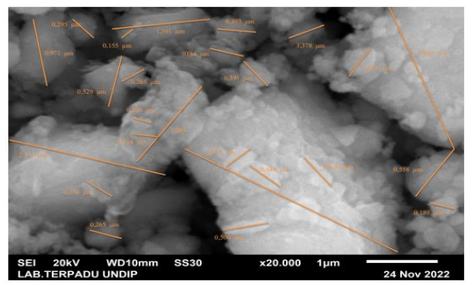

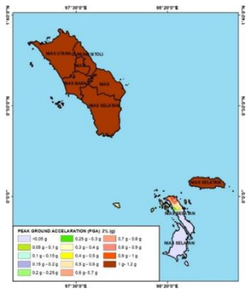

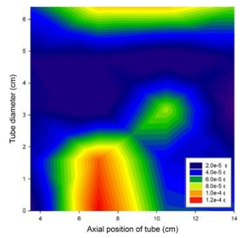

ISSN 1412 2960

Indonesian Physics Communication
Vol. 21 No. 02
Jully 2024
Department of Physics, Universitas Riau
Pekanbaru

Department of Physics
Faculty of Mathematics and Natural Sciences
Universitas Riau
Kampus Bina Widya Jl. HR. Soebrantas Km. 12.5
Simpang Baru Panam, Pekanbaru 28293

Vol. 21 No. 02
July 2024

p-ISSN 1412-2960
e-ISSN 2579-521X

Indonesian Physics Communication

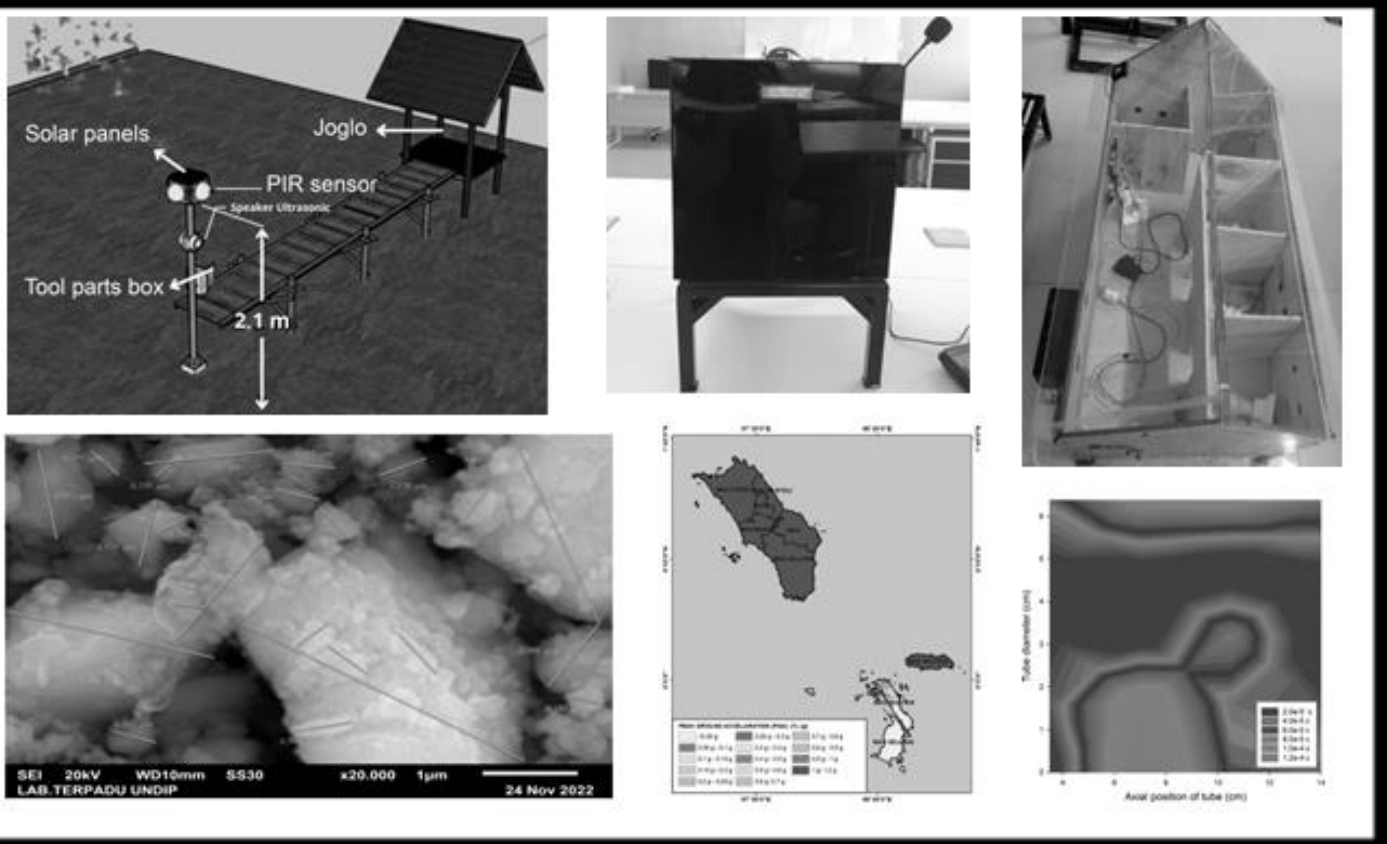

Department of Physics
Faculty of Mathematics and Natural Sciences
Universitas Riau
Kampus Bina Widya Jl. HR. Soebrantas Km. 12.5
Simpang Baru Panam, Pekanbaru 28293

Indonesian Physics Communication
Department of Physics, Universitas Riau, Pekanbaru, Indonesia
p-ISSN 1412-2960 | e-ISSN 2579-521X
Web: https://kfi.ejournal.unri.ac.id
E-mail: kfi@ejournal.unri.ac.id

Editorial Board of the Indonesian Physics Communication (IPC) Journal
Department of Physics, Faculty of Mathematics and Natural Sciences, Universitas Riau

Editorial Address:

Department of Physics, Faculty of Mathematics and Natural Sciences, Universitas Riau
Kampus Bina Widya Km 12.5 Simpang Baru Pekanbaru
Homepage: https://kfi.ejournal.unri.ac.id/index.php/JKFI
E-mail: kfi@ejournal.unri.ac.id

LIST OF CONTENTS

IPC

Indonesian Physics Communication

Department of Physics, Universitas Riau, Pekanbaru, Indonesia
p-ISSN 1412-2960 | e-ISSN 2579-521X

Vol. 21 | No. 2
July 2024

Web: https://kfi.ejournal.unri.ac.id
E-mail: kfi@ejournal.unri.ac.id

Analysis of pressure distribution in cylindrical tube fluid flow using a fiber Bragg grating

Annisa Ratna Pertiwi[1], Saktioto[1,*], Bambang Widiyatmoko[2], Dwi Hanto[2]
[1]Department of Physics, Universitas Riau, Pekanbaru 28293, Indonesia
[2]Research Center for Photonics, BRIN - KST BJ HABIBIE, South Tangerang 15314, Indonesia

*Corresponding author: saktioto@lecturer.unri.ac.id

ABSTRACT

Fibre optic sensors have garnered considerable attention from scientists, leading to the extensive use of optical fibres as sensors for monitoring strain and temperature. The increasing adoption of fibre Bragg gratings (FBG) can be attributed to their enhanced sensitivity and rapid transmission speed. The objective of this study is to examine the pressure distribution of FBGs within a cylindrical tube while subjected to vibrations from a loudspeaker and the presence of hot water vapour. The given options were of two scenarios, first scenario had a tube without water vapour and a heart sound, while the second scenario included a tube with water vapour and a heart sound. In this experiment, we strategically placed the FBG at 20 different points along the cylindrical tube to accurately detect strain values at each position. The outcomes derived from these two scenarios illustrate that temperature and air vapour pressure exert an influence on the occurrence of sound, with the highest level of tension found when hot water vapour and heart sounds are present.

Keywords: Fiber Bragg grating; fluid flow; hot water vapor; sound; strain

Received 09-08-2023 | Revised 11-10-2023 | Accepted 22-04-2024 | Published 16-07-2024

INTRODUCTION

Fiber Bragg grating (FBG) is an optical fiber with a grating in one of its segments. This grating reflects light that passes through it with a certain wavelength and passes the rest [1,2]. FBG is also widely used to detect the heart. Because the FBG system receives the human heartbeat in the form of pressure which results in changes in strain in the FBG [3-5]. Not only to strain, FBG also has high sensitivity to temperature [6,7]. This is what makes FBG widely used as a strain and temperature sensor. FBG-based sensors utilize the effect of changes in strain values, changes in strain in the FBG can be a function of temperature so by utilizing the impact of changes in strain due to temperature, the sensitivity of the sensor can be increased [8-10]. Based on the FBG sensor vibration monitoring system, the FBG sensor vibration can be designed for the detection system. Changes in the Bragg wavelength due to strain dynamics in the FBG can be measured by detecting changes in the Bragg wavelength [11,12].

This research presents an analysis of the pressure distribution resulting from a fluid flow design using a cylindrical tube where the tube contains a FBG to detect strains that occur due to vibrations from heart sounds. The variations given are: first, in the condition in the tube without water vapor and there is a heart sound, third, in the condition in the tube there is water vapor and there is a heart sound.

LITERATURE REVIEW

Optical fiber is a transmission medium that is capable of transmitting information with large capacity and high reliability. Optical fiber consists of 4 parts with the core and cladding as the main structure with an explanation of each part as follows [13-15]:

1. Core is the deepest part of an optical fiber. Made from fine glass fiber which will help the movement of light. This section has a size of 2 – 5 μm.

2. Cladding has a size of 5 – 250 μm and is made of silicone. Cladding is an outer material that protects the core and reflects the light it receives (radiates).
3. Coating/Buffer is defined as a mechanical protector that can protect optical fibers from external disturbances, such as cable bending and air humidity.
4. Strength Member and Outer, namely a fiber optic protective jacket that will protect the cable from interference that can damage the core.

FBG is an optical fiber with a grating in one of its segments. This grating reflects light that passes through it with certain wavelengths and passes the rest. FBG is widely used as a strain and temperature sensor [16]. The basic principle of FBG is transmitting and reflecting light that passes through it. Polychromatic light comes from a source that is further guided in an optical fiber. When light passes through a Bragg grating, part of the light will be reflected at a certain wavelength value or what is usually called the Bragg wavelength, and part of it will be transmitted through the FBG [17].

The Bragg wavelength due to the strain around the FBG can be expressed in the following equation [18]:

$$\Delta\lambda_{B,1} = \lambda_B (1 - p_\alpha)\varepsilon \quad (1)$$

$$\Delta\lambda_B = \lambda_{B,1} - \lambda_{B,0} \quad (2)$$

where $\lambda_{B,0}$ is the reference wavelength before the FBG is placed on the cylindrical tube, $\lambda_{B,1}$ is the wavelength after the FBG is placed on the cylindrical tube, $\Delta\lambda_{B,1}$ is the wavelength shift (nm), λ_B is the Bragg wavelength (nm), $p_\alpha \approx 0.22$ is the photo-elastic coefficient of the optical fiber, ε is the strain (με or microstrain).

Based on the FBG sensor vibration monitoring system, the FBG sensor vibration can be designed for the detection system. From the FBG strain sensor model, it can be seen that if the FBG strain is a periodic dynamic strain that changes over time and changes due to the influence of object vibrations, then the model can be used to measure the vibration period. For vibration characteristics, the main parameters are acceleration, amplitude, speed, and vibration frequency [19,20]. In this way, the FBG vibration sensing system can be designed. Changes in the Bragg wavelength due to strain dynamics in the FBG can be measured by detecting changes in the Bragg wavelength [9].

Sound is a longitudinal wave that propagates in a medium (solid, liquid, or gas). These waves are a form of energy. Sound energy comes from vibrating objects, the propagating vibrations are called waves, therefore sound propagates in the form of waves [21]. A loudspeaker is an electroacoustical transducer that converts electrical signals into sound vibrations. The electrical signal produced by the amplifier is transmitted to the loudspeaker. Speakers carry electrical signals and convert them back into physical vibrations to produce sound waves. The loudspeaker converts the electrical signal into an analog sound signal [22].

RESEARCH METHODS

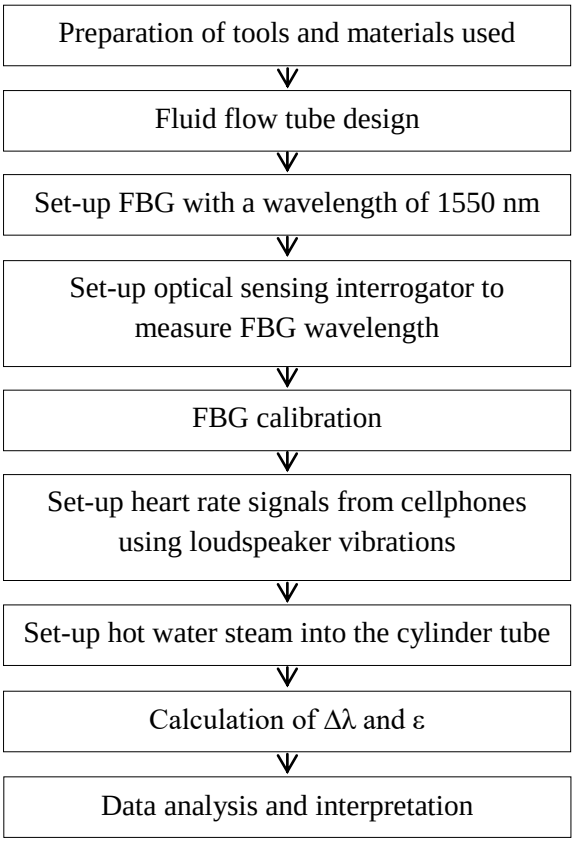

Figure 1. Research flow diagram.

The flow diagram of this research can be seen in Figure 1. This research method was carried out to analyze the pressure distribution due to sound vibrations in a cylindrical tube using a loudspeaker which was detected by the FBG and by changes in temperature in the tube due to hot water vapor being applied.

RESULTS AND DISCUSSION

In this chapter, the results of the FBG response to strains caused by loudspeaker sound vibrations and hot water vapor placed in a cylindrical tube-shaped medium are discussed. This research was divided into 2 conditions, namely the condition without water vapor and heart sounds (condition 1), and the condition given water vapor and heart sounds (condition 2).

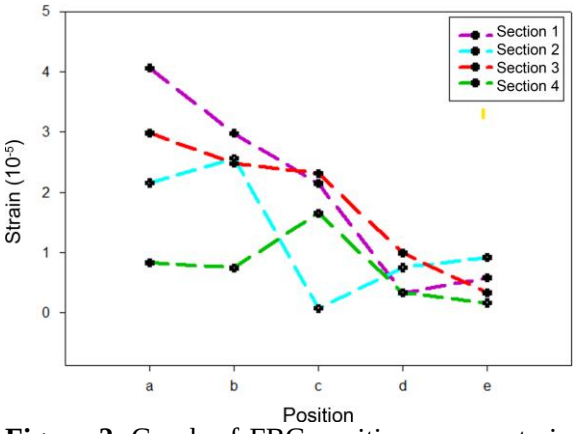

Figure 2. Graph of FBG position versus strain value under conditions without water vapor and heart sounds.

Figure 2 shows that the highest strain value is located at position 1a with a strain value of 4.059×10^{-5} ε with a flow velocity in the tube of 0.099 m/s and the lowest strain value is located at position 2c with a strain value of 7.586×10^{-7} ε with The flow velocity in the tube is 0.083 m/s. Based on the graph, it can also be seen that section 1 experienced a decrease in strain values from positions a to e with values ranging from 4.059×10^{-5} ε to 5.789×10^{-6} ε with a flow velocity range in the tube of 0.060 – 0.129 m/s.

Figure 3 shows the distribution of air in the tube when the tube is without steam while sound is given, meaning that from the bottom side, no hot steam pressure is given, but it can be seen that almost half of the change in strain value occurs at the air pressure at the top, this can be caused by from the inhomogeneous distribution of sound produced by the heartbeat so that the upper part has a relatively higher strain value than the lower part. Furthermore, measuring the pressure distribution conditions in conditions without water vapor and given that the heart sounds should appear homogeneous, but due to the high sensitivity of the strain value of the FBG measuring instrument, the FBG records extreme positions at the top with a range of 3×10^{-5} ε up to 4×10^{-5} ε and the extreme position at the bottom where the bottom of the range is 1×10^{-5} ε to 2×10^{-5} ε. It can be said that sound influences the pressure or strain also at the bottom, but lower than at the top. Another thing that causes the top is that the air experiences upward pressure, resulting in stretching strains at the top.

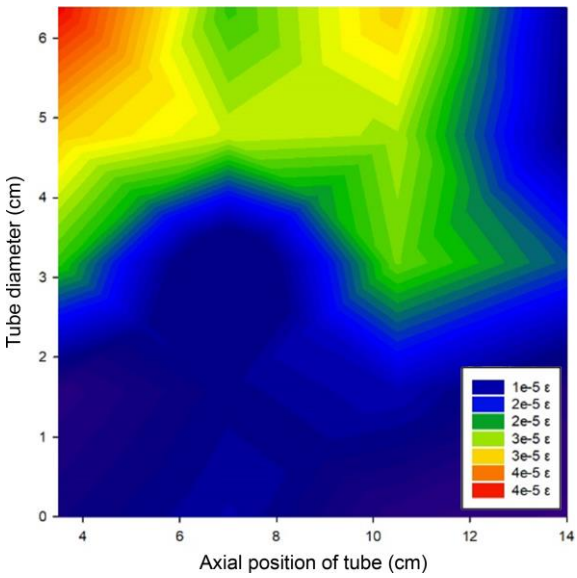

Figure 3. Distribution of strain values for conditions without water vapor and heart sounds.

Figure 4 shows that the highest strain value is located at position 2d with a strain value of 1.083×10^{-4} ε with a flow velocity in the tube of 0.076 m/s and position 2e with a strain value of 1.232×10^{-4} ε with a flow velocity in the tube of 0.129 m/s, the high strain value is due to the position of the FBG being close to the

source of hot water vapor which is around section 2. From the graph, it can also be seen that on average at position b the strain value has decreased from other positions, namely with a range of 8.271×10^{-7} ε to 1.819×10^{-5} ε with a flow velocity range in the tube in position b of 0.088 – 0.109 m/s.

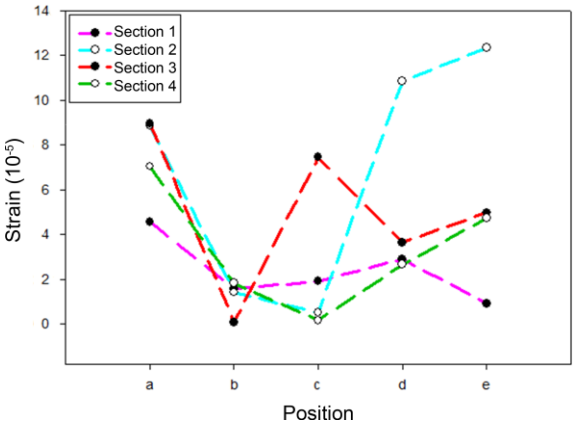

Figure 4. Graph of FBG position versus strain value in conditions of water vapor and heart sounds.

There is steam entering from below the axial axis, while on the left there is sound entering, there is an accumulation of functions between sound and steam flowing from below (see Figure 5). So, there is a resultant relationship between sound and steam. Sound is more about pressure, while steam is more about pressure, the thermal density of the air in the tube, the image shown shows an increase in extreme changes, a shift in the strain value at the sound source, and the flow reaches the middle position of the tube because the sound source is not homogeneous, but because of pressure. This sound causes the hot air to shift towards the right. Meanwhile, at the top of the tube, there is a blocked flow, namely a high strain value due to the airflow that has been blocked at the top so that it does not flow out. In the middle of the tube, sound can flow in an open cylindrical tube, this is because firstly, the effect of steam is influenced by sound, and secondly, the effect produced by water vapor is small compared to heart sounds which exert pressure on air movement, meaning the density of the surrounding air. The middle tube is controlled by sound, as evidenced by the fact that the steam does not contribute much to all points except being retained at the top and some at the bottom, where the bottom is close to the heat source and at the top is retained due to the effects of convection and conduction.

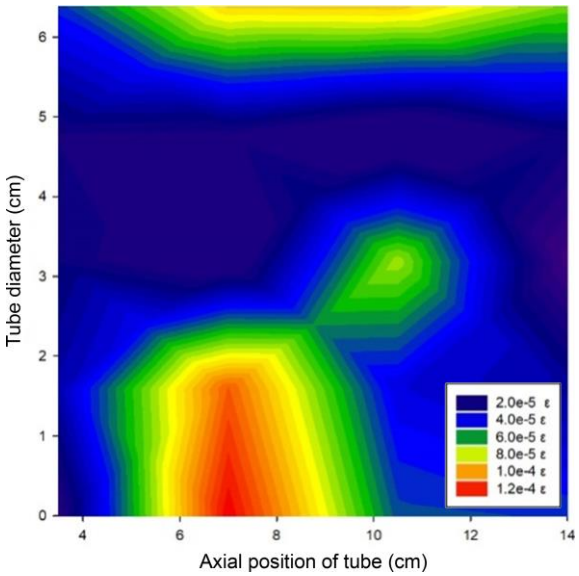

Figure 5. Distribution of strain values for conditions of water vapor and heart sounds.

CONCLUSION

A fluid flow design has been carried out to determine the strain in the Bragg lattice fibers in a cylindrical tube using FBG. The design of the tube is in the form of an FBG laying medium as a sensor to detect changes in pressure in the tube in the form of changes in strain values that occur due to the influence of sound and the influence of applied water vapor. Conditions without water vapor and heart sounds show that almost half of the change in strain value occurs in the air pressure at the top. This can be caused by the inhomogeneous distribution of sounds produced by the heartbeat so that the top part has a relatively higher strain value than the lower part. When water vapor is applied and heart sounds are given, it is shown that there is an increase in extreme changes in the shift value of the strain at the sound source and the flow reaches the middle area of the tube because the sound source is not homogeneous, but because of the sound pressure, the hot air shifts to the right.

REFERENCES

1. Shekar, P. R., Latha, D. M., Kumari, K. & Pisipati, V. G. K. M. (2021). Optimal parameters for fiber Bragg gratings for sensing applications: A spectral study. *SN Applied Sciences*, **3**(6), 666.
2. Veriyanti, V. & Saktioto, S. (2020). Tampilan birefringence pada gangguan pembengkokan serat optik komersial. *Indonesian Physics Communication*, **17**(2), 97–103.
3. Hongyao, W. (2011). Coal mine disaster rescue life sign monitoring technology based on FBG and acceleration sensor. *Procedia Engineering*, **26**, 2294–2300.
4. Fadilla, F. D. & Saktioto, S. (2021). Aplikasi sistem sensor fiber Bragg grating untuk pendeteksian simulasi denyut jantung. *Indonesian Physics Communication*, **18**(2), 151–158.
5. Saktioto, S., Maulana, A. M., Yupapin, P. & Hairi, H. M. (2023). Analysis of fluid flow in a cylindrical tube using fiber Bragg grating. *Science, Technology and Communication Journal*, **4**(1), 15–20.
6. Mishra, V., Lohar, M. & Amphawan, A. (2016). Improvement in temperature sensitivity of FBG by coating of different materials. *Optik*, **127**(2), 825–828.
7. Vaeruza, I., Kurniansyah, K. E., Darma, F. & Yulianti, I. (2019). Fabrikasi sensor serat optik plastik untuk deteksi ion logam merkuri dalam air. *Indonesian Physics Communication*, **16**(2), 123–129.
8. Zhang, Z. & Liu, C. (2017). Design of vibration sensor based on fiber Bragg grating. *Photonic Sensors*, **7**(4), 345–349.
9. Ramadhan, K. & Saktioto, S. (2021). Integrasi chirping dan apodisasi bahan TOPAS untuk peningkatan kinerja sensor serat kisi Bragg. *Indonesian Physics Communication*, **18**(2), 111–123.
10. Meyzia, B., Saktioto, S., Emrinaldi, T., Wanara, N., Hanto, D., Widiyatmoko, B. *et al*. (2024). Novel approach peak tracking method for FBG: Gaussian polynomial technique. *Science, Technology and Communication Journal*, **4**(3).
11. Kouhrangiha, F., Kahrizi, M., & Khorasani, K. (2022). Structural health monitoring: modeling of simultaneous effects of strain, temperature, and vibration on the structure using a single apodized π-Phase shifted FBG sensor. *Results in Optics*, **9**, 100323.
12. Ikhsan, R., Syahputra, R. F. & Saktioto, S. (2018). Analisis kompensasi dispersi menggunakan penguat Raman pada jaringan WDM (wavelength division multiplexing) dalam komunikasi serat optik. *Indonesian Physics Communication*, **15**(2), 88–92.
13. Saktioto, S., Defrianto, D., Hikma, N., Soerbakti, Y., Irawan, D., Okfalisa, O. *et al*. (2022). External perspective of lung airflow model via diaphragm breathing sensor using fiber optic belt. *The 4th Al-Noor International Conference for Science and Technology*, **4**(1), 1014.
14. Sutriyono, D. P. & Saktioto, S. (2017). Karakteristik pertumbuhan pelepah kelapa sawit dengan menggunakan fiber Bragg grating moda tunggal. *Indonesian Physics Communication*, **14**(1), 1026–1031.
15. Saktioto, S., Nurpadilla, R., Meyzia, B., Hairi, H. M., Fadhali, M. M., & Yupapin, P. (2024). Characteristics of human voice vibrations based on FBG strains. *Science, Technology and Communication Journal*, **4**(2), 31–36.
16. Presti, D. L., Massaroni, C., Leitao, C. S. J., Domingues, M. D. F., Sypabekova, M., Barrera, D. *et al*. (2020). Fiber bragg gratings for medical applications and future challenges: A review. *IEEE Access*, **8**, 156863–156888.
17. Hillmer, H., Woidt, C., Kobylinskiy, A., Kraus, M., Istock, A., Iskhandar, M. S. *et al*. (2021). Miniaturized interferometric sensors with spectral tunability for optical fiber technology—A comparison of size requirements, performance, and new

concepts. *Photonics*, **8**(8), 332.
18. Li, R., Tan, Y., Chen, Y., Hong, L., & Zhou, Z. (2019). Investigation of sensitivity enhancing and temperature compensation for fiber Bragg grating (FBG)-based strain sensor. *Optical Fiber Technology*, **48**, 199–206.
19. Li, T., Guo, J., Tan, Y. & Zhou, Z. (2020). Recent advances and tendency in fiber Bragg grating-based vibration sensor: A review. *IEEE Sensors Journal*, **20**(20), 12074–12087.
20. Emrinaldi, T. & Saktioto. (2016). Penentuan nilai regangan Jembatan Siak I oleh kendaraan bermotor menggunakan fiber Bragg grating. *Indonesian Physics Communication*, **13**(13), 919–926.
21. Anggelia, S., Rahmawati, R., Setiawati, A. & Kurniawati, W. (2023). Diving into the World of Sound and Light, Understanding Their Properties, Propagation and Uses. *Jurnal Pendidikan Indonesia*, **2**(1), 119–125.
22. Klippel, W. (2020). Loudspeaker and headphone design approaches enabled by adaptive nonlinear control. *Journal of the Audio Engineering Society*, **68**(6), 454–464.

IPC

Indonesian Physics Communication

Department of Physics, Universitas Riau, Pekanbaru, Indonesia
p-ISSN 1412-2960 | e-ISSN 2579-521X

Vol. 21 | No. 2
July 2024
Web: https://kfi.ejournal.unri.ac.id
E-mail: kfi@ejournal.unri.ac.id

Fabrication of a lithium-ion battery separator from cellulose acetate of empty palm fruit bunches with the addition of PVDF

Rismadani Haryanti, Romi Fadli Syahputra, Delovita Ginting*
Department of Physics, Universitas Muhammadiyah Riau, Pekanbaru 28291, Indonesia

*Corresponding author: delovita@umri.ac.id

ABSTRACT

The separator is a crucial element in lithium-ion batteries that is positioned between the anode and cathode. Its primary function is to prevent direct contact between the electrodes, hence avoiding electrical short circuits. Lithium ion battery separators are typically composed of polyvinylidene fluoride (PVDF) and polyacrylonitrile (PAN) polymers, which possess excellent ionic conductivity and mechanical qualities. Nevertheless, these polymers and materials possess numerous drawbacks, necessitating adjustments for their further development. The objective of this study is to examine the impact of incorporating novel polymers into the constituents of the separator. The alteration utilises a novel polymer called cellulose, specifically the cellulose derivative known as cellulose acetate. The cellulose acetate utilised is derived from the empty fruit bunches of oil palm trees. Cellulose acetate offers several benefits, including affordability, the ability to selectively adsorb substances, solubility in a wide range of solvents (particularly organic solvents), hydrophilicity, and its origin from renewable sources. The separator was fabricated using the reflux process, which involved mixing 5.6 g of PVDF and 0.7 g of $Al(OH)_3$ with varying amounts of CA (0.1 g, 0.2 g, and 0.3 g). The conducted tests include the thickness test, elongation test, and PSA test. According to the test results, the separator is viable and complies with the standards.

Keywords: Cellulose acetate; lithium; PVDF; separator

Received 06-09-2023 | Revised 13-10-2023 | Accepted 25-04-2024 | Published 16-07-2024

INTRODUCTION

Batteries are parts that have a very big role in human needs. Batteries are a source of electrical energy that is highly relied upon to operate electronic equipment that is portable or can be carried anywhere [1]. Lithium-ion batteries are widely used in electronic equipment because of their advantages in the faster self-discharge process and higher energy power density. Another advantage of this lithium-ion battery is that it can last longer [2]. Lithium-ion batteries consist of 3 important components, namely cathode (positive electrode), anode (negative electrode), and separator [2]. Separators have an important role in the process of preventing short circuits at the cathode anode in battery cells. The characteristics of the separator are that it has a small electrical resistance, is an insulator and has high mechanical stability [3].

Lithium-ion battery separators are generally made from polyvinylidene fluoride (PVDF), and polyacrylonitrile (PAN) polymers which have high ion conductivity and good mechanical properties [4]. This polymer still has weaknesses and needs to be developed by making modifications to the separator. Modifications can be made by mixing other polymer materials or new materials to improve the performance weaknesses of the separator [3]. Referring to research conducted by Jiang C et al [5], namely making a separator by mixing PVDF, CA, and $Al(OH)_3$ which produces a separator with an absorption value of 403.9%, a porosity of 68.6% and an ion conductivity of reaching 2.85×10^{-3} S/cm [5]. Data resulting from Jiang *et al.*'s research shows that adding new materials to the separator composition can improve separator performance. The new material that can be used is cellulose.

Cellulose is a natural polysaccharide polymer with a linear chain consisting of two anhydroglucose units that repeat up to 15,000 units. Cellulose is a very abundant natural resource on earth that can be renewed and is available not only from plants (wood, cotton, wheat, grass, etc.) but even from non-plants such as algae and bacteria [6]. Cellulose has the advantage of being biodegradable, the raw material is abundant and easy to find, having high thermal stability, and high electrochemical stability, and is easily recyclable and renewable [7]. The cellulose derivative product that is widely used in the industrial world is cellulose acetate. Membranes made from cellulose acetate polymer are hydrophilic due to the presence of groups in the polymer chain, cellulose acetate is environmentally friendly and biodegradable. Many cellulose acetate polymers are synthesized, but good cellulose acetate for membrane materials must contain a minimum of 39.5% acetyl [8]. Cellulose acetate is a material that is still not available in Indonesia. This makes cellulose fall into the category of materials that require expensive costs and take a long time to ship.

The advantages of using cellulose acetate are that it can be produced at a low cost, has selective adsorption, can dissolve in most solvents (especially organic solvents), is hydrophilic, and is made from renewable sources. Cellulose acetate is also widely used for the adsorption process or absorption of metal ions or industrial waste because of its good absorption properties [9]. The hydroxyl group in cellulose acetate has been replaced by an acetyl group which is a white solid, non-toxic, tasteless, and odorless. The commercial value of cellulose acetate is quite high because of its advantages. Based on the degree of substitution, cellulose acetate is divided into three, namely cellulose monoacetate, degree of substitution (DS) 0 – 2 with acetyl content < 36.5%. Cellulose monoacetate can be used in making plastics, paints, and lacquers. Cellulose in acetate, degree of substitution (DS) 2.0 – 2.8 with acetyl content 36.5% – 42.2%. Cellulose diacetate can be used in the manufacture of membranes, topographic films, and threads. Cellulose tri acetate, degree of substitution (DS) 2.8 – 3.9 with acetyl content 43.5% – 44.8%. Cellulose triacetate can be used in the manufacture of fabric and wrapping thread [10].

Cellulose acetate can be obtained by extracting it from natural materials, one of which is empty oil palm fruit bunches. Empty palm oil bunches (TKKS) are palm oil mill wastes that are abundant and have not been widely used. Processing 1 ton of palm oil can produce 22% – 23% EFB or 220 – 230 kg EFB [11]. The chemical content and composition contained in empty oil palm fruit bunches is 40% – 43% cellulose, 22% – 25% hemicellulose, and 19% – 21% lignin. The high cellulose content has great potential for making cellulose fibers based on transparent biopolymers [6]. TKKS decomposes more than 3 months naturally because its large size makes it difficult for TKKS to decompose due to its small surface. Reducing the size of EFB will help EFB to decompose more quickly [12].

PVDF made from fluoropolymer has strong piezoelectric and pyroelectric properties, this material is widely used because it has low strength, good response, flexibility, and lightness. PVDF has three molecular structures, namely α phase, β phase, and γ phase. The β phase is most widely used as sensors and actuators because it has the greatest piezoelectric effect. The β phase structure material requires certain fabrication techniques to obtain it by stretching (pulling) at a certain temperature and followed by polarization with high voltage DC electricity [13].

RESEARCH METHODS

The research method used is the reflux method. The tools used in this research include a synthetic distillator, grinding machine, desiccator, digital balance, stirring rod, oven, beaker, measuring cup, Erlenmeyer, magnetic stirrer, filter paper, pH paper, dropper pipette, and thermometer. The main ingredients used in this research were empty palm fruit bunches, NaOH powder, H_2SO_4 72%, NaOCl 1%,

distilled water, glacial acetic acid, acetic anhydride, sodium acetate, $Al(OH)_3$, DMAc and PVDF.

Cellulose Extraction

The empty palm oil bunches are separated first, then the empty palm oil bunches are cleaned and dried in the sun until the empty palm fruit bunches are completely dry. Dry empty bunches are ground using a grinding machine until the sample is 60 mesh. A sample of 40 grams of finely ground empty palm oil bunches was put into a synthetic distillator.

2 g of NaOH powder was first dissolved in 100 ml of distilled water and made 2 times. The NaOH liquid is mixed into the distillator and refluxed for 8 hours at 90ºC. The mixture is filtered and tested for lignin by reacting the filtrate and H_2SO_4, if there are still lumps in the filtrate, the residue is dissolved again in NaOH solution and refluxed again until there is no lignin.

Cellulose that no longer contains lignin is refluxed again for one and a half hours with NaOCl solution and 2 g of NaOH are added with a ratio of 100:1 (v/w) at a temperature of 70ºC. Then the mixture was filtered using filter paper, the filtered residue was then soaked in 100 mL of NaOH solution for 30 minutes. The mixture was filtered again and washed using distilled water until the pH was neutral. The residue was dried using an oven at 100ºC for 2 hours. The dried sample is then cooled in a desiccator and then weighed until the mass is constant.

Synthesis of Cellulose Acetate

This stage was carried out by reacting 2 g of alpha-cellulose from empty palm fruit bunches with 25 mL of glacial acetic acid and stirring for 1 hour using a magnetic stirrer at room temperature at continuous speed until the cellulose was activated. Next, the acetylation stage was carried out by adding 3 drops of H_2SO_4, 10 mL of acetic anhydride, and 5 mL of distilled water at a temperature of 40ºC. 2 mL of distilled water and 5 mL of glacial acetic acid were added to the solution and reacted for 30 minutes. 100 mL of distilled water was added to the solution and observed, the precipitate formed was then filtered and dried in an oven at 40ºC. The cellulose acetate that was obtained was then weighed and FTIR functional group identification was carried out.

Making Separators

0.7 g $Al(OH)_3$ was dissolved with 42.3 mL DMAc and stirred for 30 minutes, 5.6 g PVDF and 0.2 g cellulose acetate were added to the mixture and stirred again for 24 hours at 70ºC and ultrasonicated for 30 minutes at 27ºC. The resulting mixture is poured onto the glass substrate and flattened using a casting knife to a thickness of < 1 mm. The polymer film was left at room temperature for 1 minute, then immersed in a coagulation bath filled with a mixture of DMAc and distilled water in a ratio of 1 : 4 until the polymer film separated from the glass substrate. The polymer film was transferred to a distilled water bath for 48 hours and dried in an oven at 60ºC for 12 hours to remove residual water and solvent.

RESULTS AND DISCUSSION

Separator Thickness

Testing the thickness of the separator was carried out using a screw micrometer, calculating the thickness of the separator using the Tappi test method. The separator thickness value is obtained from the average calculation results carried out at five different points. This measurement is carried out to determine the suitability of the resulting separator for its use. The thickness of the separator also affects the mechanical properties of the separator. The separator thickness test results obtained all meet the thickness standard for application to lithium-ion batteries, namely less than 1 mm. Test result data can be seen in Table 1.

Table 1. Thickness test results.

CA Variations (g)	Separator thickness value (mm)					Average (mm)
	1	2	3	4	5	
0.1	0.12	0.11	0.80	0.80	0.12	0.390
0.2	0.15	0.10	0.15	0.10	0.15	0.130
0.3	0.20	0.20	0.19	0.20	0.20	0.198

The standard used is SNI 2-1707

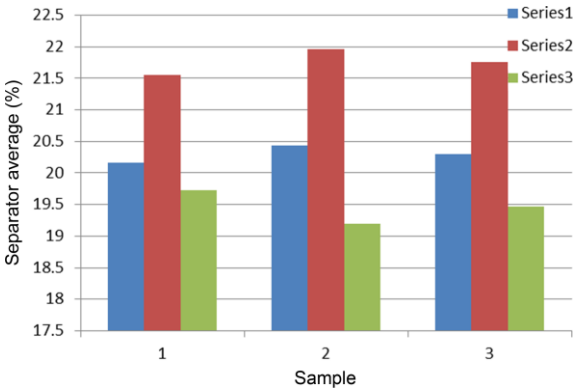

Figure 1. Separator thickness graph.

Separator Elongation

Elongation is the percentage change in film length which is calculated when the film is pulled until it breaks. The analysis results show that the average value of elongation of the separator is the highest in the 0.2 g CA addition variation, namely 21.755%, while in the 0.1 g CA variation, it is 20.305% and the 0.3 g CA variation is 19.465%. The average value of the separator extension can be seen in Table 2.

Table 2. Elongation test results.

CA sample (g)	Elongation (%)		Average (%)
	1	2	
0.1	20.17	20.44	20.305
0.2	21.55	21.96	21.755
0.3	19.73	19.20	19.465

The standard used is SNI 7818:2014

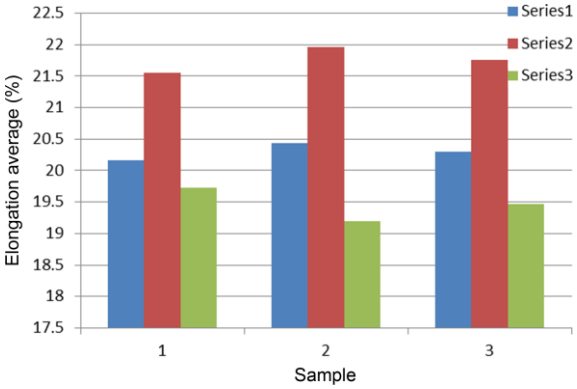

Figure 2. Graph of elongation results.

PSA Testing

Particle Size testing of CA empty oil palm bunches was carried out using HORIBA L300 Particle Size Analysis. The results of this test can be seen in Figure 3. The test results show that the smallest particle is 0.115 µm and the largest particle is 592.387 µm with an average diameter of 73.1870 µm.

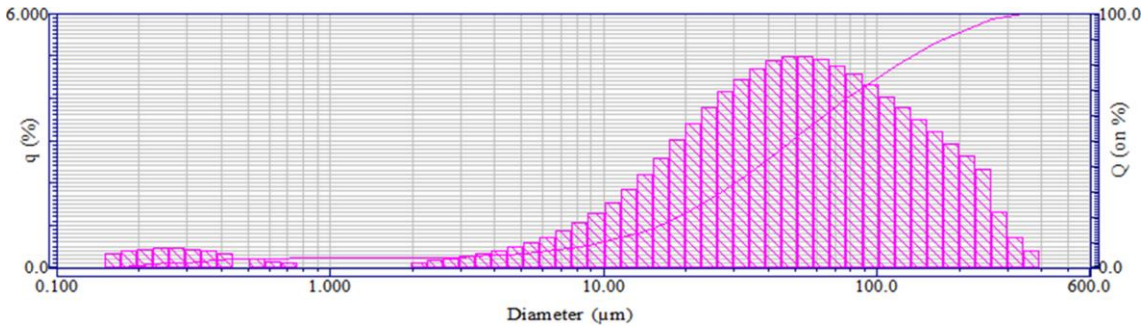

Figure 3. Graph of PSA results.

CONCLUSION

Based on the research that has been carried out, it can be concluded that the use of cellulose acetate from empty oil palm fruit bunches can be used as an alternative in making lithium-ion battery separators. The composition of the type of material the battery separator is made from can affect the results of the separator produced. The separator that has the best elongation properties is produced from a variation of PVDF 5.6 g, $Al(OH)_3$ 0.7 g with CA 0.2 g. The resulting separator is suitable for application to lithium-ion batteries because it meets separator standards.

ACKNOWLEDGMENTS

The author is very grateful to the Directorate General of Learning and Student Affairs, Ministry of Research, Technology and Higher Education of the Republic of Indonesia, the Research Institute of Muhammadiyah University of Riau and the Physics Study Program of the Faculty of Mathematics and Natural Sciences and Health.

REFERENCES

1. Nasution, M. (2021). Karakteristik baterai sebagai penyimpan energi listrik secara spesifik. *JET (Journal of Electrical Technology)*, **6**(1), 35–40.
2. Cahyono, T. P., Hardianto, T. & Kaloko, B. S. (2020). Pengujian karakteristik baterai lithium-ion dengan metode Fuzzy dengan beban bervariasi. *Jurnal Arus Elektro Indonesia*, **6**(3), 82–86.
3. Barbosa, J. C., Dias, J. P., Lanceros-Méndez, S. & Costa, C. M. (2018). Recent advances in poly (vinylidene fluoride) and its copolymers for lithium-ion battery separators. *Membranes*, **8**(3), 45.
4. Wang, S., Zhang, D., Shao, Z. & Liu, S. (2019). Cellulosic materials-enhanced sandwich structure-like separator via electrospinning towards safer lithium-ion battery. *Carbohydrate Polymers*, **214**, 328–336.
5. Cui, J., Liu, J., He, C., Li, J. & Wu, X. (2017). Composite of polyvinylidene fluoride–cellulose acetate with $Al(OH)_3$ as a separator for high-performance lithium ion battery. *Journal of Membrane Science*, **541**, 661–667.
6. Septevani, A. A., Burhani, D. & Sudiyarmanto. (2018). Pengaruh proses pemutihan multi tahap serat selulosa Dari limbah tandan kosong kelapa sawit. *Jurnal Kimia dan Kemasan*, **40**(2), 71–78.
7. Nazir, M. S., Wahjoedi, B. A., Yussof, A. W. & Abdullah, M. A. (2013). Eco-friendly extraction and characterization of cellulose from oil palm empty fruit bunches. *BioResources*, **8**(2), 2161–2172.
8. Raja, P. M. (2017). Pembuatan membran selulosa asetat dari tandan kosong kelapa sawit termodifikasi mikro zeolit alam untuk filtrasi air sungai. *Jurnal Agro Estate*, **1**(1), 27–33.
9. Riani, P., Syafrinal, S. & Putri, A. (2020). Pembuatan dan karakterisasi membran selulosa asetat dari limbah kulit kakao (Theobroma cacao L.) dengan metode inversi fasa untuk adsorpsi logam timbal. *Andalas Civil Engineering (ACE) Conference 2019*.
10. Siswati, N. D., Wachidah, A. N. & Ariyani, A. E. P. (2021). Selulosa asetat dari ampas sagu. *Jurnal Teknik Kimia*, **15**(2), 90–94.
11. Lukas, A., Ngudiwaluyo, S., Mulyono, H., Rosyadi, I., Noor, I. M. & La Teng, P. N. (2018). Analisis finansial pemanfaatan limbah tandan kosong kelapa sawit menjadi biokar untuk media tanam. *Jurnal Industri Hasil Perkebunan*, **13**(1), 37–42.
12. Nopsagiarti, T. & Ezward, C. (2018). Pengaruh ukuran cacahan tandan kosong kelapa sawit terhadap karakteristik fisik kompos TRITANKOS (Triko Tandan Kosong). *Jurnal Agroqua: Media*

Informasi Agronomi dan Budidaya Perairan, **16**(2), 132–142.

13. Nugraha, A., Ardin, M. B. & Rezani, R. (2017). Karakterisasi material polimer PVDF dengan polarisasi permukaan. *Jurnal Rekayasa Mesin*, **8**(3), 135–139.

IPC

Indonesian Physics Communication

Department of Physics, Universitas Riau, Pekanbaru, Indonesia
p-ISSN 1412-2960 | e-ISSN 2579-521X

Vol. 21 | No. 2
July 2024

Web: https://kfi.ejournal.unri.ac.id
E-mail: kfi@ejournal.unri.ac.id

Magnetic susceptibility, composition, and morphology of iron oxide particles resulting from ball milling of natural sand in the Rokan River

Elfitah Ramadhani Triana*, Salomo, Erwin Amiruddin, Rahmondia Nanda Setiadi
Department of Physics, Universitas Riau, Pekanbaru 28293, Indonesia

*Corresponding author: elfitah.ramadhani2420@student.unri.ac.id

ABSTRACT

The magnetic susceptibility value and alterations in the composition and dimensions of iron oxide particles in the natural sand from the Rokan River, which were prepared using ball milling (BM), have been measured. Prior to undergoing the BM procedure, the sample's magnetic and non-magnetic particles are initially separated using an iron sand separator and a neodymium iron boron magnet. Subsequently, a 120-gram sample was obtained and subjected to the initial stage of BM for a duration of 80 hours, resulting in the formation of a product referred to as BM1. Next, product BM1 undergoes a second stage of BM with an extended duration of 30, 40, and 50 hours. The resulting products are termed BM2A, BM2B, and BM2C, respectively. The milled balls utilised were a total of 16 combined iron balls with a diameter of 2 cm, 32 combined iron balls with a diameter of 1.5 cm, and 64 combined iron balls with a diameter of 0.7 cm. The findings indicated a positive correlation between the duration of BM rotation and the magnetic susceptibility value. Specifically, the value increased from 11,361.6 in BM1 to 12,398.7 in BM2A, 13,383.4 in BMB, and 14,541.2 in BM2C. The XRF test findings also indicated an increase in the fraction of the magnetic element, Fe, from 38.113% in BM1 to 40.133% in BMA, 41.629% in BM2B, and 42.478% in BM2C. The SEM test findings indicated a decrease in the average particle size of the samples from 696 nm to 401, 356, and 288 nm.

Keywords: Ball milling; magnetic susceptibility; natural sand; NdFeB; SEM; X-ray flourescence

Received 17-01-2023 | Revised 14-02-2023 | Accepted 31-04-2024 | Published 17-07-2024

INTRODUCTION

Indonesia is a country that has an abundance of natural resources, one of the riches that Indonesia itself has is iron sand. We can find iron sand in sand in coastal areas and sand around rivers. Indonesia, with its very unique geological, is home to iron sand deposits. Starting from Banda Aceh, at the northern tip of Sumatra, to Sarmi on the north coast of Papua. There are at least iron sand resources in Indonesia, namely 4 billion tons, while iron sand reserves are 897 million tons [1].

Iron sand contains quite strong magnetic compounds, this is because the number of Fe atoms in iron sand is greater than in other compounds. Apart from that, iron sand also contains Fe_3O_4 compounds and small amounts of titanium, silica, manganese, calcium, and vanadium. As has been reviewed by [2], the magnetic compound most often found in coastal areas or rivers is the Fe_3O_4 compound. In general, iron sand is dark gray or black. With characteristics like these, iron sand can be easily distinguished. with other sand.

The Rokan River is in Ujung Batu City, Riau Province. The distance from Pekanbaru to the Rokan River is 194.5 km or 3 hours 30 minutes by car. It is suspected that Rokan River sand has better quality iron sand compared to other rivers. This can be seen from the black and shiny color of the iron sand. Because of its superiority and uniqueness, this was the reason researchers took samples from the Rokan River.

With these abundant natural resources, we can make the best use of them. According to Yulianto and Cholil in [2], permanent magnet and thin film manufacturing, electronic engineering, and the steel industry are examples of magnetic applications in the industrial sector. Apart from that, according to opinion [1] sandy deposits, especially iron sand, are considered

very economical. This is because the minerals it contains can be used in various applications, ranging from magnetic which can be used for making steel which can be used as raw material for titanium. However, unfortunately, the use of iron sand in Indonesia is not good enough.

Particle size greatly influences the quality of a material. The flow properties and compactness of a material can be seen from the size of the powder particles. Larger-sized particles allow it to flow more easily, while smaller-sized particles will form a thicker suspension more easily and quickly [3-5]. Apart from that, [6] adds that when the size of the magnetic particle is reduced to nanometer size, it will have superparamagnetic properties.

Getting the right particle size that matches the target is a challenge for researchers. Priyadarshana [7] said that magnetite nanoparticles can be prepared using top-down and bottom-up mechanisms. Top-down mechanisms are usually created mechanically, namely by crushing magnetite en masse. Natural sand can be reduced from millimeter to micrometer to nanometer size using a tool called ball milling (BM) [8-10]. Meanwhile, the bottom-up method is a way of arranging atoms or molecules and combining them through chemical reactions to form nanostructures, namely using sol-gel techniques, chemical precipitation, and phase agglomeration.

BM is a tool or machine that can be used to smooth or even crush materials to be smaller than their original size which is widely used in the fields of biopharmaceuticals, construction, and other industries [11-13]. The BM machine is in the form of a tube that will continue to rotate at a time and speed set by the operator. By utilizing balls from various materials and various sizes, BM machines can easily do their job. According to [6], several things can influence the results of BM, including the length of milling time, the size of the BM used, and the speed of the BM. These differences can be shown by analyzing the particle size, morphology, and magnetic susceptibility.

Many studies have been carried out using the BM method, one of which is research conducted by [6] who conducted research using a combination of 0.5 cm BM; 0.7 cm and 1.5 cm, and using natural sand originating from the Suci Bengkulu River beach. As well as research in year [8] which used a combination of 60 hours and 100 hours. However, this research is different from previous research. This research uses an iron ball with a BM variation of 0.7 cm; 1.5 cm and 2 cm and the ball is milled in two stages. The first stage for 80 hours is named product BM1 and the second stage with additional time for 30, 40, and 50 hours is named BM2A, BM2B, and BM2C respectively.

It is hoped that this research will be useful for producing even smaller particle sizes, especially in crushing iron sand to nanometer sizes. This research sample was synthesized using the BM method and then characterized using the scanning electron microscope (SEM) to determine its size and the X-ray fluorescence (XRF) to determine its composition.

RESEARCH METHODS

Tools and Materials

The tools and materials used in this research are BM used as a sample crusher, power supply used as an electric voltage source, connecting cable used as a circuit connector, PS-2162 Pasco probe used as a magnetic field meter, solenoid used as a tool to measure magnetic induction, neodymium iron boron (NdFeB) magnets are used as non-magnetic and magnetic particle separators after BM, laptops are used as data storage and processing, XRF is used as a sample particle size identifier and SEM is used as a sample morphology identifier.

Determination of Magnetic Susceptibility Values

A magnetic induction value is required before a magnetic susceptibility assessment is carried out. A magnetic coil of 2500 turns is needed with a length of 10 cm and a diameter of 3 cm. The solenoid is used to measure magnetic induction as a function of current and

distance using a PASCO PS magnetic probe and is connected to a laptop running the data studio program. Calculations were carried out with a magnetic induction distance to the electromagnet of 1 mm and determined the current to be 200, 400, 600, 800, and 1000 mA.

There are three magnetic induction measurements, namely as follows:

1. Without natural river sand to obtain the magnetic induction value without a core (B_0).
2. With intact natural sand samples and natural sand samples that have been separated using the iron sand separator (ISS) method, they are inserted into the solenoid alternately and the Bs value and BISS value are obtained.
3. Natural sand samples that have been separated using the ISS method and have been subjected to BM stages 1 and 2.

Determination of magnetic susceptibility (χ_m) is obtained using the formula for the magnetic induction value B0 and with a core (B_T) as stated in (1):

$$\chi_m = \frac{B_T - B_0}{B_0} \quad (1)$$

Sample Separation Process with ISS and NdFeB Magnets

The process of separating iron sand samples from ordinary sand is carried out using the ISS or ISS method. This is a method that separates iron particles containing magnetic and non-magnetic compounds. Then the iron sand samples were weighed as much as the research target, namely 120 g. The sand that has been in BM stages 1 and 2 is then separated again using a NdFeB magnet. This aims to ensure that the sample to be tested only contains magnetic particles.

BM Process

The sand that has been weighed is then put into the BM machine. Here researchers carried out 2 stages of the grinding process. In the BM process, researchers used 16 combined iron balls with a diameter of 2 cm; 32 pieces of 1.5 cm, and 16 pieces of 0.7 cm, 64 pieces. Then the first stage of BM was carried out for 80 hours. Meanwhile, the second stage of the BM process is carried out with an additional time of 30, 40, and 50 hours.

XRF Test

Natural sand samples that had been separated using the ISS method and had been subjected to BM stages 1 and 2 were sent to the Padang State University FMIPA Laboratory to carry out XRF tests. The XRF test was carried out to determine the composition contained in the natural sand samples.

SEM Test

Natural sand samples that had been separated using the ISS method and had been ball milled in stages 1 and 2 were sent to the Diponegoro University FMIPA Laboratory to carry out SEM tests. The SEM test was carried out to determine the size of the particles that had been ball-milled.

RESULTS AND DISCUSSION

Magnetic Susceptibility

Table 1 shows the measurement data for the magnetic susceptibility value of natural sand, ISS products, BM1 for 80 hours, and BM2 (A, B, and C) for 30, 40, and 50 hours.

From Figure 1, it can be seen that the magnetic susceptibility value is increasing. The magnetic susceptibility value of natural sand is 2635.2, an increase in the ISS product of 4993.9. The cause is the separation of magnetic and non-magnetic particles using an ISS machine so that the magnetic content contained in the particles is more than natural sand. The magnetic susceptibility value continues to increase in BM products, namely at BM1 it is 11,361.6, BM2A of 12,398.7, BM2B is 13,383.4, and BM2C of 14,541.2. The preparation and separation process in BM

causes the magnetic concentration of BM products (1, 2A, 2B, and 2C) to be higher compared to ISS products.

Table 1. Magnetic susceptibility values (χm) of natural sand, ISS products, BM1 for 80 hours, BM2 (A, B, and C) for 30, 40, and 50 hours.

Product	B_0 (mT)	B_T (mT)	χ_m (10^{-5})
Iron sand	11,574	11,879	2,635.2
ISS	11,574	12,152	4,993.9
BM1	11,574	12,889	11,361.6
BM2A	11,574	13,009	12,398.7
BM2B	11,574	13,123	13,383.4
BM2C	11,574	13,257	14,541.2

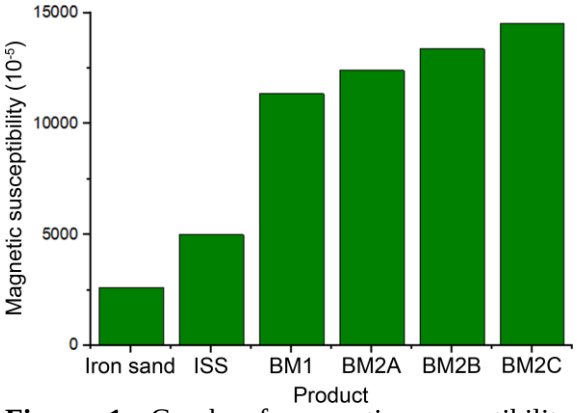

Figure 1. Graph of magnetic susceptibility value of natural sand, ISS products, BM1 for 80 hours, BM2 (A, B, and C) for 30, 40, and 50 hours

Composition of Magnetic Nanoparticles

Identification using XRF of the natural sand of the Rokan River aims to determine the elements contained in the natural sand of the Rokan River which has been in BM stage 1 (BM1) for 80 hours and BM stage 2 (BM2A, BM2B and BM2C) for 30, 40 and 50 hours.

In the first stage of BM for 80 hours, silicon (Si) has a percentage of 32.244%. Meanwhile, in the second stage of BM, Si experienced a percentage decrease of 30.159% in an additional 30 hours; 29.068% in 40 hours of additional time, and 28.564% in 50 hours of additional time. Other non-magnetic elements also experienced a decrease in percentage. Meanwhile, the iron (Fe) element in the first stage of BM for 80 hours had a percentage of 38.113%, while in the second stage of BM, the percentage increased, namely 40.133% in an additional 30 hours; 41.629% in 40 hours of additional time and 42.478% in 50 hours of additional time. And other magnetic elements also experienced a percentage increase.

Table 2. Data on Element Identification of Rokan River Natural Sand after BM Stages 1 and 2.

Element	Composition (%)			
	80 hours	110 hours	120 hours	130 hours
Al	7.814	8.167	8.634	9.379
Si	32.244	30.159	29.068	28.564
P	2.394	2.303	1.762	1.439
K	4.335	4.112	3.952	3.267
Ca	10.427	10.384	10.083	9.888
Ti	2.316	2.428	2.502	2.519
V	0.071	0.078	0.079	0.085
Cr	0.061	0.065	0.072	0.079
Mn	0.441	0.297	0.193	0.156
Fe	38.113	40.133	41.629	42.478
Ni	0.024	0.02	0.018	0.009
Cu	0.03	0.03	0.027	0.011
Zn	0.078	0.057	0.042	0.022
Pb	0.024	0.023	0.02	0.005
Other	1.629	1.744	1.919	2.099

The cause of increasing and decreasing the percentage of each element is influenced by the length of BM time. The longer the grinding time, the smaller the particle size will be, causing the collision process between the walls of the milling tube and the iron balls to become larger so that the size becomes smaller, where the non-magnetic elements that were originally still together will be split so that when they are separated with a magnet Strong NdFeB magnetic particles will be attracted more. Magnetic particles that experience separation will experience an increase in the percentage value, while non-magnetic particles will experience a decrease in the percentage value.

Morphology of Magnetic Nanoparticles

The purpose of testing using a SEM is to determine changes in particle size after BM stages 1 and 2. The results of SEM testing are

images with a magnification of 20,000× and can be processed using ImageJ software to obtain the average size of the particles. the. As seen in Figure 2 below.

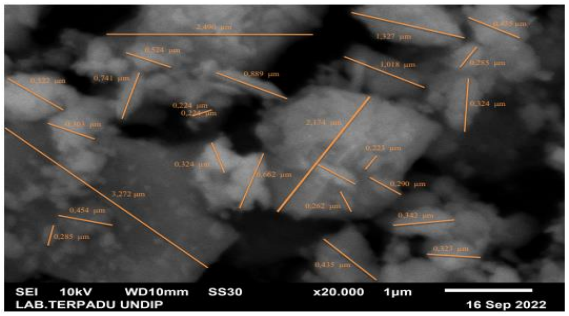

(a)

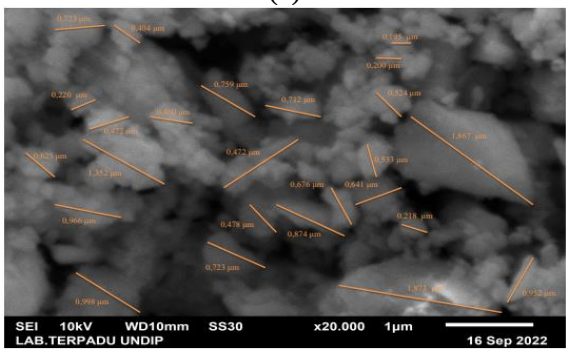

(b)

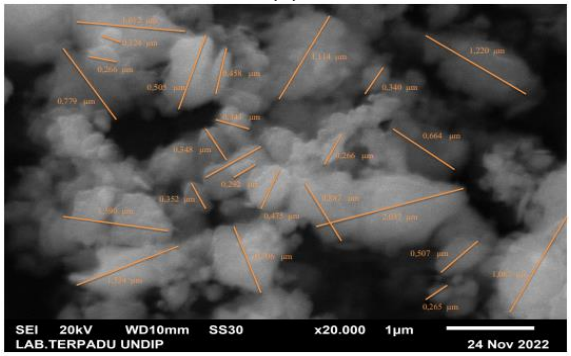

(c)

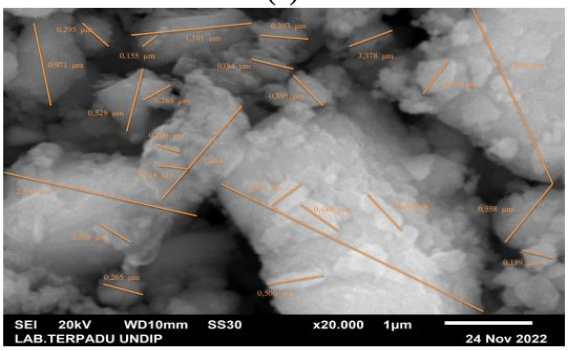

(d)

Figure 2. Size of natural sand particles in Rokan River after BM stages 1 and 2: (a) BM product 1; (b) BM product 2A; (c) BM product 2B; and (d) BM product 2C.

As shown in Figure 2 (a – d) above, the surface shape of the natural sand of the Rokan River which has been in BM stages 1 and 2 tends to be irregular. If you look closely, several nanoparticles have a round and elongated shape. In BM stage 1, the average particle size is 685 nm. Meanwhile, in BM stage 2, the average particle size is 656 nm for 30 hours; 630 nm for 40 hours; and 630 nm for 50 hours. For the average size of the BM product stage 2, namely at an additional time of 40 and 50 hours, the average size of the nanoparticles is the same. This is caused by several particles accumulating. This occurs due to the sample clumping when tested, making it a little difficult to measure the size of the sample nanoparticles.

The results of measurement tests using a SEM show that the longer the BM time, the smaller the particle size produced. Apart from that, this happens according to the physics formula, namely the momentum formula. Where the greater the mass is given, the greater the momentum that occurs. By using combined and varied milling balls, the sand particles and milling balls collide with each other and have great momentum. So the resulting BM product will be smoother.

CONCLUSION

Based on the research data obtained, it can be concluded that the magnetic susceptibility value of Rokan River natural sand which has gone through the BM process has increased along with the increase in BM rotation time of 11361.6 at BM1; 12398.7 on BM2A; 13383.4 on BM2B and 14541.2 on BM2C. The XRF identification results show that the percentage of magnetic element composition increases with increasing BM rotation time, such as Fe, namely 38.113% at BM1; 40.133% in BM2A; 41.629% on BM2B, and 42.478% on BM2C. SEM identification results show that the particle size of the natural sand of the Rokan River becomes smaller as the BM rotation time

increases, namely 685 nm at BM1; 656 nm on BM2A; 630 nm on BM2B, and 630 nm on BM2C.

REFERENCES

1. Satria, B., Masrurah, Z. & Fajar, S. J. (2021). Magnetic susceptibility and grain size distribution as prospective tools for selective exploration and provenance study of iron sand deposits: A case study from Aceh, Indonesia. *Heliyon*, **7**(12).
2. Yulianto, Y. W. & Cholil, M. (2024). Landslide susceptibility levels analysis based on geographic information system (GIS) in Simo District, Boyolali Regency. *IOP Conference Series: Earth and Environmental Science*, **1357**(1), 012044.
3. Santoso, U. T., Rodiansono, R., Junaidi, A. B., Ariyanti, C., Oktari, R., Nopitasari, P. & Hasanah, H. (2019). Pengaruh penyaringan dan pengeringan terhadap ukuran partikel oksida besi: Tinjauan karakterisasi kualitatif menggunakan mikroskop optik. *Jurnal Fisika Flux*, **1**(1).
4. Sinuraya, S., Amiruddin, E., Nurrohmah, D. & Wulandari, T. (2021). Analisa perubahan suseptibilitas magnetik dan komposisi partikel pasir alam sungai rokan sebagai fungsi kecepatan putar tabung ball milling. *Komunikasi Fisika Indonesia*, **18**(3), 225–229.
5. Alisna, S. & Sinuraya, S. (2021). Pemetaan suseptibilitas magnetik dan penentuan kandungan logam pada air gambut di Kelurahan Tuah Madani Kecamatan Tampan Pekanbaru. *Komunikasi Fisika Indonesia*, **18**(1), 12–17.
6. Laia, S. & Erwin. (2021). Suseptibilitas magnetik dan morfologi nanopartikel oksida besi dipreparasi menggunakan ball milling melalui varias bola milling. *Seminar Nasional Fisika Universitas Riau VI (SNFUR-6)*, **6**(1), 1004.
7. Priyadarshana, G., Kottegoda, N., Senaratne, A., de Alwis, A. & Karunaratne, V. (2015). Synthesis of magnetite nanoparticles by top-down approach from a high purity ore. *Journal of Nanomaterials*, **2015**(1), 317312.
8. Sinuraya, S., Amiruddin, E., Wahyuni, L. & Jesika, N. (2021). Analysis of the size and composition of natural sand particles in the Rokan River Riau Province as a function of ball milling time. *Journal of Aceh Physics Society*, **10**(3), 80–83.
9. Sirait, R. A., Salomo, S., Muhammad, J. & Taer, E. (2022). Sintesis dan karakterisasi nanopartikel oksida besi menggunakan metode ball milling dan kopresipitasi. *Indonesian Physics Communication*, 19(2), 91–98.
10. Kurniawan, R., Salomo, S., Erwin, E. & Defrianto, D. (2022). Pengaruh doping mangan terhadap komposisi dan sifat kristalinitas partikel oksida besi pasir alam Sungai Rokan dipreparasi dengan metode ball milling. *Indonesian Physics Communication*, **19**(2), 113–118.
11. Li, Z., Wang, Y., Li, K., Lin, W. & Tong, X. (2018). Study on the performance of ball mill with liner structure based on DEM. *Journal of Engineering & Technological Sciences*, **50**(2).
12. Salomo, S. & Yosefi, N. R. (2022). Pengaruh doping tembaga terhadap suseptibilitas magnetik dan komposisi serta sifat kristalinitas pasir alam sungai rokan dipreparasi dengan metode ball milling. *Indonesian Physics Communication*, **19**(3), 154–160.
13. Nurhidayah, I., Sinuraya, S., Amiruddin, E. & Setiadi, R. N. (2023). Analisa perubahan suseptibilitas dan komposisi serta ukuran partikel oksida besi sebagai fungsi kecepatan putaran tabung ball milling. *Indonesian Physics Communication*, **20**(1), 75–82.

IPC

Indonesian Physics Communication

Department of Physics, Universitas Riau, Pekanbaru, Indonesia
p-ISSN 1412-2960 | e-ISSN 2579-521X

Vol. 21 | No. 2
July 2024
Web: https://kfi.ejournal.unri.ac.id
E-mail: kfi@ejournal.unri.ac.id

Utilization of young coconut fiber activated carbon with pre-carbonization variations as a supercapacitor electrode

Winda Nofriyanti, Awitdrus*
Department of Physics, Universitas Riau, Pekanbaru 28293, Indonesia

*Corresponding author: awitdrus@lecturer.unri.ac.id

ABSTRACT

A supercapacitor is an electrochemical device that integrates power supply and charge storage capabilities. The primary constituents of a supercapacitor consist of electrodes, separator, electrolyte, and current collector. This work focuses on the production of carbon electrodes using coconut fibre biomass waste. The carbonisation process is carried out at three different temperatures: 200ºC, 225ºC, and 250ºC. The resulting samples are labelled as SC-200, SC-225, and SC-250, respectively. The production of Carbon electrodes involves multiple procedures, including pre-carbonization, chemical activation using a $ZnCl_2$ activator at a concentration of 0.5 M, followed by carbonisation using N_2 gas at a temperature of 600ºC, and physical activation using CO_2 gas at a temperature of 750ºC. The mass reduces by 23.01%, 27%, and 36.51% following pre-carbonization. The sample with the greatest density value is SC-225, which has a mass loss percentage of 41.66%. The results of cyclic voltammetry indicate that the SC-225 supercapacitor cell has the maximum capacitance value of 199.82 F/g. To summarise, the SC-225 temperature can function as an activated carbon electrode that enhances the performance of the supercapacitor electrode.

Keywords: Electrode carbon, pre-carbonization, supercapacitor, young cocofiber

Received 20-02-2023 | Revised 27-06-2023 | Accepted 10-05-2024 | Published 17-07-2024

INTRODUCTION

The increase in energy consumption along with the progress of economic development poses a serious threat to humans and the environment, encouraging us to innovate regarding energy [1-3]. Rapid technological developments in fields such as electronics, digital telecommunications, and transportation have caused an increase in energy consumption [4,5]. The currently available energy sources are not commensurate with the energy needs that must be met, making people think critically about alternative energy. Alternative energy is becoming important as a relatively cheap, renewable, and abundantly available source to help meet energy needs [6-8].

The energy requirement that is currently most widely used is electrical energy. Electrical energy is an important factor in supporting development. The demand for electrical energy continues to increase so a breakthrough energy storage device is needed [4,9]. Some of the energy storage devices used today are batteries and capacitors. However, several researchers have found energy storage devices with higher capacitance. This storage medium is called a supercapacitor. Supercapacitors or in other words double-layer electrochemical capacitors are used as energy storage devices which have advantages including a long life cycle, fast charge-discharge, high power density, safe when used, and good temperature characteristics [10-12]. Supercapacitor electrodes include the materials used, namely nanotubes, carbon graphene, and activated carbon [13-15].

The biomass currently used to make supercapacitor carbon electrodes is coconut fiber. Indonesia is the largest coconut producer. Coconut plantations in Indonesia cover 3.5 million hectares, and 17.7 million tonnes of coconuts are produced annually. The products produced are copra and crude oil for various

applications, but coconut production produces quite a lot of agricultural waste, one of which is young coconut fiber. It is known that coconut production contributes around 35% of the 6.2 million tons of coconut fiber produced as waste in Indonesia every year [16-18]. This study focuses on the role of the influence of pre-carbonization temperature on mass loss, density properties, and specific capacitance of the resulting supercapacitor cells.

RESEARCH METHODS

This research method explains the procedure for making supercapacitor cells. Young coconut fiber was obtained from Pangkalan Kerinci, Pelalawan Regency. Cut the coconut fibers into several pieces and then separate the fibers with a cork. Coconut fiber is dried in the sun for 2 days until the mass obtained remains constant. 30 grams of coconut fiber was weighed and placed in a pre-carbonized tube, then the bottom was covered with aluminum foil to make it airtight. After that, the tube was put into an electric oven. Refining the samples was carried out using a mortal and pestle, however, to produce a smoother sample a ball milling process was required for ± 20 hours.

The fine samples were then sifted using a 53 µm sieve. Chemical activation uses the activating agent $ZnCl_2$ 0.5 M. Then, pellets are printed using a hydraulic press. Carbonization was carried out using N_2 gas at a temperature of 600ºC and physical activation using CO_2 gas. Next, the sample was soaked in a beaker containing distilled water, then dried, and then polished to reduce the thickness and diameter of the carbon pellets. Several components for making supercapacitor cells are a separator, electrolyte, current collector, and carbon electrodes from young coconut fiber. Electrochemical characterization of activated carbon electrodes was carried out by making a supercapacitor cell and calculating it using cyclic voltammetry.

RESULTS AND DISCUSSION

Density Analysis

Figure 1 is the result of carbon pellet density data before and after pyrolysis. In carbonization, stronger carbon atomic bonds are formed which changes the young coconut fiber sample into pure carbon and increases the carbon content [19]. The decrease in density is also caused by physical activation, where CO2 reacts with carbon to form a new pore structure due to erosion of the walls between the pores. Shows that all samples experience a decrease in density as the pre-carbonization temperature increases. Samples with higher pre-carbonization temperature variations cause erosion of the carbon walls, reducing the surface area and pore structure formed before pyrolysis. The effect of higher temperatures can also destroy existing pores so that they accumulate and cover the previous surface area.

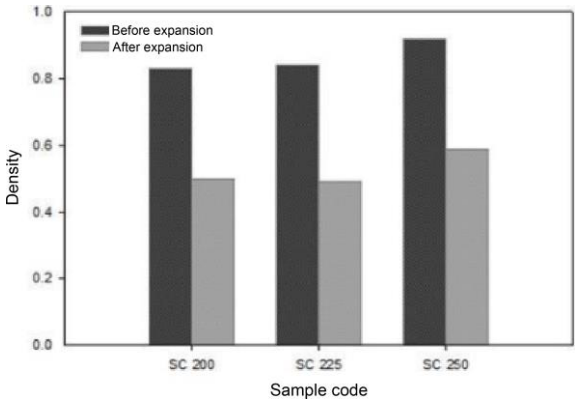

Figure 1. Percentage density graph of carbon electrodes.

Figure 1 shows the largest shrinkage percentage of the electrode in the SC-225 sample and the lowest density shrinkage in the SC-250 sample. During the carbonization process, the density decreases due to elements other than carbon disappearing. SC-225 experiences more shrinkage because the bonds between the elements oxygen, hydrogen, and carbon are weakened. Pre-carbonization is the first step that needs to be considered because the optimum temperature provides better density.

Cyclic Voltammetric Analysis

A voltammogram curve is formed as in Figure 2 with a scanning rate of 2 mV/s for each pre-carbonization variation. In the voltammogram curve, you can also see the charging current (Ic) and discharging current (Id) values. The current density value, namely the charge current (Ic) is the current that occurs when the charge comes from the electrolyte which breaks down into ions when the voltage is increased and the discharge current (Id) is the current when the voltage is lowered. Cyclic voltammetry curves have a rectangular closed area and some curves show a slight increase in current or have a hump in the curve with a certain voltage range [20]. The SC-225 curve has a larger curve area and width than SC-200 and SC-250, which indicates that the pre-carbonization temperature has a great influence on the specific capacitance results obtained. The optimal temperature, the thin thickness of the separator, and the carbon electrode mass are closely related to obtain the specific capacitance value. The specific capacitance of the SC-225 is an optimal temperature which has a specific capacitance value of 156.48 F/g.

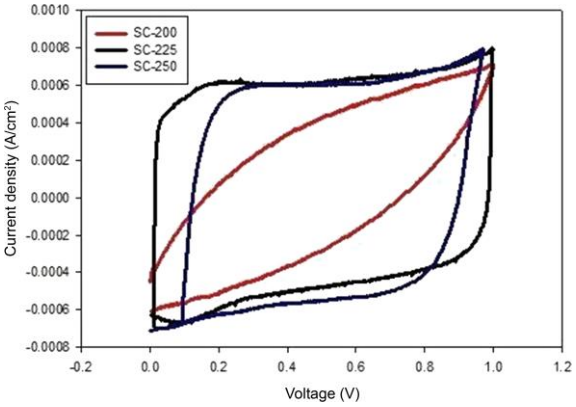

Figure 2. Cyclic voltammetry voltammogram curve of 1 mV/s.

CONCLUSION

P The research that has been carried out can conclude that young coconut fiber biomass can be used as a supercapacitor cell electrode. The SC-225 sample had the largest percentage of density shrinkage at 41.66% and the specific capacitance value was 199.82 F/g.

REFERENCES

1. Libich, J., Máca, J., Vondrák, J., Čech, O. & Sedlaříková, M. (2018). Supercapacitors: Properties and applications. *Journal of Energy Storage*, **17**, 224–227.
2. Nopriansyah, R. & Awitdrus, A. (2023). Pemanfaatan limbah serabut kelapa muda sebagai elektroda karbon superkapasitor dengan variasi konsentrasi aktivator $ZnCl_2$. *Indonesian Physics Communication*, **20**(3), 301–305.
3. Jaiswal, K. K., Chowdhury, C. R., Yadav, D., Verma, R., Dutta, S., Jaiswal, K. S. & Karuppasamy, K. S. K. (2022). Renewable and sustainable clean energy development and impact on social, economic, and environmental health. *Energy Nexus*, **7**, 100118.
4. Lestari, A. N. I., Farma, R., Asyana, V. & Awitdrus, A. (2020). Fabrikasi dan karakterisasi elektroda karbon dari biomassa serabut buah nipah dengan variasi konsentrasi aktivator KOH. *Komunikasi Fisika Indonesia*, **17**(3), 127–133.
5. Suwandi, D. A. & Awitdrus, A. (2021). Karakterisasi sifat elektrokimia elektroda karbon berbahan pelepah aren menggunakan larutan elektrolit Na_2SO_4. *Indonesian Physics Communication*, **18**(1), 88–92.
6. Zhang, X., Han, S., Fan, C., Li, L. & Zhang, W. (2015). Effects of pre-carbonization on the structure and performance of hard carbon in lithium cells. *Journal of Solid State Electrochemistry*, **19**, 715–721.
7. Simanjuntak, M. T. & Awitdrus, A. (2022). Fabrikasi elektroda karbon dari sabut kelapa muda dengan aktivasi fisika sebagai aplikasi superkapasitor. *Indonesian Physics Communication*, **19**(2), 65–68.

8. Hanifa, Z. & Awitdrus, A. (2022). Pembuatan Elektroda Karbon dari Biomassa Sabut Kelapa Muda dengan Aktivator KOH Sebagai Aplikasi Sel Superkapasitor. *Indonesian Physics Communication*, **19**(1), 45–50.
9. Simanjuntak, A. C., & Awitdrus, A. (2022). Karakterisasi sifat elektrokimia elektroda karbon aktif berbasis limbah sabut kelapa muda menggunakan separator membran kulit telur ayam. *Indonesian Physics Communication*, **19**(1), 31–34.
10. Handayani, R. & Taer, E. (2019). Pengaruh waktu aktivasi terhadap sifat fisis dan elektrokimia sel superkapasitor Dari Sabut Pinang. *Indonesian Physics Communication*, **16**(2), 87–90.
11. Putri, M. S. D., Awitdrus, A. & Manullang, R. K. (2020). Penyerapan logam berat Pb dan Cu menggunakan karbon aktif berbasis mahkota nanas dengan variasi konsentrasi kalium hidroksida. *Indonesian Physics Communication*, **17**(1), 30–34.
12. Awitdrus, Rukmana, D. V. & Farma, R. (2016). Pengaruh waktu perendaman dalam pembuatan karbon aktif cangkang buah ketapang dengan pengaktifan kimia berbantuan iradiasi gelombang mikro. *Indonesian Physics Communication*, **13**(13), 870–875.
13. Habibah, M. D. (2016). Variasi holding time suhu aktivasi karbon aktif dari tempurung kluwak (Pangium edule) sebagai elektroda pada superkapasitor. *Inovasi Fisika Indonesia*, **5**(1), 19–22.
14. Widarti, Awitdrus, Farma, R. & Iwantono. (2016). Pengaruh daya iradiasi gelombang mikro terhadap sifat-sifat fisika karbon aktif kayu Eucalyptus. *Indonesian Physics Communication*, **13**(12), 773–780.
15. Rahim, A. H. A., Ramli, N., Nordin, A. N. & Wahab, M. F. A. (2021). Supercapacitor performance with activated carbon and graphene nanoplatelets composite electrodes, and insights from the equivalent circuit model. *Carbon Trends*, **5**, 100101.
16. Hebbar, K. B., Abhin, P. S., Sanjo Jose, V., Neethu, P., Santhosh, A., Shil, S. & Prasad, P. V. (2022). Predicting the potential suitable climate for coconut (Cocos nucifera L.) cultivation in India under climate change scenarios using the MaxEnt model. *Plants*, **11**(6), 731.
17. Junita, E., Pane, T. C. & Darus, M. B. (2023). Processing coconut husk waste to gain profit in Tanjung Pura Subdistrict, Langkat Regency, North Sumatera Province. *IOP Conference Series: Earth and Environmental Science*, **1241**(1).
18. Sekali, S. U. K. & Awitdrus, A. Fabrication of carbon electrodes from young coconut fiber by varying the carnonization temperature as a supercapacitor application. *Indonesian Physics Communication*, **21**(1), 63–66.
19. Kurniawan, P., Taer, E., Malik, U. & Taslim, R. (2018). Pengaruh Konsentrasi KOH Terhadap Sifat Fisis Dan Elektrokimia Elektroda Karbon Dari Limbah Kulit Durian Sebagai Sel Superkapasitor. *Indonesian Physics Communication*, **15**(1), 62–66.
20. González-García, P. (2018). Activated carbon from lignocellulosics precursors: A review of the synthesis methods, characterization techniques and applications. *Renewable and Sustainable Energy Reviews*, **82**, 1393–1414.

IPC

Indonesian Physics Communication

Department of Physics, Universitas Riau, Pekanbaru, Indonesia
p-ISSN 1412-2960 | e-ISSN 2579-521X

Vol. 21 | No. 2
July 2024

Web: https://kfi.ejournal.unri.ac.id
E-mail: kfi@ejournal.unri.ac.id

Earthquake vulnerability mapping based on probabilistic seismic hazard analysis (PSHA) in the Nias Islands, Indonesia

Astri Angraeni[1], Lailatul Husna Lubis[1,*], Ratni Sirait[1], Reinhard Sipayung[2]
[1]Department of Physics, Universitas Islam Negeri Sumatera Utara, Deli Serdang 20353, Indonesia
[2]Class I Geophysical Station, BMKG, Deli Serdang 20353, Indonesia

*Corresponding author: lailatulhusnalubis@uinsu.ac.id

ABSTRACT

The Nias Islands are categorised as seismically active, making them susceptible to earthquakes. The Nias Islands region is situated on the ring of fire and a subduction line that experiences annual movement, which is the primary factor contributing to its susceptibility to earthquakes. The occurrence of earthquakes in the Nias Islands is supported by a documented record of 7,152 incidents with a magnitude strength more than 4 Mw from 1910 to 2022, indicating a 500-year return period. In order to assess the susceptibility of the Nias Islands region to earthquakes, a process called earthquake vulnerability mapping is conducted. This involves utilising the probabilistic seismic hazard analysis (PSHA) approach to calculate the peak ground acceleration value. The investigation commences with gathering seismic events within the study region from the IRIS and BMKG catalogues. The earthquake data was subsequently transformed from magnitude to M_w (magnitude moment), and then de-clustered to isolate the primary event from the entire dataset of earthquakes. First, the a-value and b-value are calculated in order to identify the background earthquake source. Then, PSHA processing is conducted to calculate the spectral acceleration value for each predefined grid. The processing findings indicate that the peak ground acceleration (PGA) value at time 0 s ranges from 0.05 – 1.2 g, the PGA value at time 0.2 s ranges from 1 – 1.2 g, and the PGA value at time 1 s ranges from 0.4 – 0.5 g.

Keywords: Earthquake; Nias Islands; PGA; PSHA

Received 18-08-2023 | Revised 21-11-2023 | Accepted 15-05-2024 | Published 18-07-2024

INTRODUCTION

Indonesia is a country located in the meeting area of three large plates in the world, namely the Indo-Australian plate, the Pacific plate, and the Eurasian plate. The movement of the Eurasian plate and the Indo-Australian plate towards the north suppresses the movement of the relatively stationary Eurasian plate. The movement caused by these three plates will cause collisions that cause earthquakes in Indonesia [1]. This is proven by the record of 51,855 earthquakes occurring in Indonesia from 1907 to 2016 with a magnitude ≥ 4.5 magnitude moment (M_w) [2].

The Nias Islands region is one of the regions in Indonesia with a record of significant and destructive earthquakes. Zebua (2018) explains that the Nias Islands are one of a group of islands on the west coast of Sumatra which is located on the ring of fire along the junction between the Indo-Australian plate and the Eurasian plate. These geographical conditions caused the Nias Islands region to experience earthquakes [3].

The morphological conditions in the Nias Islands region also support the occurrence of earthquakes. Where the morphological conditions are dominated by hills, valleys, and coastal land. The rocks are pre-tertiary (sedimentary rocks and metamorphic rocks), tertiary (sedimentary rocks), and quaternary deposits (coastal alluvial, swamps, and rivers). if rocks of pre-tertiary and tertiary age experience quaternary deposits and weathering, they will be broken down, loose, not yet compact and will strengthen the effects of shocks which makes them prone to earthquakes. Apart from that, the morphology of hills covered with weathering rocks is prone to

ground movement because it is triggered by large earthquake shocks and is also supported by high rainfall [4]. Meanwhile, the geological condition of the Nias Islands consists of several formations which can be seen in Figure 1, namely the Labuhanhiyu formation, Rapa-Rapa Formation, Alluvium, Hiligeho formation, Guunung Bala formation, Sipika formation, Bancuh Tanah Bala, Gunung Sitoli formation, Lelematua formation, and Gomo formation.

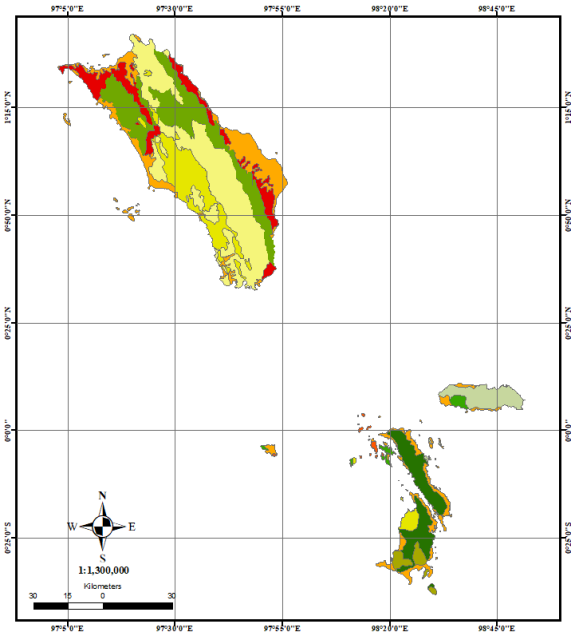

Figure 1. Geological map of the Nias Islands.

In historical records, Nias has experienced four earthquakes that were classified as destructive, in 1861 with a magnitude of 8.5 M_w, in 1907 with a magnitude of 7.4 M_w, in 2004 with a magnitude of 9.2 M_w, and in 2005 with a magnitude of 8.7 M_w. The last earthquake in 2005 claimed the lives of up to two thousand people and destroyed many buildings. Other impacts cause environmental damage, where the earth's surface is lifted and lowered by around one to three meters along the west coast of Nias, the southern and eastern parts of Simelue, and Banyak Island [1].

Natawidjaya (2007) has also explained that in the range of events the earthquake that occurred in 1861 had ruptured the same segment in 2005 [5]. The Nias segment last released its stored energy about 145 years ago. Thus, there is still the potential for earthquakes to occur in the area. One effort that can be made to anticipate and minimize the damage caused by earthquakes is by creating an earthquake vulnerability map which is made by analyzing the value of ground acceleration or peak ground acceleration (PGA).

The PGA value is expressed in g (gravitational acceleration = g) or m/s^2 (1 g= 9.81 m/s^2 or in gal where 1 gal is equal to 0.01 m/s^2, 1 g = 981 gal) [6]. The resulting PGA value shows the level of disaster risk that occurs and can be used as consideration for disaster mitigation, building structure design, and spatial planning in the Nias Islands [7].

Two methods can be used to obtain the PGA value, namely deterministic seismic hazard analysis (DSHA) and probabilistic seismic hazard analysis (PSHA). This research was carried out using the PSHA method which is a technique for analyzing earthquake events for a certain anniversary period by creating the possibility of various levels of ground movement in the research area. This method can also provide a clearer framework so that uncertainty factors can be calculated, identified, and combined with rational approach methods to get a more complete picture of earthquake events thousands of years into the future. This also depends on the completeness of the data in the form of maximum obstacles in the research area, earthquake data, and the natural period or frequency of earthquakes by considering how big the risk of an earthquake occurring. The disadvantage of this method is that many assumptions or uncertainties arise in carrying out the analysis so control or reference parameters are needed [8].

$$P[I \geq i] = \int_r \int_m P[I \geq i; m, r]\, f_m(m) f_r(r) dm\, dr \quad (1)$$

RESEARCH METHODS

The research was conducted from May to July 2023 at the Class I Deli Serdang Climatology Station, Medan City. The research area is on the Nias Islands, North Sumatra Province with coordinates -2.984º – 2.994º N and 96º – 98.349º E.

Data processing in this research was assisted using Microsoft Word 2019, Microsoft Excel 2019, Visio, Notepad++, Matlab R2007b, Zmap v6, USGS_PSHA 2007, and ArcGIS 10.8 software. The data used in this research include seismic data for the Nias Islands from 1910 to 2022, a base map of Indonesia, a base map for the North Sumatra district, a base map for the North Sumatra sub-district, and data on the PGA and spectral acceleration (SA) values of the Nias Islands from 1910 to 2022 has been processed.

This research began by analyzing earthquake sources in the research area and collecting earthquake catalog data from the IRIS and BMKG catalogs. Earthquake data was collected from 1910 to 2022 at coordinates -2.984º – 2.994º N and 96º – 98.349º E and magnitude > 4 M_w. The catalog data is then converted to a magnitude scale for each scale value obtained in analyzing earthquake risk. This is done to standardize the data with a scale that has been established in Indonesia, namely the M_w scale [9]. Then de-clustering is carried out by separating the earthquake between foreshock and aftershock using time and distance criteria to get the main earthquake. De-clustering earthquake data using Zmap and Matlab software [10].

The data that has been de-clustered is then modeled according to the earthquake source by interpreting geological, geographic, and seismotectonic conditions based on secondary data resulting from earthquakes in the Nias Islands from 1910 to 2022. This earthquake source zone modeling will provide an overview of earthquake events, earthquake frequency, and the relative shift of plates. The earthquake source area is classified into three sources, namely fault earthquake sources, subduction earthquake sources, and background earthquake sources.

The final process carried out in the Zmap software is determining the a-value and b-value parameters and the attenuation function. Determine the a-value and b-value parameters used to predict the maximum earthquake value from the earthquake source. This parameter is determined using the maximum likelihood equation [11]. The attenuation function is based on the similarity of geological and tectonic conditions in a research area. Currently, the Indonesian region does not have data that can be used to derive the attenuation function, so data is needed from other regions that have similar geological and seismotectonic characteristics to the research area. The attenuation function will be adjusted to the earthquake source mechanism that has been modeled.

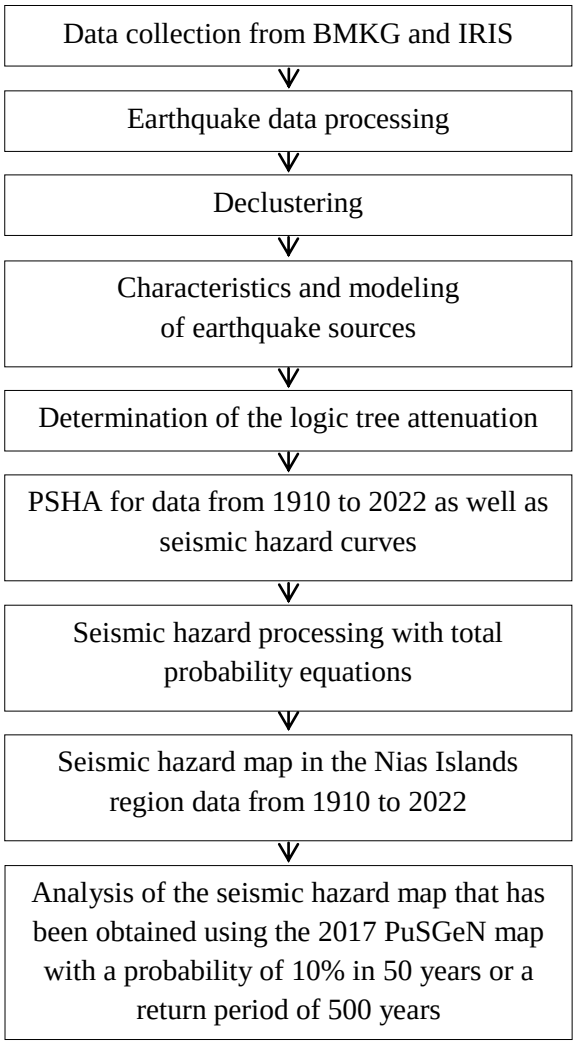

Figure 2. Flow diagram of research procedures.

The results obtained are then analyzed using the PSHA method with Equation (1). Processing earthquake data using this method will produce indicator values for vibration acceleration parameters in the bedrock (PGA and SA). This analysis was carried out with the

help of USGS_PSHA software. The final result of the earthquake vulnerability analysis in this study is a map of the maximum earthquake acceleration in the bedrock for a probability of exceeding 10% in the 50-year earthquake return period of 500 years. This processing process can be seen in the research procedure flow diagram in Figure 2.

RESULTS AND DISCUSSION

The source of the earthquake in the Nias Islands area greatly influences the PGA and SA values. The earthquake source consists of three sources, namely fault earthquake sources, subduction earthquake sources, and background earthquake sources. Each of the earthquake source models will be combined and produce an earthquake vulnerability map. By entering the parameter values from the three earthquake sources, the seismic hazard distribution value for all earthquake sources is obtained. The probabilistic seismic hazard calculation is carried out on a probability of exceeding 10% within a 50-year earthquake return period of 500 years.

The results of this research are the values of maximum ground acceleration or PGA and the SA response in bedrock in short periods (T = 0.2 s) and long periods (T = 1 s) in bedrock. Where each acceleration period represents a period of structure vibration for each level. For example, in 0 seconds, it will have quite an influence on the vibration of the building foundation. Then 0.2 seconds will represent the shortest period of vibration of the structure, namely a two-story building. Meanwhile, for a long period of 1 second, it will represent the shock that occurs in a ten-story building. So, if the building stands in an area with a fairly high ground acceleration value at the surface and has a natural structural period that is the same as the earthquake period, then it is certain that there will be implications and resonances that cause the building to possibly experience shocks strong enough to cause damage to the building.

The range of PGA values obtained in the Nias Islands region will be classified into three ranges, namely low range (PGA < 0.05 g and PGA < 0.25 g), medium range (0.25 g < PGA < 0.7 g), and high range (PGA < 0.7 g and PGA > 1.2 g) which can be seen in Figure 3.

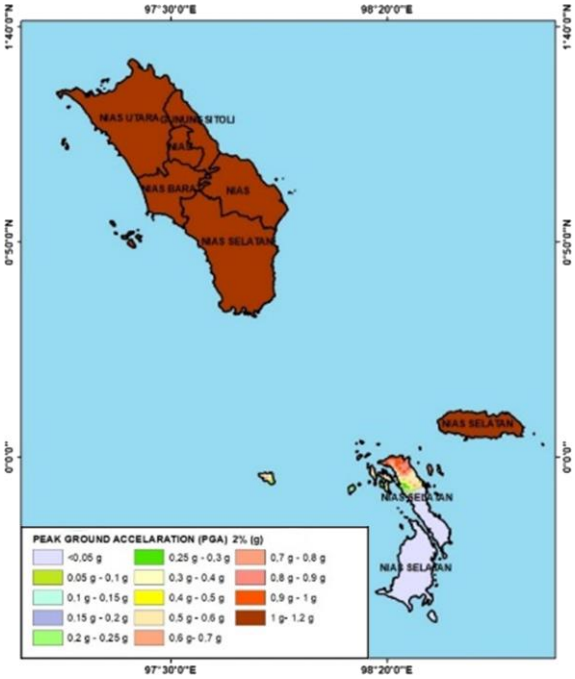

Figure 3. Map of ground acceleration values in bedrock (PGA) at spectral conditions T = 0 second for a probability of exceeding 10% in 50 years.

The PGA value in the South Nias Regency area has a PGA value that is classified as low to high. Meanwhile, Gunung Sitoli, North Nias, Nias, and West Nias regencies have a high range because the areas with relatively high PGA values are close to the Andaman-Sumatra and Nias subduction earthquake source route (megathrust).

The map of ground acceleration on bedrock in the period T = 0.2 seconds shows a range of ground acceleration values in the range of 1 – 1.2 g which is relatively high and covers the five districts of the Nias Islands, namely South Nias, Nias, West Nias, Gunung Sitoli, and North Nias (Figure 4).

Analysis of ground acceleration in bedrock for the period T = 1 s shows a range of ground acceleration values ranging from 0.4 – 0.5 g as shown in Figure 5. The T = 1 s spectral value in the five districts on the Nias Islands is in the medium range with yellow contours.

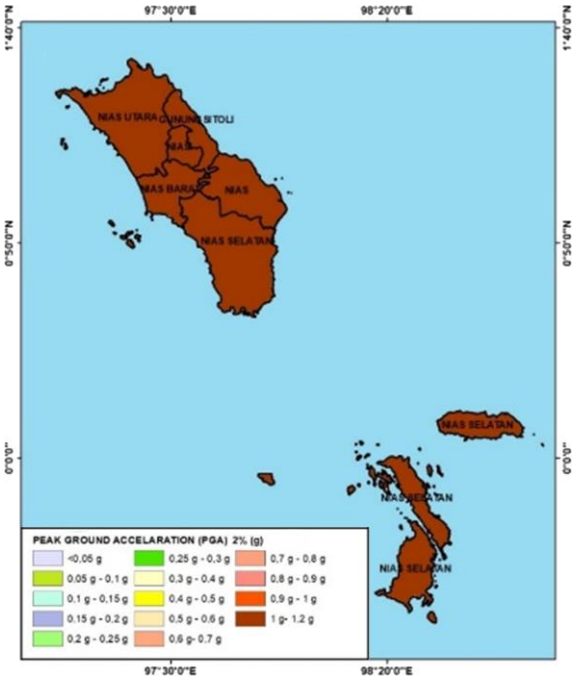

Figure 4. Map of ground acceleration values in bedrock at spectral conditions T = 0.2 s for a probability of exceeding 10% in 50 years.

Based on the results of the PSHA values obtained, almost the entire Nias Islands area is classified as moderate to dangerous damage due to the effects caused by the aftermath of the earthquake disaster. The values obtained by applying the PSHA method are by PSHA theory. PSHA theory states that the resulting PGA and SA values are influenced by the distance of the earthquake source. So the map projects a relatively high range of PGA and SA values along the subduction route (megathrust) Andamana-Sumatra and Nias.

As for this research, validation of the results of earthquake hazard mapping using the PSHA method was compared with the results of seismic hazard values with research that had been carried out in PuSGeN 2017, and it was found that there were differences. These differences include the PGA value in the period T = 0 s, the research results have a range of < 0.05 – 1.2 g, while the 2017 PuSGeN map has a range of < 0.7 g to > 0.8 g. Meanwhile, the SA value (T = 0.2 s) has a range of 1 – 1.2 g, while the 2017 PuSGeN map has a range of > 1.2 g. And likewise, the SA value (T = 1 s) has a range of 0.4 – 0.5 g in the research results, and 0.4 – 0.6 g in the 2017 PuSGeN map [12,13].

This difference in results is due to the earthquake catalog data source and different time ranges from PuSGeN 2017, fault and subduction earthquake source parameters are more widely used in PuSGeN 2017 because the research area covers a global scale. The data source and use of equations in the USGS_PSHA software in this study can also be the cause of differences in research results.

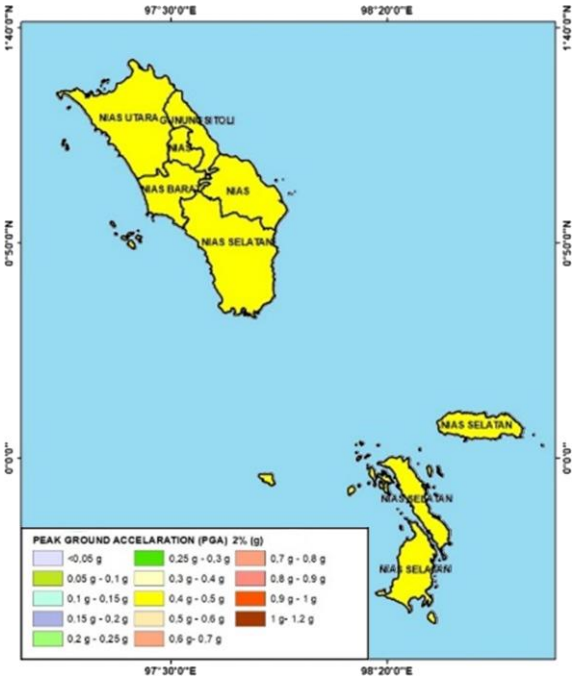

Figure 5. Map of ground acceleration values in bedrock at spectral conditions T = 1 s for a probability of exceeding 10% in 50 years.

Based on the overall results of the ground acceleration values in bedrock, this is an encouragement that the Nias Islands region is an area that is classified as vulnerable to earthquakes. This shows that the traces of earthquakes that occurred on the Nias Islands were quite significant and several earthquakes were recorded which caused quite serious damage. The subduction zone around the Nias Islands is the earthquake route that absorbs and releases the most earthquake energy. The subduction zone consists of Andamana-Sumatra and Nias. This is also supported by the environmental geology information map for the spatial plan (Intra Urban) for the Nias Islands region made by the Department of Energy and Mineral Resources, showing that the Nias

Islands region is dominated by areas with medium to high potential for ground movement and alongside roads. has a relatively high tsunami potential.

CONCLUSION

Based on the research that has been carried out and analyzed, several conclusions have been obtained, namely that the maximum ground acceleration value in the Nias Islands region from 1910 to 2022 has a PGA value with a relatively low to high classification with a value range of < 0.05 – 1.2 g, SA of T = 0.2 s with a relatively medium classification with a value range of 0.4 – 0.5 g, and SA of T = 1 s with a relatively high classification with a value range of 1 – 1.2 g

ACKNOWLEDGMENTS

The author would like to thank the Head of the Deli Serdang Class I Geophysics Station who gave the author the opportunity to carry out research and process the PSHA to completion, as well as to all parties involved.

REFERENCES

1. Khoiridah, S., Ibad, M. I. & Setyonegoro, W. (2017). Validasi Potensi Tsunami Berdasarkan Estimasi Durasi Patahan dan Pemodelan Tsunami di Wilayah Barat Sumatra (Studi Kasus: Gempa Bumi Nias 2005 dan Mentawai 2010). *OLDI (Oseanologi dan Limnologi di Indonesia)*, **2**(1), 39–54.
2. Irsyam, M., Wayan, S., Fahmi, A., Sri, W., Wahyu, T., Danny, H. N. *et al*. (2010). *Ringkasan hasil studi tim revisi peta gempa Indonesia 2010*. Bandung.
3. Zebua, A. W. (2018). Analisis gaya gempa bangunan rumah tinggal di wilayah gempa tinggi. *Siklus: Jurnal Teknik Sipil*, **4**(1), 23–35.
4. Badan Geologi. (2023). Diakses pada tanggal 17 Maret 2023, https://geologi.esdm.go.id/id/.
5. Natawidjaja, D. H. (2007). *Gempabumi dan tsunami di Sumatra dan upaya untuk mengembangkan lingkungan hidup yang aman dari bencana alam*. Laporan KHL, LIPI, Jakarta.
6. Kurniawan, R. (2017). Pemetaan ground acceleration menggunakan metode probabilistic seismic hazard analysis di propinsi Nusa Tenggara Barat pada zona megathrust. *Proceeding Seminar Nasional Teknologi Informasi dan Kedirgantaraan (SENATIK)*, **3**, 132–137.
7. Irwansyah, E. & Winarko, E. (2015). Zonasi daerah bahaya kegempaan dengan pendekatan peak ground acceleration (PGA). *Seminar Nasional Informatika (SEMNASIF)*, **1**(5).
8. Baker, J. W. (2013). An introduction to probabilistic seismic hazard analysis. *White Paper Version*, **2**(1), 79.
9. Pasau, G. & Tanauma, A. (2011). Pemodelan sumber gempa di wilayah Sulawesi Utara sebagai upaya mitigasi bencana gempa bumi. *Jurnal Ilmiah Sains*, 202–209.
10. Wiemer, S. (2001). A software package to analyze seismicity: ZMAP. *Seismological Research Letters*, **72**(3), 373–382.
11. Aki, K. (1965). Maximum likelihood estimate of b in the formula log N= a-bM and its confidence limits. *Bulletin of the Earthquake Research Institute, Tokyo University*, **43**, 237–239.
12. IRIS Earthquake Browser. (2023). Diakses pada tanggal 17 Maret 2023, http://ds.iris.edu/ieb/.
13. Irsyam, M., Sri, W., Danny, H. N., Irwan, M., Ariska, R. *et al*. (2017). *Peta sumber dan bahaya gempa Indonesia tahun 2017*. Bandung: Kementerian Pekerjaan Umum dan Perumahan Rakyat.

IPC

Indonesian Physics Communication

Department of Physics, Universitas Riau, Pekanbaru, Indonesia
p-ISSN 1412-2960 | e-ISSN 2579-521X

Vol. 21 | No. 2
July 2024

Web: https://kfi.ejournal.unri.ac.id
E-mail: kfi@ejournal.unri.ac.id

Design an Arduino-based rice ATM machine system using RFID and ultrasonic sensors

Andi Dhika Putranta Makullawu
Department of Physics, Universitas Islam Negeri Sumatera Utara, Deli Serdang 20353, Indonesia

Corresponding author: companydsd665@gmail.com

ABSTRACT

A system has been developed for an Arduino-based rice ATM machine that utilises RFID and ultrasonic sensors. The system employs a quantitative research strategy and is designed to automatically distribute rice to the public. This device utilises the Arduino Uno microcontroller as its primary controller. The sensors employed for detection of rice quantity in the rice ATM machine are Ultrasonic Sensors. The activation card reader utilised to dispense rice is an radio frequency identification (RFID) reader. The output components responsible for the operation of the rice ATM machine are a Servo Motor, a 2X16 LCD, and a Buzzer. The study yielded satisfactory results as each component tested and utilised in the rice ATM machines successfully executed the controller programme commanded by Arduino. This programme effectively dispensed rice in the desired quantity, detected unauthorised cards, and accurately determined rice balances. Furthermore, the application of these components proved to be straightforward and uncomplicated. In public, this can be demonstrated through testing conducted on individual components or machines. RFID technology is used to read the frequency from the RFID card, while ultrasonic sensors detect the quantity of rice and generate a code using a buzzer. Additionally, an LCD display provides comprehensive information about the rice ATM's status, which users can easily comprehend. The mechanical system of the servo motor enables the movement of the exit door for rice weighing over 15 kg.

Keywords: Arduino Uno; distribution; radio frequency identification; rice ATM

Received 24-08-2023 | Revised 29-11-2023 | Accepted 21-05-2024 | Published 19-07-2024

INTRODUCTION

The Indonesian government has implemented many social policies to meet the needs of low-income people to meet the main needs of the poor, one of which is the Raskin rice social assistance which is intended for underprivileged or poor people, although many are also unable to meet the main needs of the poor [1]. Irresponsible individuals always take advantage of loopholes by taking advantage of a distribution system that is not always monitored, so that the amount and timing of Raskin rice distribution can be corrupted and no longer useful for the recipients [2].

One of them is the case in Garut where the former village head in Garut misappropriated social assistance funds in the form of Raskin rice for three consecutive years, namely from 2014 to 2016 by not distributing Raskin rice to distribution points [3,4]. Based on the problems above, the author found one way to minimize the opportunity for fraud in the distribution of Raskin rice which could be exploited by irresponsible individuals for personal gain, namely by using Arduino. Based on the problems above, the author wants to conduct research and develop a tool in the form of a rice automated teller machine (ATM) with the title "Design of an Arduino-based rice ATM machine system using RFID and ultrasonic sensors". This final project aims to maximize the distribution system to the community by minimizing the weaknesses of previous research and conducting research on making automatic rice ATMs to maximize the process of distributing Raskin rice social resources to aid recipients, in this case, the community, so that it becomes more useful. This research aims to design an Arduino-based rice ATM system

using RFID and ultrasonic sensors and to determine the performance of an Arduino-based rice ATM using RFID and ultrasonic sensors.

LITERATURE REVIEW

ATM is an electronic machine that allows bank customers to withdraw money and check their savings accounts without needing to be served by a human "teller". Many ATMs also allow depositing money or checking amounts, transferring money, or even buying stamps. Initially, ATM technology was used to assist customers in making cash withdrawals where there were no bank branches [5].

An ATM requires a card as an intermediary between humans and machines. A card has a line called a magnetic chip. The magnetic chip functions as a sensor to detect the owner's identity. The magnetic chip is very sensitive to various situations, for example, if the magnetic chip is rubbed against an object then the magnetic chip has lost its function. because if there is friction on the magnetic chip, the ATM cannot detect the ATM card owned by a customer [6].

In 1939 Simjian patented an early ATM prototype which later proved less successful [7]. Some argue that a Scotsman named James Goodfellow was the earliest patent holder (1966) for a modern ATM and John D White (from Docutel) in the United States is also often referred to as the inventor of the first free-standing ATM design [8]. In 1967, John Shepherd-Barron invented and installed an ATM at Barclays Bank in London [9]. A year later (1968), Don Wetzel invented the American-made ATM [10]. ATMs only became an important part of banking starting in the 1980s [11,12].

Rice is a basic need for Indonesians. According to the big Indonesian dictionary (KBBI), the meaning of the word rice is rice whose skin has been removed (which becomes rice after being cooked) [13]. Another meaning of rice is grain as explained in the Qur'an, Surah Al-An'am, Verse 95. Allah Subhanahu Wa Ta'ala says, which means "Indeed, Allah is the one who grows grain (rice) and seeds (dates). He brings out the living from the dead and brings out the dead from the living. That is Allah's (power), so why do you still turn away?" [14].

Based on the explanation above, it can be concluded that rice is a class of grains (rice grains) that God grows on the face of the earth as a source of life for mankind and as a source of life, the distribution of rice should be something more useful, based on the big language dictionary Indonesia (KBBI) ATM is an automated teller machine for dispensing cash using techniques such as using a card that has a chip [15]. From the 2 explanations above, it can be concluded that a rice ATM is an automated teller machine that is used to withdraw rice grains which are one of the sources of life or an electronic machine that allows ATM cardholders to withdraw their rice without needing to be served by a human and is automatic.

The following is an example of research on rice ATMs that was previously carried out, the first is research entitled "Automatic Raskin collection machine using RFID based on an Arduino microcontroller" [16]. amounting to 1 kg and does not have a monitoring system for the amount of rice filled in the tank, which is contrary to the author's goal of making it easier to distribute rice because it will complicate the distribution process and is ineffective. Next is the final assignment entitled "Implementation of a rice ATM design using Arduino Uno R3 DIP ATMega328P and PLC Siemens S7-300" [17] in this tool the weakness is the use of a program logic controller (PLC) because it has a high sensitivity to environmental conditions, especially hot temperatures because it can damage the tool itself and then What is also a weakness is that the rice ATM must be placed in an open place to reduce pressure when applying it to many rice ATM users, in this case the public, the next weakness is the monitoring system for the amount of rice in the rice storage tank which this tool does not have ATM, then the final project entitled "Rice ATM with RFID activation system" [18] this research aims to

maximize distribution to remote areas such as rural areas. This research has weaknesses in real time relies on signals and is not equipped with media in the form of an LCD as a provider of information. words and numbers to become one-way information between the user and the machine.

RESEARCH METHODS

Research Time

This research is planned for January 1 – January 15, 2023.

Research Place

This research was conducted in the lecture building of the Faculty of Science and Technology, North Sumatra State Islamic University, Medan, Jl. Golf Course No.120, Kp. Tengah, Pancur Batu District, Kab. Deli Serdang, North Sumatra.

Research Tools

The tools used in this research are as follows:

1. Arduino Uno as a clipboard chip to control the work of the design system.
2. The Ultrasonic Sensor functions to detect the amount of rice in the rice atm.
3. Servo motor as a torque that opens and closes the rice exit door.
4. RFID reader as an RFID tag reader to open the rice exit door on the rice ATM machine.
5. RFID tag provides a command code to the RFID reader to open the rice ATM door.
6. The 2X16 LCD functions as a display to display the situation inside the rice storage tube.
7. The relay functions as a controller connecting the system circuit.
8. Electric soldering is used to bond components with tin.
9. PCB functions as a place for designing components.
10. Stepdown functions to reduce voltage.
11. Jumper cables function to connect several components.

Materials Used in Research

The materials used in the research were rice, which served as a test material for the working of rice ATMs

Complete Range of Tools

This chapter will present an explanation of the complete series of tools. The complete series of tools aims to simulate the component design process using a project board using designed software before assembling and placing components on the tool with a mechanical design in its original version.

RESULTS AND DISCUSSION

In this chapter, the results of tool testing will be discussed, and a discussion on how the tool system that was created works and data will be collected on the rice ATM with the title "Design and Build an Arduino-Based Rice ATM System Using RFID and Ultrasonic Sensors" which aims to find out how the whole tool works. and the performance of each component of the tool so that it can produce valid data and the tool can work according to its function and purpose.

Research Result

In the research results, it was found that by testing and calibrating each component and sensor used as well as testing the tool as a whole by looking at the performance of each tool, the output results and discussion will be written into data that can be seen in the form of a test table which has been carried out several times on each component and the machine as a whole, the rice ATM is a system that works as an automatic system for taking rice with the name of the machine "Arduino-based rice ATM machine system design using RFID and ultrasonic sensors", this machine uses hardware

consisting of Arduino as a microcontroller board, RFID as a card detection sensor, Ultrasonic Sensor as a distance sensor that measures the height of the rice, Servo Motor as the torque that moves the rice exit door, LCD plays the role of providing exit signals and uses command application software using the C programming language which can be sent to the Arduino board and stored on the microcontroller. The appearance of the rice ATM can be seen in Figure 1.

Testing of the machine as a whole was carried out five times using three different types of RFID cards with the desired amount of rice of 1 kg and 0.5 kg. The experimental data for the rice ATM can be seen in Table 1.

Figure 1. Rice ATM.

Table 1. Rice ATM experimental data.

Test	Card series	Rice out (kg)	Rice exact (kg)	RFID initialization
1	42 AC 80 2D	0.25	0.5	Accepted
2	52 34 44 2D	0.5	0.5	Accepted
3	B4 59 16 22	0.6	1	Accepted
4	42 D6 17 2D	1.1	1	Accepted
5	42 B1 5D 2D	2.2	2	Accepted

Testing All Component Functions

In this sub-chapter, testing will be carried out on all components and discussions will be held to determine the performance of each sensor and other components to be used as a source for collecting research data with thorough and gradual implementation. Before testing the tool as a whole, a more complex test is needed to determine the number of errors or damage values in the rice ATM by testing each component of the tool first before placing it on the mechanical part. Meanwhile, each data taken will be presented in the form of a table containing information. is quantitative and is explained physically for each percentage error that each component has with the following formula:

$$Error = \frac{V_{Experimental} - V_{Exact}}{V_{Exact}} \times 100\% \quad (1)$$

CONCLUSION

Based on the results of trials that have been carried out on sensor characterization and linearity along with machine performance tests, it was concluded that the Arduino-based rice ATM system design using RFID and ultrasonic sensors was designed by starting with testing the characteristics and linearity of the sensors. When the sensor and output work according to commands and the results are optimal with an error percentage below 10%, coding of the entire circuit is then carried out using the Arduino IDE application. If the electrical, programming, and mechanics are complete, the Rice ATM is ready to be tested. The performance of the Arduino-based Rice ATM Machine using RFID and an Ultrasonic Sensor can work according to program commands and all components run when the RFID TAG is attached, the servo motor moves according to the data read by the RFID reader, the buzzer

sounds when the ultrasonic sensor reads the amount of rice that exceeds the limit normal in the sense that the amount of rice is low and the LCDs information that can be read by Rice ATM users.

REFERENCES

1. Ketmoen, A. (2022). Implementation of the poor rice program in an effort to support and improve community food security (case study in Air Mata Village, Kota Lama District, Kupang City). *Jurnal REP (Riset Ekonomi Pembangunan)*, **7**(2), 271–294.
2. Alcadipani, R. & de Oliveira Medeiros, C. R. (2020). When corporations cause harm: A critical view of corporate social irresponsibility and corporate crimes. *Journal of Business Ethics*, **167**(2), 285–297.
3. Aspiranti, T., Amaliah, I. & Shaharuddin, A. (2023). Poverty Alleviation Pattern: Top Down or Bottom Up Approach? (Indonesia and Malaysia Benchmarking). *KnE Social Sciences*, 354–368.
4. Basuki, A. T. & Nengsih, W. (2024). Analysis of factors affecting poverty in districts and cities in West Java. *ProBisnis: Jurnal Manajemen*, **15**(2), 74–84.
5. Indrayani, C. W., Aritra, S. & Muda, I. (2019). Customer satisfaction as intervening between use automatic teller machine (ATM), internet banking and quality of loyalty (Case in Indonesia). *International Journal of Financial Research*, **10**(6), 54–66.
6. Osakwe Charity, I. & Akunna Racheal, C. (2023). Assessing bank customers perception and ease of using automated teller machines in Awka Metropolis. *International Journal of Trend in Scientific Research and Development*, **7**(1), 332–338.
7. Chandrasekaran, S. & Narayanan, S. M. (2019). Perception of digital payment in professionals. *Emerging Trends in Banking, Insurance and International Trade*, 106–109.
8. Gibbs, E. (2024). Foreign direct investment policy, multinationals, and subsidiary entrepreneurship success and failure in post-war Scotland. *Business History*, **66**(4), 927–949.
9. Gupta, R. (2022). A Study on Growth and Usage of ATM/POS in India: Pre and Post Covid19. *Journal of Positive School Psychology*, 11872–11881.
10. Sri, M. S., Chaithanya, J. K. & Dhruthiee, N. (2022). Design and implementation of smart atm under idle application. *2022 7th International Conference on Communication and Electronics Systems (ICCES)*, 1410–1417.
11. Singh, R. K. H., Radzi, W. N. W. M., Isa, E. V. M. & Saraih, U. N. (2020). An investigation of customer satisfaction towards the service quality of ATM machine. *Journal of Social Science and Humanities*, **3**(5), 35–39.
12. Maixé-Altés, J. C. (2019). The digitalization of banking: A new perspective from the European savings banks industry before the Internet. *Enterprise & Society*, **20**(1), 159–198.
13. Juliana, S. (2024). Analysis of language mistakes in description text works of BIPA Students. *Talenta Conference Series: Local Wisdom, Social, and Arts (LWSA)*, 7(2), 184–189.
14. Zaini, N. S. M. & Mohd, R. A. (2022). The concept of plant-based food in Verse 99 of Surah Al-An'Am: A thematic study of Tafsīr Mafātīhul Ghayb. *Maʿālim al-Qurʾān wa al-Sunnah*, **18**(2), 176–190.
15. Sari, F. K., Fadly, Y. & Ramadhan, P. R. (2022). The effect of changes in the value of conventional interbank transfers and digital banks in technological development. *Britain International of Humanities and Social Sciences (BIoHS) Journal*, **4**(2), 246–257.
16. Billah, M. M., Nugroho, A. B. & Auliq, M. A. (2018). *Mesin otomatis pengambilan raskin menggunakan RFID berbasis*

mikrokontroler arduino. Undergraduate Thesis, Universitas Muhammadiyah Jember.
17. Nasution, T. H. (2019). *Implementasi Rancangan ATM beras menggunakan Arduino uno R3 DIP AT Mega 328P dan PLC Siemens S7-300*. Undergraduate Thesis, Universitas Muhammadiyah Sumatera Utara.
18. Mallawakkang, M. N. (2020). *ATM beras dengan sistem aktifasi RFID*. Doctoral dissertation, Universitas Hasanuddin.

IPC

Indonesian Physics Communication

Department of Physics, Universitas Riau, Pekanbaru, Indonesia
p-ISSN 1412-2960 | e-ISSN 2579-521X

Vol. 21 | No. 2
July 2024

Web: https://kfi.ejournal.unri.ac.id
E-mail: kfi@ejournal.unri.ac.id

Implementation of gas leak detection and security systems in smart homes

Sonya Sasmita Simanjuntak*, Mulkan Iskandar Nasution, Nazaruddin Nasution
Department of Physics, Universitas Islam Negeri Sumatera Utara, Deli Serdang 20353, Indonesia

*Corresponding author: sonya.sasmita@uinsu.ac.id

ABSTRACT

Leakage of liquified petroleum gas (LPG) cylinders or devices is still one of the main causes of fires known for its flammability so that leaks in LPG are at high risk of fire. To overcome this, a tool is made to prevent crime or gas leaks that often occur to homeowners. This research was conducted to find out the security control system for homeowners and overcome if a gas leak occurs. The method used in this tool is the method of designing a tool to detect gas leaks and a security system at home when left by the owner. From the test results of the prototype that has been designed, the error percentage is 1.6% and also in the MQ2 sensor section where the distance conditions and variables used are distance, time and gas source so that if gas is detected, the fan will turn on and an sms message will appear on the smartphone.

Keywords: Buzzer; GSM module; MQ2 sensor; RTC

Received 26-10-2023 | Revised 12-01-2024 | Accepted 29-05-2024 | Published 22-07-2024

INTRODUCTION

The role of liquefied petroleum gas (LPG) at this time is vital for human life both in households and in industry, and LPG gas is very cheap, so it is easier to use. However, LPG gas can hurt human health and even cause significant losses if it is not used carefully, especially if it is not known that there has been a leak from the LPG gas cylinder or storage area. Leakage of LPG cylinders or devices is still one of the main causes of fires. LPG gas that leaks has an odor so normal leaks are easy to detect. However, if the leaking gas seeps into water pipes, electrical installations, or under carpets, it will be difficult for the human sense of smell to detect. Apart from that, AC and room heaters can also cover the smell of LPG gas. LPG gas is known for its flammability nature, so leaks in LPG equipment pose a high fire risk. Due to its sensitive nature, special attention must be paid to this fuel type. So a warning system is needed to deal with gas leaks.

To prevent these leaks, a tool was created that will detect gas leaks, namely by using the MQ-2 sensor, so that fires that arise due to gas leaks can be prevented. This detection tool using MQ -2 is a tool that detects the concentration of flammable gas and also as an output for reading analog voltage [1,2]. Apart from that, people also spend a lot of time outside the house, with busy activities that make homeowners forget several things, such as locking the door of the house or checking the condition of equipment in the house whether it is off or on, even in some cases resulting in crimes occurring at home [3-5]. To overcome this problem, an automatic smart home control device based on Arduino Uno was created.

This tool will help homeowners detect strangers entering the house, whether through doors, windows, or even through holes in the wall that would unexpectedly become an entry point for criminals [6,7]. This system is also equipped with a buzzer as an alarm which will activate when an unknown object enters the house [8,9]. Apart from that, this system can also be controlled via smartphone with SMS notifications to make things easier for users. This is an effort to provide security for the house to avoid unwanted things such as theft, gas leaks, and fires in the home environment [10-12].

The way the smart home SMS system works is that first the Arduino will initialize it, set the input-output, and initialize it to connect to the SIM800L module and read data from the DS3231 RTC module. Arduino reads the gas sensor output in the form of an analog voltage which is then converted into a digital value using the ADC feature. The converted value will be compared with the reference value that has been input into the Arduino program. If the sensor reading value exceeds the reference value, the fan will activate and the Arduino will carry out the process of sending an SMS using the SIM800L module containing the message "gas detected". If the sensor reading is below the reference value, the fan will be inactive and the Arduino will carry out the process of sending an SMS using the SIM800L module containing the message "gas condition is safe". Arduino also reads the magnetic door sensor. If the magnetic door switch sensor is active, the Arduino will activate the buzzer, and if the magnetic door switch sensor is inactive, the Arduino will deactivate the buzzer [13].

LITERATURE REVIEW

A smart home is a house that connects an internet network or communications with electrical equipment that can be controlled, such as controlling lights and also the security of the house. A smart home has its benefits, such as providing better comfort, more guaranteed safety and security [14].

Security is something you need to pay attention to because it can have a very bad impact on the homeowner. High crime rate, especially theft which ends in murder. Of course, this is a very serious concern in society. Moreover, the world has become increasingly sophisticated, such as doing things that can be controlled remotely. A smart home is also a system that combines technology with services specifically used in the home environment which aims to help with daily activities at home, increasing the security, efficiency, and comfort of its occupants automatically according to user controls that have been programmed via a computer or smart home. residence so that it can be controlled anywhere [1, 15, 16].

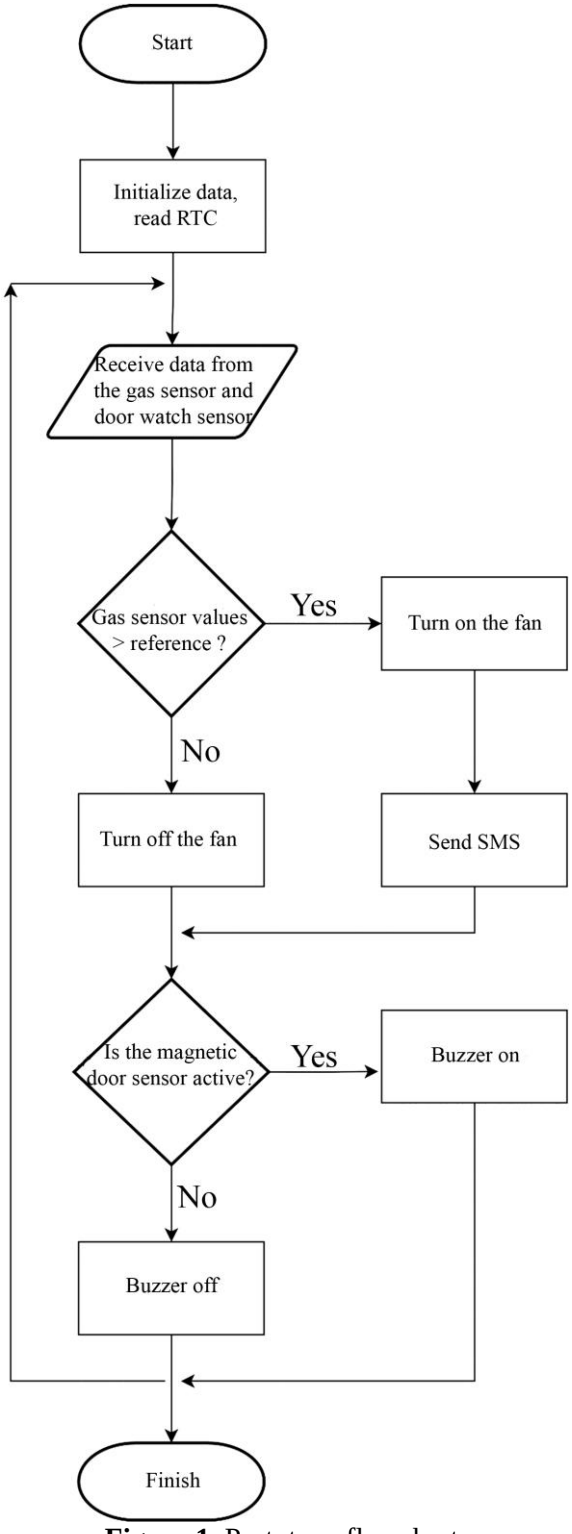

Figure 1. Prototype flowchart.

The parameters that will be controlled in this research are gas leak detection with an MQ2 sensor and a magnetic door sensor as security

for the house. In this system software and hardware such as sensors and other devices will be used to control and automate it.

A flow diagram is a graphic depiction of the steps and sequence of procedures of a program to explain the stages of the research process from start to finish. This flow diagram will make it easier for readers to understand the research methodology used.

RESEARCH METHODS

This research was carried out using quantitative methods. The tools used in this research include laptops, smartphones, SMS, and lighters. The main materials used in this research include Arduino Uno, SIM800L GSM module, MQ2 sensor, buzzer, magnetic sensor, DS3231 RTC module, LM2596 stepdown, adapter, liquid crystal display (LCD).

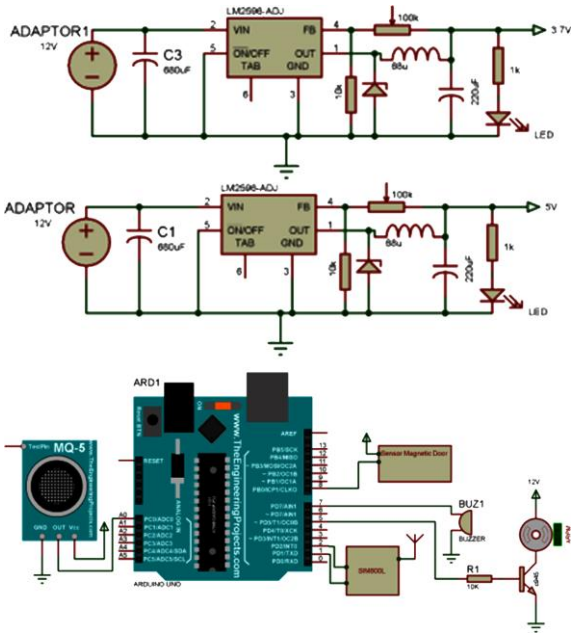

Figure 2. Research series.

The research was carried out by assembling all the materials in an electronic circuit. All components are assembled to produce a circuit that can work according to commands that have been input into the Arduino IDE software.

The method used in this tool is a tool design method for detecting gas leaks and a security system for the house when it is left by the owner. So from these results, if a gas leak occurs in the LPG cylinder and the ADC value is above 700, the fan will automatically turn on and the GSM module will send an SMS to the smartphone with the message "Gas detected" and if the ADC value is below 700 then the fan will turn off and then the GSM module will send a message to the Smartphone with the SMS "Gas is safe". And for the security part of the house, that is by using a magnetic door sensor which is placed on the door, then the real time clock (RTC) module is set according to the clock on the smartphone, if the door is opened then the buzzer will sound, and if the door is opened outside of the RTC setting time then the house in a safe condition. The design of a gas leak detection tool and security system for a smart home with SMS notifications can be seen in Figure 3.

Figure 3. Results of a series of tools.

RESULTS AND DISCUSSION

Testing On Power Supplies

Testing the power supply which functions to reduce the LM2596 Stepdown voltage. Where

in this research 2 LM2596 stepdown's were used, for the first stepdown it was used to reduce the voltage from 12 volts to 5 volts which will later be connected to the Arduino, and for the second stepdown it was used to reduce the voltage from 12 volts to 3 volts which will later be connected to the SIM800L GSM Module. Then 3 adapter tests were carried out using a power supply where the initial voltage and final voltage were % error and the average error was obtained, namely 1.6%. The test results on the power supply system can be seen in Table 1.

Table 1. Power supply test results.

Testing	Initial voltage (V)	Rated voltage (V)	Voltage difference (V)	Errors (%)
1	12	12.3	0.4	2.5
2	12	12.1	0.2	0.8
3	12	12.2	0.1	1.6

Gas Sensor Testing

Gas sensor testing, namely response time, fan condition, status, and also the ADC reference value on the LCD. If the gas is brought close to the MQ2 sensor, the display on the LCD is the ADC value, whereas if the ADC value is above 700 then the fan will be on and the GSMSIM800L module will send a gateway SMS to the smartphone with the status "gas detected", and if the ADC value is below 700 then the fan is not on and the message on the SMS is "Gas is safe".

Table 2. Power supply test results.

Response time (s)	Fan condition	Status	ADC value
10	On	Gas detected	700
30	Off	Safe gas	300
16	On	Gas detected	723
40	Off	Safe gas	280
50	On	Gas detected	740

From the results of the Table 2, the response time starts from the fastest, namely 10 seconds, and the longest response time is 50 seconds.

DS3231 RTC Module Testing

The RTC on this tool functions as a continuous time count. This test serves to compare the time on the RTC with the time on the smartphone. So this RTC is a timer for the magnetic door which is placed on the door and the buzzer is the alarm. When the RTC time is set, for example from 12 pm to 5 am, if the door is opened between 12 pm to 5 am, the magnetic door will respond and the buzzer will sound. If the door opens outside the hours set on the RTC, the door condition is safe. In the table above is the RTC test as the difference between the clock on the smartphone and the clock on the RTC. After testing, the highest difference obtained was 10 seconds, this was due to the difference in the IC chip embedded in the laptop using CMOS, while the DS3231 IC chip was used in the RTC, as well as the transfer speed of the Arduino code.

SIM800L GSM Module Testing

The GSM SIM800L module is an electronic device that can be installed with a SIM card, which can connect to the GSM network and can also connect to all networks with GPRS starting from 2G, 3G, or others. At this testing stage, it is based on the length of time sent via a smartphone that was previously connected to the Arduino, then the Arduino will carry out the SMS-sending process using the GSM module. Where the SMS says "gas detected" with the sim card used in this research being an XL card which then sends an SMS to the Telkomsel network.

The distance between the GSM module is not a problem as long as there is still a GSM network available and it is also ensured that everything is connected correctly and that there is a GSM network. On the GSM module, there is an LED which will later determine whether the GSM module is active or inactive. If the LED lights up three times then the module is active, however, if the LED flashes more quickly three times it means the GSM module is not active. The results in the table above

show that each test has a different time because it depends on the network and the fastest delivery is 10 seconds and the longest is 50 seconds.

Door Magnetic Sensor Testing

Testing on the magnetic door is carried out to see whether the sensor can read the condition of the door being closed or not and this test is also carried out by adjusting the time that is changed on the RTC module. If the magnet coincides with the sensor, the system will judge that the door is closed and has been regulated according to the provisions in the RTC. If it doesn't match, the buzzer will automatically sound.

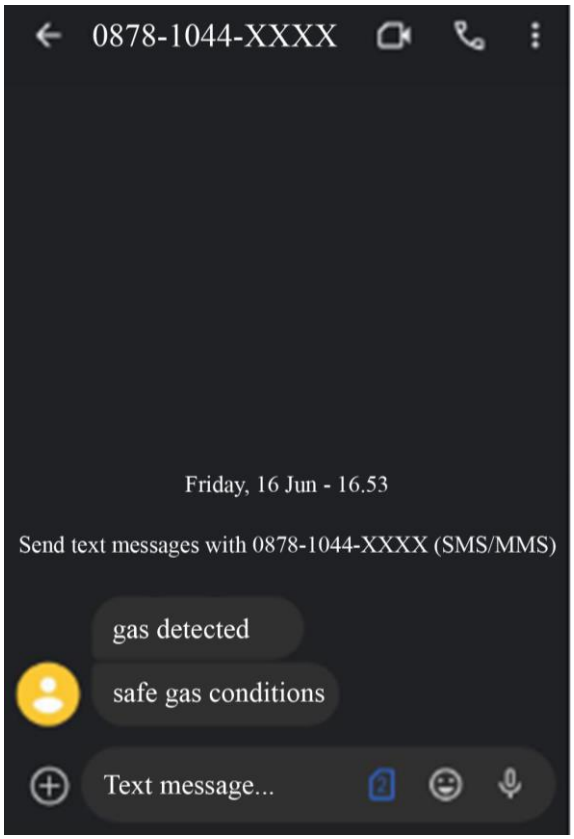

Figure 4. Display of SMS.

This tool is also equipped with an SMS system which is used as a smart home condition monitoring system. SMS (ShortMessage Service) is an application used to send and receive SMS. This SMS can also be sent via telephone in just a few seconds as long as it is within the GSM service range. In this research, SMS is used as a notification if a gas leak occurs. If the value on the sensor reader exceeds the reference value, the fan will activate and the Arduino will carry out the process of sending an SMS using the SIM800L GSM module containing the message "gas detected". If the sensor reader is below the reference value, the fan will be deactivated and the Arduino will carry out the process of sending an SMS using the GSM Module containing "safe gas conditions".

The result of the smart home being designed is a technological concept that must be developed so that it can be implemented in everyday human life. The definition of a smart home here is an electronic network technology that is integrated between electronic devices and household appliances so that they can be monitored and controlled. Examples include gas leak systems and home security. Based on the background above, this research designed an automatic tool that will be linked to a smart home because it can be done with a technological concept. The parameters that will be controlled in this research are gas leak detection with an MQ2 sensor and a magnetic door sensor as security for the house. In this system, software and hardware such as sensors and other devices will be used to control and automate other home activities and also have their benefits such as providing better comfort.

CONCLUSION

Based on the results of the prototype testing that has been carried out, the conclusion is that this prototype test is a home security control system on a smart home prototype that has been designed, using sensors and modules that can run well so that it makes it easier for users to monitor using SMS and has been equipped with a security system. which has been connected to the smartphone. The prototype has been designed using an MQ2 sensor with variable conditions used, namely distance and time of the gas source. So if gas is detected, the fan will turn on and an SMS message will appear on the smartphone.

REFERENCES

1. Andesta, D. & Ferdian, R. (2018). Sistem keamanan sepeda motor berbasis mikrokontroler dan modul GSM. *Journal of Information Technology and Computer Engineering*, **2**(02), 51–63.
2. Sunanda, W., Barkah, H. & Arkan, F. (2022). Notifikasi SMS untuk pendeteksi kebocoran pada kompor gas. *Jurnal Teknik Elektro Indonesia*, **3**(1), 168–184.
3. Al Fani, H., Sumarno, S., Jalaluddin, J., Hartama, D. & Gunawan, I. (2020). Perancangan alat monitoring pendeteksi suara di ruangan bayi RS Vita Insani berbasis Arduino menggunakan buzzer. *Jurnal Media Informatika Budidarma*, **4**(1), 144–149.
4. Fattah, M. I. N., Siregar, S. & Soegiarto, D. (2015). Rancang bangun prototype sistem keamanan untuk smart home monitoring. *eProceedings of Applied Science*, **1**(3).
5. Himawan, F. P., Sunarya, U. & Nurmantris, D. A. (2017). Perancangan alat pendeteksi asap berbasis mikrokontoller, modul GSM, sensor asap, dan sensor suhu. *eProceedings of Applied Science*, **3**(3).
6. Hutagalung, D. D. (2018). Rancang bangun alat pendeteksi kebocoran gas dan api dengan menggunakan sensor MQ2 dan flame detector. *Jurnal Rekayasa Informasi*, **7**(2).
7. Khakim, Lukmanul, Afriliana, I. & Sulasmoro, A. (2023). *Kupas tuntas penggunaan sensor MQ2 dan MQ5 pada alat proteksi kebocoran gas LPG rumah tangga berbasis mikrokontroler*. Tangerang: Penerbit Nem.
8. Kurniawan, H., Triyanto, D. & Nirmala, I. (2019). Rancang bangun sistem pendeteksi dan monitoring banjir menggunakan Arduino dan website. *Coding Jurnal Komputer dan Aplikasi*, **7**(1).
9. Kusumah, H. & Pradana, R. A. (2019). Penerapan trainer interfacing mikrokontroler dan internet of things berbasis ESP32 pada mata kuliah interfacing. *Journal Cerita*, **5**(2), 120–134.
10. Mahmuda, W. & Edidas, E. (2021). Rancang bangun Sistem Rumah Pintar Berbasis Arduino Uno. *Voteteknika*, **9**(3), 44–51.
11. Munawar, Z., Sastradipraja, C. K., Komalasari, R., Putri, N. I., Ma'sum, H., Mandowen, S. A., Mogi, I. K. A., Muliantara, A., Rahmad, I. F., Kmurawak, R. M. & Nurwarsito, H. (2023). *Fundamental internet of things (IoT): memahami teori dan penerapannya*. Kaizen Media Publishing.
12. Nurfaizal, H. (2023). Rancang bangun sistem keamanan rumah terintegrasi telegram menggunakan mikrokontroler ATMega328. *Faktor Exacta*, **16**(1).
13. Santoso, H. (2018). *Monster Arduino 3 implementasi internet of things pada jaringan GPRS*. Jakarta: Elang Sakti.
14. Septryanti, A. & Permana, E. S. (2020). Pengaman pintu rumah berbasis sensor sidik jari dan magnetic sensor. *Journal of Coumputer Engineering, System and Science*, **5**(2), 306–307.
15. Wahyuddin, S. & Maulana, A. (2023). *Pemrograman mobile*. Sumatera Barat: PT Global Eksekutif Teknologi.
16. Zambak, M. F. (2022). Monitoring pemakaian listrik berbasis mikrokontroler. Medan: Universitas Muhammadiyah Sumatera Utara.

IPC

Indonesian Physics Communication

Department of Physics, Universitas Riau, Pekanbaru, Indonesia
p-ISSN 1412-2960 | e-ISSN 2579-521X

Vol. 21 | No. 2
July 2024

Web: https://kfi.ejournal.unri.ac.id
E-mail: kfi@ejournal.unri.ac.id

Application of solar panels in IoT-based bird pest control tools

Fitri Harahap*, Nazaruddin Nasution, Mulkan Iskandar Nasution
Department of Physics, Universitas Islam Negeri Sumatera Utara, Deli Serdang 20353, Indonesia

*Corresponding author: fitri.harahap@uinsu.ac.id

ABSTRACT

The use of solar panels in bird pest control equipment in the rice field zone is based on the internet of things (IoT), which aims to create bird pest control equipment for farmers. This control system is equipped with a PIR sensor whose role is to determine the presence of birds in the rice field zone. The distance range when a bird is found is 5 meters, and an ultrasonic speaker will be active when there is bird movement in the rice field. This speaker uses an ultrasonic wave frequency of 20 kHz. RTC testing is used as a timer to reset the number of invasions in 1 × 24-hour intervals at 00.00 WIB. Next, there is a test of sending (transmitter) and receiving (receiver) LoRa material information near ± 450 meters, information to be sent and placed on the dashboard things board.

Keywords: ESP32; internet of things; RTC DS3231; sensor PIR

Received 25-08-2023 | Revised 20-01-2023 | Accepted 07-06-2024 | Published 23-07-2024

INTRODUCTION

Indonesia is an agricultural country, one of Indonesia's crops is rice which is the staple food of Indonesian citizens. Rice or in Latin Oryza sativa is one of the most cultivated plants in today's civilization. In Indonesia itself, rice is the staple food every day for Indonesian citizens, therefore Indonesia is a country that is synonymous with rice as the main food of its population. In the process of planting rice, there are challenges that farmers will experience, one of which is bird pests. The increasing problem of bird pest attacks can cause serious damage to rice so farmers' rice harvests decrease. Bird pest attacks generally range from when the rice is 25 to 30 days old (the period when rice flowers develop). Various obstacles to rice cultivation give rise to shaky food security [1-3].

Bird pests are one of the main enemies of farmers who can harm plant production. The bird population continues to increase causing crop yields to decrease. On average, bird pests eat 5 – 10 g of rice. Attacks by groups of birds have disturbed farmers planting rice. Bird pest attacks include consuming rice grains during the ripening period of milk or rice with a planting period of 70 days. Due to bird invasions, rice production fell by 30% – 50%. Over the last 10 years, the development of Indonesian rice production has increased, and in 2045 the Ministry of Agriculture of the Republic of Indonesia designated Indonesia as the world's food basket, to ensure the stability of rice production in the years to come, making it necessary to estimate early the problems encountered in rice production. One of them is the difficulty of controlling rice-eating bird pests [4-6].

Solar panels are equipment that can convert solar energy into electrical energy or as it is often called photovoltaic. In PLTS, solar panels are the most important component and use WP units. Solar panels are not only environmentally friendly, but they also have advantages, one of which is saving on electricity bills [7-9]. With today's technological developments and problems, the author got the inspiration to create another alternative, namely producing equipment to control pests. One of them is by using solar panels as a voltage source for bird pest control equipment in the rice field zone based on the internet of things (IoT) using an ESP32 microcontroller based on the IoT. PIR sensors to detect pest movements and ESP32 are used for monitoring. So it can help farmers

to be more efficient in monitoring using IoT in rice fields. IoT is a concept to expand the benefits of continuously connected internet connectivity to monitor pests on rice plants.

LITERATURE REVIEW

Pests are the causes of destruction in plants which can be seen using the five senses, namely the eyes. In the rice field area, there are many pests, one of which is a group of small birds that eat seeds or are often called sparrows. Farmers generally make equipment to control bird pests by using strands of rope provided with objects that make a sound when the rope is pulled. This causes the birds to be startled and fly away from the rice so they can't eat. The sparrow or bond (Latin: genus Lonchura) is a small bird and also a seed eater, this species is widespread in tropical areas including Indonesia. This bird generally inhabits areas of grass, rice fields, grasslands, bushes, and forest edges [10-12].

Solar panels are a device system that converts light and sunlight energy into electrical energy through a photovoltaic impact process also called photovoltaic cells (PV for short). The electrical voltage produced from a solar cell system is very small, around 0.6V without load or 0.45V with load. To obtain a large enough electrical voltage as desired, several solar cells can be arranged in a series circuit. Solar cells are made from semiconductor materials, namely silicon, which functions as an insulator at low temperatures and as a conductor when there is power and heat. In simple terms, the working principle of the solar panel system is that when sunlight hits the solar panel, the valence electrons in the solar cell material will experience movement from N to P, so that at the output stop pole of the solar panel it will create an electric current. The amount of electrical energy depends on the number of solar cells combined in the solar panel and the number of serious rays of solar radiation that hit the solar panel [13-15].

IoT is access to electronic features via the internet. Access to this feature occurs due to human contact with the feature or by using a network to share information, share access, and also think about the security involved in access. This IoT was first reported by Kevin Aston in 1999. The Internet of Things is used in a collection of features that are connected to other features on the internet network. This feature consists of Things whose job is to record information in an area or object. The results of the recording are in the form of information, after which they are forwarded or sent to an application located on the internet. The information obtained is then processed further to show the data stored behind a set of information. IoT can be developed using universal electronic devices such as Arduino for more specific needs and IoT can also be developed as an integrated application with the Android operating system [16-19].

RESEARCH METHODS

The research method used is a qualitative method starting from initialization and initial values which regulate input-output parameters and so on while also setting initial values. Followed by reading the input, in this case, the PIR sensor which reads or detects the movement of objects, namely birds in the rice field area. In this system, the sensor reads in several directions such as north, east, south, and west. If the PIR sensor hits an object, the speaker will automatically sound and the program will calculate and compare the number of attacks according to each direction or concerning certain limits. This research was designed based on the block diagram shown in the following image.

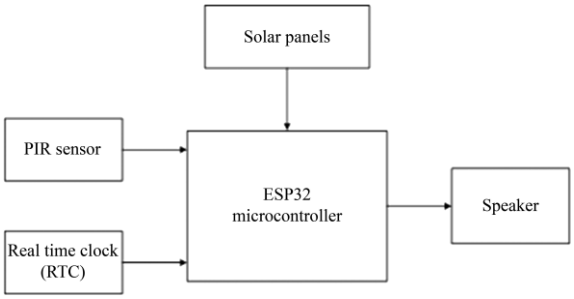

Figure 1. Block diagram.

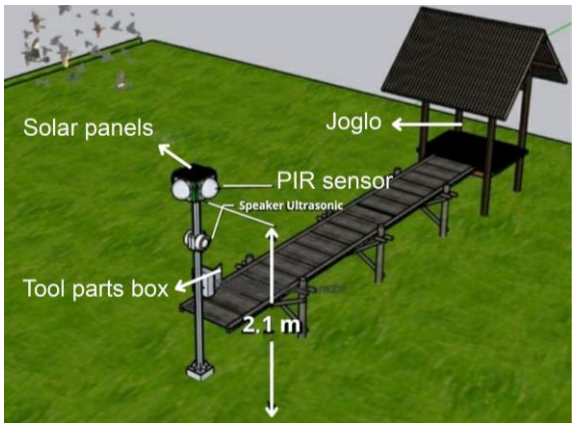

Figure 2. Tool design.

In this design, a telemetry data set is created to reset data on the status of the north, east, south, and west PIR sensors. The counter reset every 24 hours will be zeroed via the website or server using the LoRa module which functions as a radio frequency. Next, the telemetry data set will send data to the gateway and the gateway will receive data from the node which then parses the data. After the telemetry data is converted to another format, the telemetry data will be sent to the thingsboard to be stored and the client PC will access or display the latest data. An illustration of the tool design can be seen in Figure 2.

The overall prototype design of the bird pest control tool consists of a 20wp solar panel, 4 PIR sensors, a speaker, and a box of tool components placed in the rice field area. Next is the prototype design of a bird pest control tool in the sensor section and the sensors used are 4 PIR sensors.

RESULTS AND DISCUSSION

Power Supply Testing (Solar Panels)

Testing solar panels is to ensure that the voltage produced is by the requirements of the equipment system that will be used. The output voltage required by the components in the device is around 5 V. We can see the results of testing the solar panel power supply voltage for each component in Table 1.

Table 1. Power supply testing.

Solar panel voltage (Battery Scc) (V)	Solar panel voltage (Battery multimeter) (V)	Battery output voltage (Stepdown) (V)	Deviation Vin (%)
13.60	13. 38	5.01	1.61
13.90	13. 85	5.01	0.35
13.10	13.00	5.01	0.76
14.00	13.91	5.01	0.64
14.20	14.00	5.01	1.40

PIR Sensor Testing

PIR sensor testing aims to find out whether an object emits infrared rays or not. This PIR sensor is used to identify bird movements in rice fields. An application that uses infrared rays connected to an ESP32 microcontroller to see bird movements can be seen in the following program. PIR sensor test results data can be seen in Table 2.

Table 2. PIR sensor testing table.

Test	Object distance (m)	Condition	Digital value
1	1	Detected	1
2	2	Detected	1
3	3	Detected	1
4	4	Detected	1
5	5	Not detected	0
6	6	Not detected	0
7	7	Not detected	0

DS3231 RTC Testing

The RTC DS3231 test aims to reset the number of bird attacks in rice fields where the attack data will be reset once every 24 hours automatically, namely at 00.00 WIB. Then the data is stored on the thingsboard dashboard. The RTC DS3231 test results data are shown in Table 3.

Table 3. DS3231 RTC test result.

DS3231 RTC	Actual Schedule	D (%)
Sunday, August 13 2023 09:59:55 WIB	Sunday, August 13 2023 10:00:00 WIB	8.33
Sunday, August 13 2023 12:59:55 WIB	Sunday, August 13 2023 13:00:00 WIB	8.33
Sunday, August 13 2023 15:59:55 WIB	Sunday, August 13 2023 16:00:00 WIB	8.33
Monday, August 14 2023 11:59:55 WIB	Monday, August 14 2023 12:00:00 WIB	8.33
Monday, August 14 2023 16:59:55 WIB	Monday, August 14 2023 17:00:00 WIB	8.33

SX1278 LoRa Module (Long Range) and Thingsboard

This research was carried out using LoRa which is supported by many factors, one of which is the advantages of LoRa which are difficult to find on other devices. The main advantage of LoRa is that LoRa is a low-cost device because the LoRa device includes the sensors needed during research, apart from requiring a low cost, LoRa is classified as a device with low power consumption because LoRa only requires around 13 mA-15 mA so a device can be used for a long period.

Apart from that, LoRa devices support research over long distances where LoRa devices can transmit data. In this research, the first 2 types of LoRa are used as transmitters, where the LoRa SX1278 module, PIR sensor, and speaker relay are connected to the ESP32. Meanwhile, the second functions as a receiver, where the RTC and LCD modules are connected to the ESP32 and then forwarded to the thingsboard dashboard. The IoT bird pest control design works by using solar panels as a voltage source, ESP32, PIR sensor, 16x2 LCD, RTC DS3231, ultrasonic speaker relay, and LoRa module.

PIR sensor which aims to identify bird movements in rice fields. The ultrasonic speaker relay aims to turn on or turn off the ultrasonic speaker if bird movements are detected or not detected by birds around the rice fields. This ultrasonic speaker uses ultrasonic wave frequencies. RTC is used to reset the number of bird attacks in the rice fields and the attack data will be reset every 1 × 24 hours at 00.00 WIB. The LoRa module has a working procedure when a tool in the rice field (transmitter) detects bird movements, the ultrasonic speaker will activate, then the detection data will be sent to a tool at home (receiver) which will then forward the data to the thingsboard dashboard so that the rice field owner can monitoring the number of attacks and movement/detection of birds in the rice fields. The maximum distance that the tool can send and receive is ± 450 m. Overall, IoT-based bird pest control tools in rice fields function well.

CONCLUSION

In this research, it can be concluded that the use of solar panels as a voltage source for controlling bird pests in rice fields is based on IoT which uses ESP32, PIR sensors, RTC,

ultrasonic speakers and LoRa modules. The way the system uses solar panels as a voltage source for controlling bird pests in rice fields based on the IoT is based on microcontroller commands through sensor detection and schedules. The PIR sensor aims to detect birds in rice fields with a range of ≤ 5m. Then the ultrasonic speaker will be active if there is bird movement in the rice field area. This speaker uses ultrasonic wave frequencies.

REFERENCES

1. Angriawan, B., Jatmiko, S. T. M. T. & Umar, S. T. (2015). *Pembasmi hama menggunakan gelombang ultrasonic dengan memanfaatkan panel surya (Solar cell)*. Doctoral dissertation, Universitas Muhammadiyah Surakarta.
2. Aroeboesman, F. N., Ichsan, M. H. H. & Primananda, R. (2019). Analisis kinerja LoRa SX1278 menggunakan topologi star berdasarkan jarak dan besar data pada WSN. *Jurnal Pengembangan Teknologi Informasi dan Ilmu Komputer*, **3**(4), 3860–3865.
3. Moh Noor Al Azam, S. K. M. M. T. (2022). *Cara Cepat Belajar IoT: ESP32: Pengenalan Dan Instalasi Arduino IDE*. Radnet Digital Indonesia.
4. Hardiansyah, M. Y. (2020). Pengusir hama burung pemakan padi otomatis dalam menunjang stabilitas pangan nasional. *Jurnal ABDI (Sosial, Budaya dan Sains)*, **2**(1).
5. Hidayat, K., Hasani, M. C., Mardiyah, N. A. & Effendy, M. (2021). Strategi pengisian baterai pada sistem panel surya standalone berbasis kontrol PI multi-loop. *Jurnal Teknik Elektro*, **13**(1), 25–33.
6. Jakaria, D. A. & Fauzi, M. R. (2020). *Aplikasi smartphone dengan perintah suara untuk mengendalikan saklar listrik menggunakan Arduino*. *Jurnal Teknik Informatika (JUTEKIN)*, **8**(1).
7. Meliala, S., Putri, R., Saifuddin, S. & Sadli, M. (2020). Perancangan penggunan panel surya kapasitas 200 WP on grid system pada rumah tangga di pedesaan. *JET (Journal of Electrical Technology)*, **5**(3), 100–111.
8. Mehta, M. (2015). ESP8266: A Breakthrough in wireless sensor networks and internet of things. *International Journal of Electronics and Communication Engineering & Technology*, **6**(8), 7–11.
9. Modjo, A. S. (2012). *Rancang bangun alat pengendali hama burung pemakan bulir padi sawah (Oryza Sativa L.) sistem mekanik elektrik*. Teknologi Hasil Pertanian Universitas Negeri Gorontalo.
10. Muliadi, M., Imran, A., & Rasul, M. (2020). Pengembangan tempat sampah pintar menggunakan ESP32. *Jurnal Media Elektrik*, **17**(2), 73–79.
11. Nugroho, A. A. (2018). *Prototipe Sistem Pengusir Hama Burung Berbasis Computer Vision*. Universitas Sanata Dharma Yogyakarta.
12. Robby, A. N. & Firmansyah, A. (2022, December). Prototype Lampu otomatis Pencegah Hama Berbasis Panel Surya. *Prosiding Seminar Nasional Hi-Tech (Humanity, Health, Technology)*, **1**(1).
13. Roslinawati, E., Prihatini, W. & Haryoko, T. (2019). Variasi ciri morfometrik burung Bondol di Indonesia. *Zoo Indonesia*, **26**(2).
14. Nurtado, A. (2020). Simulasi bel sekolah otomatis berbasis Arduino Uno. *Jurnal Manajemen dan Teknik Informatika (JUMANTAKA)*, **3**(1).
15. Sumadikarta, I., No, J. A. P. I. & Lama, K. (2020). Perancangan smarthome berbasis Arduino Nodemcu Esp8266 (Studi kasus: Griya Setu Permai). *Jurnal Ilmiah Fakultas Teknik LIMIT'S*, **16**(1).
16. Suhaeb, S. (2017). *Mikrokontroler dan interface*. Makassar: UNM.
17. Sulaiman, A. A. (2018). *Sukses swasembada Indonesia menuju lumbung*

pangan dunia 2045. Jakarta: IAARD Press.
18. Toyib, R., Bustami, I., Abdullah, D. & Onsardi, O. (2019). Penggunaan sensor passive infrared receiver (PIR) untuk mendeteksi gerak berbasis short message service gateway. *Pseudocode*, **6**(2), 114–124.
19. Wilianto, W. & Kurniawan, A. (2018). Sejarah, cara kerja dan manfaat internet of things. *Matrix: Jurnal Manajemen Teknologi Dan Informatika*, **8**(2), 36–41.

IPC

Indonesian Physics Communication

Department of Physics, Universitas Riau, Pekanbaru, Indonesia
p-ISSN 1412-2960 | e-ISSN 2579-521X

Vol. 21 | No. 2
July 2024

Web: https://kfi.ejournal.unri.ac.id
E-mail: kfi@ejournal.unri.ac.id

Reducing free fatty acid and peroxide levels in refining used cooking oil made from activated carbon from Barangan banana peels

Dian Frasisca*, Ety Jumiati, Masthura Masthura
Department of Physics, Universitas Islam Negeri Sumatera Utara, Deli Serdang 20353, Indonesia

*Corresponding author: dianfrasisca@gmail.com

ABSTRACT

Everyday life requires a food processing component known as cooking oil. Repeated use of cooking oil can reduce its quality and cause it to have high levels of free fatty acids and peroxides. The purpose of this study was to find out how to purify cooking oil using activated carbon made from Barangan banana peels to reduce the amount of free fatty acids and peroxide value. The activated carbon samples used in this study were sample A (5.5 g), sample B (10.5 g), and sample C (15.5 g). Sample C with 15.5 g of activated carbon had a free fatty acid test result of 0.16% and a peroxide number of 3.91 mek O_2/kg which was the best result in this study, and was in accordance with SNI 01-7709-2019.

Keywords: Activated carbon, Barangan banana peel, used cooking oil

Received 26-08-2023 | Revised 27-01-2023 | Accepted 16-06-2024 | Published 23-07-2024

INTRODUCTION

Cooking oil is a crucial need in society. Cooking oil is usually used as a frying medium, but is also often used as a raw ingredient in commercial kitchens. Usually cooking oil after frying, which is called used cooking oil. Used cooking oil is produced when more frying is done, and usually causes the oil to smoke, darken, and have an unpleasant taste. Repeated use of cooking oil poses health risks. Cooking oil will be damaged if cooked repeatedly at high temperatures (150ºC to 200ºC), so it can harm the body and trigger various diseases such as fat buildup in blood vessels, cancer, and other conditions [1]. The nutritional value and quality of fried foods will be affected by oil damage. Some cooking oils will oxidize when heated at very high temperatures. Food that has been contaminated by oxidation will taste less delicious, have an unattractive color, and cause damage to some vitamins and degradation of fatty acids [2].

Cooking oil refining is a strategy used to reduce the amount of used oil used. In the purification process, activated carbon is used as an adsorbent. Amorphous carbon compounds, such as activated carbon, can be made from carbon-containing materials that have undergone certain expansions to increase their surface area. Activated carbon has a surface area of 300 – 3,500 m^2/g and functions as an adsorbent [3]. Materials that contain carbon elements, one of which comes from waste such as banana peels, can be used to make active carbon [4].

Banana peel has a carbonization value of 96.56% and is a substance that contains the element carbon [5]. Bananas are a fruit that is relatively popular among people [6]. Banana plants are considered flexible plants. All parts such as roots, stems, leaves, and tubers have benefits [7].

Bananas are quite productive, but the amount of banana peels that are wasted is also increasing. These banana skins are simply thrown away after post-harvest of the bananas without further processing. Therefore, it causes a lot of banana peel waste to be thrown away, so there is a need for improvement efforts to increase the usability of banana peels [8]. The cellulose and lignin content of banana peels ranges from 7.6% – 9.6% and 6% – 12% respectively. Banana peels absorb better and do

not interfere with the adsorption process if the lignin content is less than 15%. Banana peel waste is expected to act as an adsorbent [9].

RESEARCH METHODS

Experimental methodology is being used in this research. The research instruments were a knife and cutting board, mortar, size 42 Whatman filter paper, funnel, beaker glass, Erlenmeyer, thermometer, 80 mesh sieve, magnetic hotplate stirrer, digital balance, oven, and furnace. Remains of banana peels from household waste, used cooking oil from fried food sellers and distilled water are the materials used in this research.

The procedures carried out in this research were making activated carbon from Barangan banana peels, testing used cooking oil before purifying it, and purifying and testing used cooking oil using activated carbon made from Barangan banana peels.

Making Activated Carbon from Barangan Banana Peels

Banana skin is cleaned and then cut into small pieces. After that, it was dried using an oven at a temperature of 180ºC for 3 hours and 20 minutes, then the Barangan banana peel was carbonized using a temperature of 400ºC with a holding time of 1.5 hours, after that, it was activated using a temperature of 600ºC with a holding time of 45 minutes, then carbonized. actively washed using distilled water and ground using a mortar then sieved using an 80 mesh sieve.

Testing Used Cooking Oil before the Refining Process

Prepare a sample of used cooking oil, then test it using the peroxide value and free fatty acid test parameters. Next, the test results are compared with SNI 01-7709-2019.

Purify and Test Used Cooking Oil Using Activated Carbon Made from Barangan Banana Peel

Put used cooking oil into 3 beakers, 50 g each. Then add 5.5 g, 10.5 g, and 15.5 g of activated carbon to each beaker glass. After that, stir each beaker glass using a magnetic hotplate stirrer at a temperature of 100ºC – 110ºC for 80 minutes. After stirring, it is cooled and then filtered using Whatman filter paper number 42. Then the results of each filter are placed in a sample bottle and tested. After that, the test results are compared with SNI 01-7709-2019.

RESULTS AND DISCUSSION

The results and discussion in this research are testing the levels of free fatty acids and peroxides before and after purification using activated carbon from Barangan banana peels.

Free Fatty Acids in Used Cooking Oil before and after Refining

The test results of used cooking oil before and after refining can be seen in Table 1.

Table 1. Free fatty acids before and after refining used cooking oil.

Sample	Free fatty acid test results		SNI 01-7709-2019 (%)
	Before purification (%)	After purification (%)	
A	1,46	0,41	0,3
B	1,46	0,23	
C	1,46	0,16	

From Table 1 above, the value of free fatty acids in used cooking oil before refining is 1.46%. The free fatty acid values after purification using activated carbon for samples A, B, and C were respectively 0.41%, 0.23%, and 0.16%.

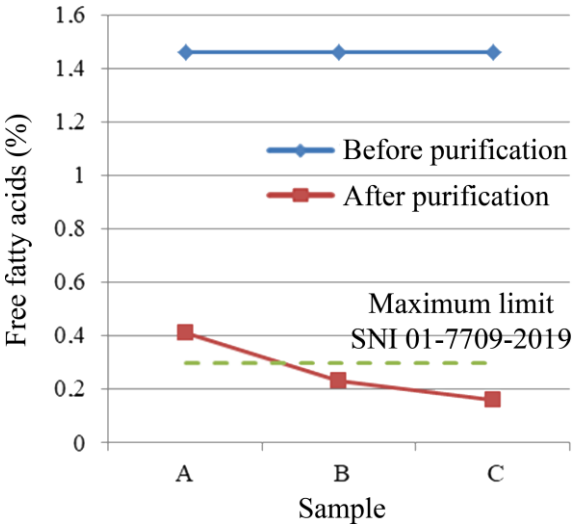

Figure 1. Graph of free fatty acids from used cooking oil before and after refining

Based on Table 1 above, free fatty acids in used oil before and after refining can be seen in Figure 1. Based on the graph, the greater the variety of activated carbon used, the better the purification results will be. This is also by the research of Oko *et al.* (2020) [10].

The decrease in free fatty acid values in sample A was 71%, sample B was 84% and sample C was 89%. This decrease is due to the presence of silanol groups (Si-OH) in carbon that has been activated with acid. The silanol group will be linked to the carbonyl oxygen group (C=O) on the free fatty acid so that the free fatty acid molecule can be adsorbed on the surface of the activated carbon [11].

Peroxide Number in Used Cooking Oil before and after Refining

The peroxide number is a quality standard for cooking oil that must be met. The test results of used cooking oil before and after refining can be seen in Table 2.

Table 2. Peroxide numbers before and after refining used cooking oil.

Sample	Peroxide value test results		SNI 01-7709-2019 (**mek O_2/kg**)
	Before purification (%)	After purification (%)	
A	4.82	4.79	
B	4.82	4.73	10
C	4.82	3.91	

From Table 2 above, the peroxide value in used cooking oil before refining produces a result of 4.82%. When purifying using activated carbon, sample A obtained a yield of 4.79%. When purifying using activated carbon, sample B obtained a yield of 4.73%. When purifying using activated carbon, sample C obtained a yield of 3.91%. For more clarity, you can see in Figure 2.

From the research that has been carried out, the more variations of activated carbon used, the better the purification will be and will result in a reduction of 0.6% for sample A, 1% for sample B, and 18% for sample C. The decrease in content is because activated carbon has the following adsorbent properties [3]. This is also by research by Oko *et al.* (2020) which states that the more variations of carbon used, the better the purification results will be [10].

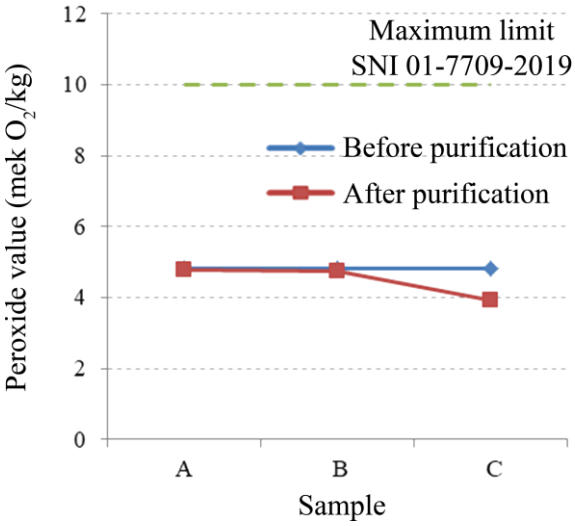

Figure 2. Graph of the peroxide value of used cooking oil before and after refining.

CONCLUSION

Based on this research, it can be concluded that the results obtained from testing used

cooking oil before refining using activated carbon from Barangan banana peels obtained a free fatty acid value of 1.46%, and a peroxide value of 4.82 mek O_2/kg. Purification of used cooking oil using a variation of sample A activated carbon produced 0.41% free fatty acids which did not meet SNI 01-7709-2019 and the peroxide value decreased to 4.79 mek O_2/kg which still met SNI 01-7709-2019. The activated carbon variation of sample B produces free fatty acids, namely 0.23% and a peroxide value of 4.73% which meets SNI 01-7709-2019. The activated carbon sample C produces 0.16% free fatty acids and a peroxide value of 3.91 mek O_2/kg which meets SNI 01-7709-2019.

REFERENCES

1. Ariani, D., Yanti, S. & Saputri, D. S. (2017). Studi kualitatif dan kuantitatif minyak goreng yang digunakan oleh penjual gorengan di kota Sumbawa. *Jurnal Tambora*, **2**(3).
2. Noriko, N., Elfidasari, D., Perdana, A. T., Wulandari, N. & Wijayanti, W. (2012). Analisis penggunaan dan syarat mutu minyak goreng pada penjaja makanan di food court UAI. Jurnal Al-Azhar Indonesia Seri Sains dan Teknologi, **1**(3), 147–154.
3. Dewi, R., Azhari, A. & Nofriadi, I. (2021). Aktivasi karbon dari kulit pinang dengan menggunakan aktivator kimia KOH. *Jurnal Teknologi Kimia Unimal*, **9**(2), 12–22.
4. Lubis, R. A. F., Nasution, H. I. & Zubir, M. (2020). Production of activated carbon from natural sources for water purification. *Indonesian Journal of Chemical Science and Technology*, **3**(2), 67–73.
5. Abdi, C., Khair, R. M. & Saputra, M. W. (2015). Pemanfaatan limbah kulit pisang kepok (Musa acuminate L.) sebagai karbon aktif untuk pengolahan air sumur kota Banjarbaru: Fe Dan Mn. *Jukung (Jurnal Teknik Lingkungan)*, **1**(1).
6. Rai, I. N., Sudana, I. M., Astawa, I. N. G., Dwiyani, R. & Fitriani, Y. (2019). Direct organogenesis in vitro propagation of local balinese banana with thidiazuron. *International Journal of Life Sciences*, **3**(3), 32–40.
7. Hartono, A. (2013). Pelatihan Pemanfaatan Limbah Kulit Pisang Sebagai bahan dasar pembuatan kerupuk. *AJIE (Asian Journal of Innovation and Entrepreneurship)*, **2**(3), 198–203.
8. Nasir, N. S. W., Nurhaeni, N. & Musafira, M. (2014). Pemanfaatan arang aktif kulit pisang kepok (*Musa normalis*) sebagai adsorben untuk menurunkan angka peroksida dan asam lemak bebas minyak goreng bekas. *Natural Science: Journal of Science and Technology*, **3**(1).
9. Widayana, S., Kurniawati, I. & Susilowati, S. (2022). Pemanfaatan Limbah Kulit Pisang Kepok Sebagai Bioadsorben pada Penurunan Warna Minyak Bekas Penggorengan. *Jurnal Pendidikan Tambusai*, **6**(2), 10191–10202.
10. Oko, S., Mustafa, M., Kurniawan, A. & Muslimin, N. A. (2020). Pemurnian minyak jelantah dengan metode adsorbsi menggunakan arang aktif dari serbuk gergaji kayu ulin (Eusideroxylon zwageri). *Jurnal Riset Teknologi Industri*, **14**(2), 124.
11. Sari, R. M. & Kembaren, A. (2019). Pemanfaatan karbon aktif ampas dalam mereduksi asam lemak bebas (free fatty acid) pada minyak goreng bekas sebagai biodiesel. *Talenta Conference Series: Science and Technology (ST)*, **2**(1), 124–128.

IPC

Indonesian Physics Communication

Department of Physics, Universitas Riau, Pekanbaru, Indonesia
p-ISSN 1412-2960 | e-ISSN 2579-521X

Vol. 21 | No. 2
July 2024

Web: https://kfi.ejournal.unri.ac.id
E-mail: kfi@ejournal.unri.ac.id

Design of a coffee bean dryer prototype based on the internet of things

Ardian Afandi*, Masthura Masthura, Nazaruddin Nasution
Department of Physics, Universitas Islam Negeri Sumatera Utara, Deli Serdang 20353, Indonesia

*Corresponding author: ardianafandi234@gmail.com

ABSTRACT

Coffee is one of the plants that is widely cultivated in tropical countries such as Indonesia. Coffee plantation commodities at least contribute a lot to the Indonesian economy, which creates foreign exchange, farmer income, industrial raw materials, employment, and regional development. This research aims to design coffee bean dryer equipment using a heater as a heating element instead of sunlight for the process of drying coffee beans. When the temperature has reached 60°C, the heater will turn off briefly, and if the set time has not expired, the heater will always be alive. If the humidity does not decrease, the fan will fail. In this research, using experimental research procedures where each measurement is used effectively by each sensor so that the measurement results of each sensor are accurate. From the test results, it can be concluded that the initial weight before drying was 1000 grams, while the weight after drying was 880 grams.

Keywords: Coffee; DHT22 sensor; IoT

Received 02-11-2023 | Revised 10-02-2023 | Accepted 21-06-2024 | Published 24-07-2024

INTRODUCTION

Coffee is one of the plants that is widely cultivated in tropical countries such as Indonesia, a coffee plantation commodity that contributes greatly to the Indonesian economy, which creates foreign exchange, income for farmers, industrial raw materials, employment opportunities, and regional development [1-4]. To enjoy a cup of coffee, the coffee beans must be dried. This is generally done traditionally, by drying directly in the sun [5-7]. However, the weakness in terms of drying is that it is very dependent on the weather and requires quite a large space. Coffee beans also have to be raised when it is cloudy and when it rains. Because drying is postponed or cannot be done during the rainy season, production will automatically decrease. As a result, coffee beans require a lot of space and a long time for drying [8-12].

With the rapid growth of technology, activities continue to become easier to try. The internet of things (IoT) is an action carried out by using the internet or network as a tool to connect [13]. One of the benefits of the IoT is an application or website that can collect information such as temperature, humidity, drying time, and the condition of coffee beans to enable monitoring [3,14].

The concept of the IoT describes how objects are connected to the internet and can share information through connectivity. IoT refers to items that can be identified separately as virtual images in an internet-based structure, such as the ability to exchange information and remote control [15-17].

This research aims to create a prototype of an automatic coffee bean drying system that uses a DHT22 sensor to determine temperature and humidity, and a heater to heat the coffee beans during the drying process. It is hoped that this prototype will help coffee farmers in the process of determining. For this reason, the author chose the title prototype of IoT-based automatic coffee bean drying equipment that has temperature and humidity control. Drying coffee must be done at a temperature of between 50°C and 60°C because at this temperature the movement of water particles and evaporation take place well. Very high drying temperatures can cause damage to the surface of the beans (case hardening), make it difficult to move water particles in the beans,

and cause the dried coffee beans to be less good. The relative humidity (RH) of coffee that is good for drying coffee is 39% – 56% [5].

LITERATURE REVIEW

Siti Nutyanti Afriani's study in 2019 was entitled Web Server Based Automatic Coffee Bean Drying System Prototype. According to research results, this system has the ability to open and close the roof according to weather conditions. In addition, if the drying chamber temperature changes and the air humidity or water vapor content is low in the drying chamber, this system will operate the lamp as an artificial dryer. By using a web server to control and monitor the system remotely, this system makes it easier for humans to dry the coffee beans [2].

This study was conducted by Asyiva Nurbaeti (2021) with the title development of IoT-based coffee bean drying equipment. The initial weight before curing was 250 grams and the weight after curing was 247 grams. This is caused by a decrease in water content in coffee beans. An average temperature of 49,750ºC and an average humidity of 46.8% can be measured by the DHT22 sensor. The process of drying data from the device to Google Firebase takes an average of 0.01 seconds or 10 milliseconds, which is a very good delay [11].

RESEARCH METHODS

The method used in this research is an experimental method where the coffee bean dryer uses a heater with IoT based temperature and humidity control, where this coffee bean dryer is capable of drying 1 kg of coffee beans at a temperature of 60ºC for 4 hours, and the dryness of the coffee beans is by SNI No. 01-2907-2008. There is an influence of temperature and holding time in the dryer on the moisture content of the coffee beans produced. The higher the temperature and holding time, the lower the water content of the coffee beans. This research requires several pieces of equipment, namely a multimeter, soldering iron, scissors, tin, screws, pliers, duct tape, and a screwdriver. On the other hand, the components used are DHT22, DC motor, 12 Volt 5A power supply, relay, dimer, heater, buzzer, RTC DS3231.

System Block Diagram Design

The preparation of this concept is logical thinking in achieving effective output aimed at producing sensor measurement data and a coffee heating system that is expected to run according to SNI. The design of the equipment block diagram in this research is shown in the following block diagram.

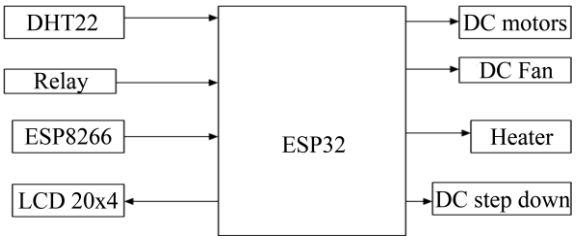

Figure 1. Design of the system block diagram.

In this research, a block diagram was designed using an ESP32 microcontroller which was used to connect the designed prototype. The ESP32 microcontroller was used as the microcontroller for the designed tool. In this research, 1 unit of ESP32 microcontroller was used. used as a dryer tube swivel. DHT22 is used as a temperature and humidity sensor, and LCD 20x4 is used to monitor sensor measurement results on the prototype. The 12 Volt 5A power supply is used as a voltage supplier or provides DC. The relay connects the heating element source to the electrical power source and is part of the ESP32 output. Dimers are used as speed regulators in DC motors. Tool terminal blocks act as connectors and isolate the electric current in the tool circuit. The heater is used as a heater. Bazzer as a sound indicator. RTC DS3231 as a timer.

Software System Design

In this research, a software system was designed using a flowchart as a diagram to

determine the working system of the prototype. The flowchart can be seen in the image below (Figure 2).

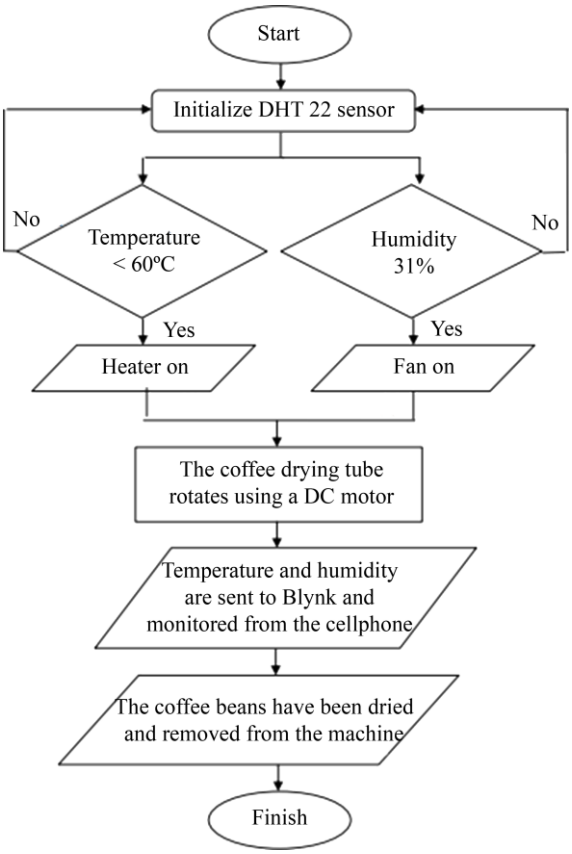

Figure 2. Design of a flow chart.

Test Design and Equipment Characteristics

The test design and equipment characteristics are made based on a prototype system which is used to determine the level of sensor accuracy and performance which aims to ensure that when the ON button is turned on, all components used in the compound box and coffee bean drying tube will be active, starting from the LCD screen which shows the temperature in the tube is measured by the DHT22 and the time is set by the RTC, then the heater that is on will produce heat in the coffee bean dryer tube. When the temperature in the tube has reached the desired high point, the heater will turn off and will come back on again when it has decreased. Then the buzzer will be active when the coffee bean dryer has been used at the time that has been set.

RESULTS AND DISCUSSION

DHT22 Sensor Testing

The DHT222 temperature sensor functions to detect the temperature in the coffee bean drying tube chamber. The DHT22 temperature sensor readings will be processed by the ESP32 and the output from the DHT22 sensor will control the heater via relay. This temperature sensor test is carried out to find out whether the sensor can work properly and correctly according to the plan that has been made.

To see the accuracy of the temperature reading, the DHT22 sensor temperature reading value is compared with the digital thermometer reading value in the same period. The temperature sensor comparison device is carried out using a digital thermometer. Test results of the DHT22 temperature sensor value by automatically measuring the thermometer visually.

Figure 3. Comparative testing of DHT22 and digital temperature.

Based on the data from the temperature measurement comparison results in Table 1, the initial temperature value (room temperature) was obtained at 36°C, with a time value of 10 minutes and humidity 58%, a time value of 20 minutes, namely a temperature of 41°C with a humidity of 45%, the time value 30 minutes is a temperature of 44°C with 39% humidity, a time value of 40 minutes is a temperature of 46°C with a humidity of 36%, a time value of 50 minutes is a temperature of 47°C with a humidity of 34%, a time value of 60 minutes is a temperature of 48°C with humidity 33%. a time value of 70 minutes is a temperature of

48°C with a humidity of 32%, a time value of 80 minutes is a temperature of 48°C with a humidity of 31%, a time value of 90 minutes is a temperature of 49°C with a humidity of 31%, a time value of 100 minutes is a temperature of 49°C with 31% humidity, a time value of 110 minutes, namely a temperature of 49°C with a humidity of 31%, a time value of 120 minutes, namely a temperature of 49°C with a humidity of 31%, so the average error value from the temperature measurement comparison data is 1.6%.

Table 1. Test results for DHT22 and digital temperature.

Time (minutes)	Digital temperature (ºC)	DHT22 (ºC)	Humidity (%)
10	37	36	58
20	44	41	45
30	46	44	39
40	47	46	36
50	48	47	34
60	49	48	33
70	49	48	32
80	49	48	31
90	48	49	31
100	48	49	31
110	49	49	31
120	49	49	31
Average	46.91	46.1	36

Relay Testing

In relay testing, the ESP32 functions to process the heater and fan data so that the relay can control the heater as a heat source. Based on the picture above, this test was carried out using ESP32 as a data processor that gives commands to the relay. The output on the relay will be connected directly to the heater and fan. relay test results with the DHT22 temperature sensor. When the temperature reaches a maximum temperature of 60°C, the heater will stop being active automatically and if the temperature is below 60°C, the heater will become active again. Testing the relay that is connected directly to the DHT22 temperature sensor can work well.

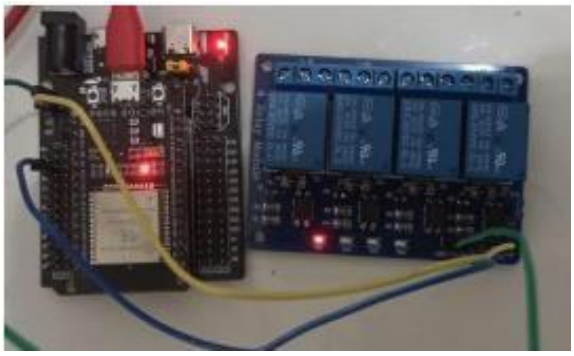

Figure 4. Relay testing.

Heater Testing

In this heater test, the PLN electricity flow that flows to the power supply and then to the heater will produce heat which will spread in the dryer tube and when the reference temperature that has been set has exceeded the reference temperature limit, the heater will turn off and the heater will turn on when the temperature is below 60°C. Here is the DC voltage. If the relay is active, the heater will be active given a voltage of 220 V. And if the voltage is 0 V, the heater will not be active. The heater will turn on when the temperature and time buttons have been set, such as setting a temperature of 60°C and a time of 4 hours, then the heater will turn on and the heat coming out of the heater will spread in the tube which will dry the coffee beans in the tube. The heater will turn off briefly when the temperature exceeds the maximum limit of 60°C from the set temperature and will turn back on when the temperature is below 60°C, and the heater will turn off automatically when the time set on the RTC has finished.

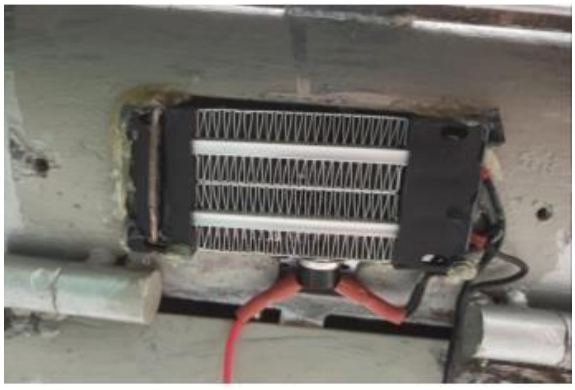

Figure 5. Heater testing.

Blynk Testing

Blynk is a platform for Android applications that aims to control ESP32 modules and similar modules via the internet. This application is used to control hardware devices and display sensor data. The way the Blynk application works is that first install the application, then open the Blynk application on Android, then create the sensors that you want to display and test, they will appear as in the image below.

Figure 6. Blynk application testing.

The results of the coffee bean dryer using 1 kg of coffee beans or the equivalent of 1000 grams require a drying time of 4 hours at a temperature of 60°C with a coffee bean weight of 880 grams. This test requires knowing what percentage of water content is contained in the coffee beans called wet base water content and before drying called dry base water content using a formula.

Where Bk (final weight) while Ba (water weight), Bk is the final weight after drying which was tested using 1000 grams of coffee beans, Bk was obtained at 880 grams while Ba (water weight) was obtained by reducing the initial weight of the coffee beans before drying with Final weight of coffee beans after drying. Ba = 1000 – 880 = 120 grams. So to find out the percentage of dry water content, here is the calculation:

Content (%) = (In. w – Fin. w) / In. w x 100%
= ((1000 – 880) / 1000) x 100%
= 12%

So it can be concluded that the water content in coffee beans after drying the water content in coffee beans is 12%.

Table 2. Condition of coffee beans in the drying tube.

Time (hours)	Temperature (°C)	Weight (grams)	Coffe Condition
0	28	1000	Wet
1	60	925	Humid
2	60	918	Half dry
3	60	898	Half dry
4	60	880	Dry

CONCLUSION

Based on the results of the research that has been carried out, it can be concluded that the coffee bean dryer uses a heater with IoT based temperature and humidity control, where this coffee bean dryer is capable of drying 1 kg of coffee beans at a temperature of 60°C for 4 hours, and the dryness of the coffee beans is by SNI No. 01-2907-2008. There is an influence of temperature and holding time in the dryer on the water content of the coffee beans produced. The higher the temperature and holding time, the lower the water content of the coffee beans. When the ON button is turned on, all components used in the compound box and coffee bean drying tube will be active, starting from the LCD screen which displays the

temperature in the tube as measured by the DHT22 and the time set by the RTC, then the heater which is on will produce heat in the tube coffee bean dryer. When the temperature in the tube has reached the desired high point, the heater will turn off and will come back on again when it has decreased. Then the buzzer will be active when the coffee bean dryer has been used at the time that has been set.

REFERENCES

1. Alhabsyi, M. F., Lengkey, L. C. C. E. & Ludong, M. M. (2021). Perbandingan mutu biji kopi robusta (Coffea canephora) hasil pengeringan secara pengasapan dan penjemuran di perkebunan kopi Desa Purworejo Kabupaten Bolaang Mongondow Timur. *Cocos*, **4**(4).
2. Afriani, S. N., Suroso, S. & Hadi, I. (2019). Prototype sistem pengering biji kopi otomatis berbasis web server. *Prosiding SENIATI*, **5**(2), 214–218.
3. Bimo, B., Nugroho, W., Hanif, M. H., Mandasari, R. I. M. & Hidayati, H. (2018). Jemuran pakaian portabel berbasis IoT. *E-Proceeding of Applied Science*, **4**(2), 669–674.
4. Budiharjo, M. Z. (2018). *Rancang bangun mesin sangrai kakao berbasis Arduino Uno*. Jember.
5. Dhamayanthie, I. (2022). Analisis metode pengurangan kadar air pada biji kopi. *Jurnal Pendidikan Tambusai*, **6**(2), 12056–12065.
6. Dwi. S. & Okta, E. (2018). Rancang bangun system monitoring pengering pakaian berbasis Arduino menggunakan implementasi IoT. *JATI Jurnal Mahasiswa Tekni Informatika*, **2**(2).
7. Hanur, M. F. A. (2016). *Rancang bangun alat pemutusan kWh meter sebagai proteksi berbasis Arduino*. Jember.
8. Kifli, N. W. (2018). *Prototype sistem monitoring kadar air biji kopi berbasi Arduino Uno*. Indonesia.
9. Kurniasih, S. (2021). *Smart cabinet pengering pakaian berbasis NodeMCU dengan fuzzy logic*. Doctoral dissertation, Politeknik Harapan Bersama Tegal.
10. Maulana, R., Jamaluddin, J. & Finawan, A. (2018). Rancang bangun pengendalian proses pada sistem pengering biji kopi berbasis mikrokontroler. *Jurnal TEKTRO*, **2**(2).
11. Nurbaeti, A., Kusumawardani, M. & Darmono, H. (2021). Rancang bangun alat pengering biji kopi berbasis internet of things. *Journal of Telecommunication Network (Jurnal Jaringan Telekomunikasi)*, **11**(2), 74–80.
12. Prastowo, B., Karmawati, E., Rubiyo, Siswanto, Indrawanto, C. & Munarso, S. J. (2010). *Budidaya dan Pasca Panen Kopi*. Eska Media: Jakarta.
13. Siswanto, A., Sitepu, R., Lestariningsih, D., Agustine, L., Gunadhi, A. & Andyardja, W. (2020). Meja tulis adjustable dengan konsep smart furniture. *Widya Teknik*, **19**(2), 97–108.
14. Sihombing, B. S. & Kirana, I. O. (2022). Rancang bangun alat pengering biji kopi berbasis mikrokontroler Arduino Uno. *STORAGE: Jurnal Ilmiah Teknik dan Ilmu Komputer*, **1**(1), 8–15.
15. Sutono, S. & Nursoparisa, A. (2020). Perancangan sistem kendali automatisasi control debit air pada pengisian galon menggunakan modul Arduino. *Media Jurnal Informatika*, **11**(1), 33.
16. Sudarmaji, S. (2017). Work system analysis of power supply in optimizing electricity on personal computer (PC). *Turbo: Jurnal Program Studi Teknik Mesin*, **6**(2).
17. Suryadi, S. (2017). Sistem kendali dan monitoring listrik rumahan menggunakan ethernet sheeld dan RTC (Real time clock) Arduino. *Jurnal Teknologi dan Rekayasa*, 2(1).

IPC

Indonesian Physics Communication

Department of Physics, Universitas Riau, Pekanbaru, Indonesia
p-ISSN 1412-2960 | e-ISSN 2579-521X

Vol. 21 | No. 2
July 2024

Web: https://kfi.ejournal.unri.ac.id
E-mail: kfi@ejournal.unri.ac.id

The effect of variations in corncob activated carbon filter media with zeolite in digging well water purification

Ridwan Yusuf Lubis*, Ety Jumiati, Arif Amri Panggabean
Department of Physics, Universitas Islam Negeri Sumatera Utara, Deli Serdang 20353, Indonesia

*Corresponding author: ridwanyusuflubis@uinsu.ac.id

ABSTRACT

Water is the most important element in human life, because almost all human activities require water, especially clean water which has a main function that cannot be replaced by other compounds. The aim of this research was to determine the quality of dug well water after the filtering process using corncob activated carbon and zeolite, as well as to find out which variations are optimal for obtaining clean water according to the Republic of Indonesia Minister of Health Regulation No. 32 of 2017. The strategy used to obtain clean water is the filtration technique. by organizing zeolite and activated carbon. The samples used came from Bandar Setia Village, Percut Sei Tuan District, Deli Serdang Regency, North Sumatra Province. Activated carbon is made from corn cobs which are activated with a 10% H_3PO_4 solution for 24 hours. The composition of the purification system is varied into three, variation A is zeolite 75% and active carbon 25%, variation B is zeolite 50% and active carbon 50%, and variation C zeolite 25% and active carbon 75%. The greatest variation in reducing parameters in dug well water is variation A with a turbidity value of 3.7 NTU, Mn of 0.011 mg/l and $KMnO_4$ of 5.8 mg/l. It can be explained that the results of this test are in accordance with clean water standards based on the PERMENKES Republic of Indonesia No. 32 of 2017. The results of this research that are most optimal in reducing parameters in dug well water are variation A.

Keywords: Activated carbon; clean water; corn; filtration; zeolite

Received 05-11-2023 | Revised 21-02-2023 | Accepted 26-06-2024 | Published 24-07-2024

INTRODUCTION

Perhaps the most basic human need is clean water, the human body contains almost 68% water content. Healthy water must meet physical, compound, and bacteriological requirements [1]. Polluted dug well water has a terrible impact on human life and spotless water, the quality of which is increasingly decreasing. Polluted well water is very bad for human activities which are usually used for drinking, washing, and other activities [2].

Corn cobs contain cellulose (41%), hemicellulose (36%), and lignin (6%). Because cellulose and hemicellulose are found in corn cobs in large quantities, they have the potential to be used as active carbon [3]. Activated carbon is a chemical compound with an amorphous form and has a very large surface area. Assuming the surface area is more prominent, the carbon assimilation limit imposed will be higher. Making activated carbon undergoes two activations, namely physical and chemical. Activated carbon is very often used in water purification processes due to the high absorption capacity contained in active carbon and its ability to absorb molecules in the form of organic and inorganic compounds [4].

Zeolite is a mineral that is often used in efforts to treat clean water and drinking water. The zeolite used in the filter media can increase oxygen, provide freshness to the water, and also act as an absorbent for light lime substances in the water. Zeolite can also filter iron in water, but in small amounts, and is also often used in aquariums and water purification [5]. A lot of water is used by humans, so the level of well water contamination will change the quality of the dug well water due to the location of the dug well being too close to the septic tank and

too shallow which will result in changes in the color and temperature of the water [6].

A tool used to solve water problems that has the function of filtering and removing contaminants in water is called a water filter. The water filter used by researchers for dug well water uses a physical process with a composition of activated carbon and zeolite as the basic ingredients, aiming to obtain clean water that is suitable for use by the community [7]. The efforts made by researchers are to find out how corncob-activated carbon and zeolite are used in water filter applications to know the quality of dug well water after the filtering process and compare variations in water filter designs that have the best value according to the Republic of Indonesia Minister of Health Regulation No. 32 of 2017 [8].

RESEARCH METHODS

The materials for the research were activated carbon from corncob waste that had been cleaned and dried, H_3PO_4 solution, distilled water, and dug well water. The tools used in this research were the furnace, oven, balance, and 100 cm PVC pipe [9]. The following are the research stages:

- Clean the corn cobs.
- Wash the corn cobs using water.
- Reduce the size of the corn cob.
- Dry the corn cobs for 7 days using sunlight.
- Carbonize the corn cobs for 30 minutes at 500ºC.
- Activated corncob-activated carbon using H3PO4 solution for 24 hours [10].
- Use distilled water to wash the activated carbon until the pH returns to neutral.
- In an activated carbon oven at 100ºC for 1 hour.
- Collected corncob-activated carbon to be used as filtering material [11].
- Filtering design.

This research was carried out by applying a water filter with dug well water which was tested before and after filtering with physical parameters in the form of turbidity and chemical parameters in the form of manganese and organic substances. This research uses three variations of filtering, the first variation is 75% zeolite: 25% active carbon, the second variation is 50% zeolite: 50% active carbon, and the third variation is 25% zeolite: 75% active carbon.

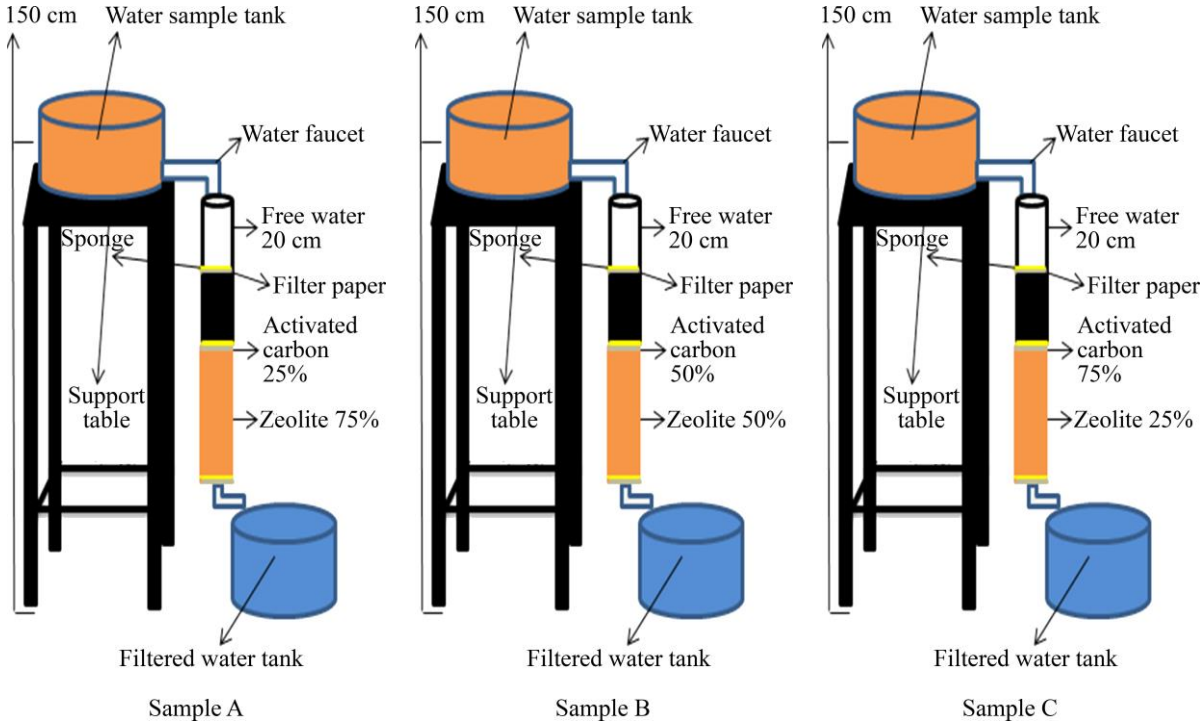

Figure 1. Filter design series [12].

RESULTS AND DISCUCCION

Turbidity

Based on the data Table 1, the turbidity value in dug well water before filtering is 27.6 NTU, indicating that it does not meet the clean water requirements. The turbidity value after filtering by varying the composition of the water filter tool obtained a value for sample A of 3.7 NTU, sample B of 4.94 NTU, and sample C of 3.85 NTU, by the Republic of Indonesia Minister of Health Regulation No. 32 of 2017 concerning clean water.

Table 1. Turbidity test results in dug well water.

Sample	Turbidity test results (NTU)		PERMENKES RI No. 32 Year 2017
	Before	After	
A		3.70	
B	27.6	4.94	25 NTU
C		3.85	

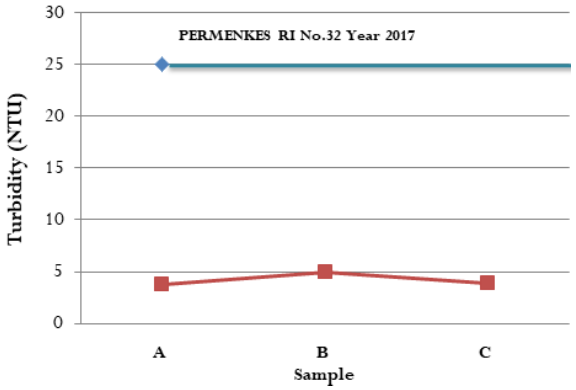

Figure 2. Effect of reducing turbidity after filtering.

Based on Figure 2. The turbidity level decreased the most in sample A, where the more zeolite content contained in the filter tool, the better it would reduce the turbidity level in dug well water with the composition of sample A being 75% zeolite: 25% active carbon. The increase in sample B results could be due to the turbidity levels absorbed in the variation A treatment, the composition of which was used again in the variation B filtering treatment.

The test results according to those carried out by Sulianto (2020), show that the reduction in turbidity levels in the water occurs when the zeolite content is greater in the filtration system [13].

Manganese

Based on the data Table 2, shows that the manganese value in dug well water before filtering is 1.296 mg/l, indicating that it does not meet the requirements for clean water. The manganese value after filtering by varying the composition of the water filter device was obtained for sample A of 0.011 mg/l, sample B of 0.337 mg/l, and sample C of 0.083 mg/l, by the Republic of Indonesia Minister of Health Regulation No. 32 of 2017 concerning clean water.

Table 2. Manganese test results in dug well water.

Sample	Manganese results (NTU)		PERMENKES RI No. 32 Year 2017
	Before	After	
A		0.011	
B	1.296	0.337	0.5 mg/l
C		0.083	

Based on Figure 3. The manganese content decreased the most in A, where the more zeolite content contained in the filter tool, the better it was to reduce the manganese content in dug well water with the composition of sample A being 75% zeolite: 25% activated carbon.

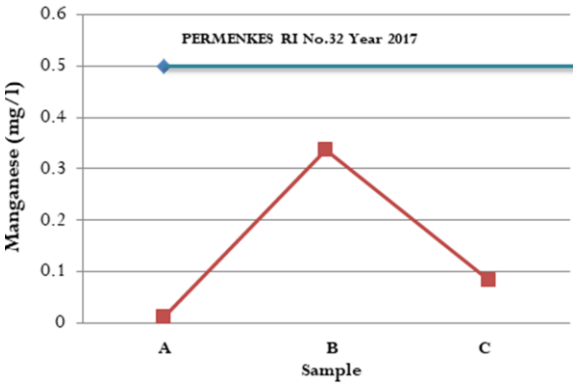

Figure 3. Effect of manganese reduction after filtering.

The increase in sample B results could be due to the manganese levels absorbed in the variation A treatment, the composition of which was used again in the variation B filtering treatment. The test results according to those carried out by Rahman (2013), show that the reduction in manganese levels in water occurs when the zeolite content is greater in the filtration system [14].

Organic Substances

Based on the data Tabel 3, shows that the value of organic substances in dug well water before filtering is 12.3 mg/l, indicating that it does not meet the requirements for clean water. The value of organic substances after filtering by varying the composition of the water filter tool obtained a value of sample A of 5.8 mg/l, sample B of 9.4 mg/l, and sample C of 8.6 mg/l, by the Republic of Indonesia Minister of Health Regulation No. 32 of 2017 concerning clean water.

Table 3. Test result of organic substances in dug well water.

Sample	Organic results (NTU)		PERMENKES RI No. 32 Year 2017
	Before	After	
A		5.80	
B	12.3	9.40	10 mg/l
C		8.60	

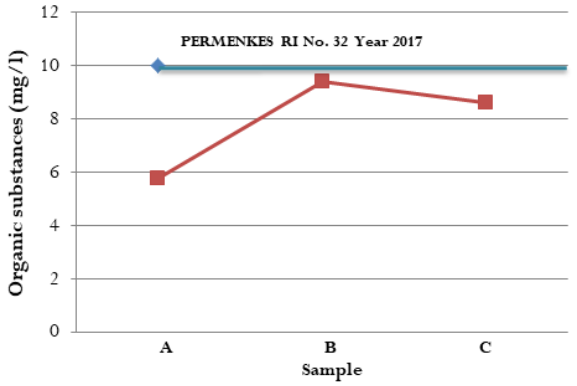

Figure 4. Effect of reducing organic substances after filtering.

Based on Figure 4, The levels of organic substances decreased the most in sample A, where the more zeolite content contained in the filter tool, the better it will reduce the levels of organic substances in the water. dug well with the composition of sample A is 75% zeolite: 25% active carbon. The increase in sample B results could be due to the level of organic substances absorbed in the variation A treatment, the composition of which was used again in the variation B filtering treatment. The results of tests carried out by Kadaria (2017) [15], showed that the greatest level of reduction in organic substances in peat water was found in the greater amount of zeolite.

CONCLUSION

Efforts to treat clean water to reduce turbidity in dug well water, namely sample A at 86.59% (27.6 NTU to 3.7 NTU), sample B at 82.10% (27.6 NTU to 4.94 NTU), and sample C was 86.05% (27.6 NTU to 3.85 NTU). The reduction in manganese levels in sample A was 99.15% (1.296 mg/l to 0.011 mg/l), sample B was 73.99% (1.296 mg/l to 0.337 mg/l), and sample C was 93.59 % (1.296 mg/l to 0.083 mg/l). The decrease in organic substance levels in sample A was 52.84% (12.3 mg/l to 5.8

mg/l), sample B was 23.57% (12.3 mg/l to 9.4 mg/l), and sample C was 30.08% (12.3 mg/l to 8.6 mg/l). The most optimal variation in reducing water parameters is variation A which has the greatest influence in reducing turbidity levels, manganese levels, and organic substances based on the Republic of Indonesia Minister of Health Regulation No. 32 of 2017.

REFERENCES

1. Sihombing, I. F. (2019). *Analisa kadar fluorida (F¯) dan kekeruhan pada air minum dan air bersih di Balai Teknik Kesehatan Lingkungan dan Pengendalian Penyakit (BTKLPP) Kelas 1 Medan, Doctoral dissertation*, Universitas Sumatera Utara.
2. Masthura & Jumiati, E. (2017). Peningkatan kualitas air menggunakan metode elektrokoagulasi dan filter karbon. *Jurnal Ilmu Fisika dan Teknologi*, **1**(2), 1–6.
3. Munfiah, S. & Ariabawani, R. M. P. (2015). Kemampuan karbon aktif tongkol jagung dalam menurunkan kekeruhan air. *Scientific Journal of Medsains*, **1**(1), 30–34.
4. Agustin, D. A. R. (2020). Pembuatan dan karakterisasi karbon aktif dari tongkol jagung dengan aktivator H_3PO_4 sebagai adsorben logam timbal (Pb), Doctoral dissertation, Universitas Islam Negeri Maulana Malik Ibrahim.
5. Hartayu, R., Putra, D. & Zainal, A. (2019). Pembuatan filter air Sederhana. *Jurnal Abdikarya: Jurnal Karya Pengabdian Dosen dan Mahasiswa*, **3**(2), 132–137.
6. Pangaribuan, L. V. (2018). *Penentuan kadar amoniak dalam air sumur bor dan pada air filter, dilakukan pada Jalan Medan Permai*. Doctoral dissertation, Universitas Sumatera Utara.
7. Nasution, J. A. (2021). *Pembuatan filter berbasis karbon aktif biji durian, zeolit, dan pasir untuk penjernihan air*. Doctoral dissertation, Universitas Islam Negeri Sumatera Utara.
8. Permenkes, R. I. (2017). Standar PERMENKES RI No. 32 Tahun 2017 *tentang standar mutu kesehatan lingkungan dan persyaratan kese hatan air untuk keperluan higiene sanitasi kolam renang solus per aqua, dan pemandian umum*. PERMENKES RI, Indonesia.
9. Rahmatika, H. N., Purwanto, P. & Narto, N. (2015). Pengaruh variasi ketebalan media filtrasi sistem up-flow terhadap kadar Fe, Mn, dan kekeruhan air sumur gali di RT 08 RW 02, Ngampilan, Kota Yogykarta. *Sanitasi: Jurnal Kesehatan Lingkungan*, **6**(3), 142–150.
10. Indariani, F. (2018). *Karakteristik arang aktif tongkol jagung (Zea mays Linn) dengan penambahan asam fosfat (H_3PO_4) pada beberapa variasi suhu aktivasi*. S1 Thesis, Universitas Mataram.
11. Meilianti, M. (2020). Pembuatan karbon aktif dari arang tongkol jagung dengan variasi konsentrasi aktivator natrium karbonat (Na_2CO_3). *Jurnal Distilasi*, **5**(1), 14–20.
12. Daulay, A. H., Manalu, K. & Masthura, M. (2019). Pengaruh kombinasi media filter karbon aktif dengan zeolit dalam menurunkan kadar logam air sumur. *JISTech (Journal of Islamic Science and Technology)*, **4**(2).
13. Sulianto, A. A., Aji, A. D. S. & Alkahi, M. F. (2020). Rancang bangun unit filtrasi air tanah untuk menurunkan kekeruhan dan kadar mangan dengan aliran upflow. *Jurnal Sumberdaya Alam Dan Lingkungan*, **7**(2), 72–80.
14. Rahman, A. R. (2013). *Perbedaan penurunan kandungan mangan (Mn) pada berbagai komposisi zeolit-karbon aktif*

dalam air sumur gali. Universitas Siliwangi, Tasikmalaya. Indonesia.
15. Kadaria, M. K. P. U. U. (2017). Pemanfaatan cangkang kerang darah (Anadara granosa) dan zeolit sebagai media filter keramik untuk pengolahan air gambut. *Jurnal Teknologi Lingkungan Lahan Basah*, **5**(1), 1–10.

IPC

Indonesian Physics Communication

Department of Physics, Universitas Riau, Pekanbaru, Indonesia
p-ISSN 1412-2960 | e-ISSN 2579-521X

Vol. 21 | No. 2
July 2024

Web: https://kfi.ejournal.unri.ac.id
E-mail: kfi@ejournal.unri.ac.id

Designing a mosque charity box with voice recognition and GPS based on the internet of things

Ainun Azizah*, Masthura Masthura, Mulkan Iskandar Nasution
Department of Physics, Universitas Islam Negeri Sumatera Utara, Deli Serdang 20353, Indonesia

*Corresponding author: ainunazizah0603@gmail.com

ABSTRACT

A security system for mosque donation boxes has been designed and built with the goal of developing a tool that can identify mosque charity box theft using the Internet of Things. The ATmega328P and ESP-32 microcontrollers are the two used in this device. Additionally, a GPS module, speech recognition, and an HC-SR04 ultrasonic sensor are included with this tool. This demonstrated that the Neo-6M GPS Module was used quite accurately with a distance difference of about 3 m. The test results from the GPS on the mosque's donation box obtained latitude and longitude points of 3.492006 and 98.587856, respectively, while the coordinate points on Google Maps were 3.491760 and 98.587943. The HC-SR04 ultrasonic sensor's purpose is to track movement in the Afterwards, a buzzer or early-warning alarm will ring, and Wi-Fi will notify the telegram application of the coordinates. This tool also includes a pretty contemporary voice recognition-based system for opening and closing donation boxes, which can accurately record, recognize, and detect sound.

Keywords: Atmega328P; GPS; HC-SR04; internet of things; voice recognition

Received 09-12-2023 | Revised 27-03-2023 | Accepted 07-06-2024 | Published 25-07-2024

INTRODUCTION

Every year many cases occur related to mosque charity boxes, including burglary and theft of charity boxes. In some cases of robbery, the thief not only took the money in the charity box but also took the charity box to destroy the evidence. Mosques that escape supervision are an opportunity for thieves to carry out their activities [1].

In general, every mosque still uses locks such as padlocks as a form of security for charity boxes, and the security system is said to be very adequate. Based on this, a charity box security system is needed which is equipped with an early warning system [2].

According to [3], the use of GPS technology is more effective in dealing with theft because it can find location coordinates with the help of the GPS module. The charity box locking and opening uses voice recognition instead of conventional keys such as padlocks, and there is an early warning alarm using a buzzer. This charity box is also based on the internet of things using a telegram bot. The goal is that if the ultrasonic sensor detects movement from the charity box or the charity box is stolen, the system will send an automatic message to the telegram bot in the form of the coordinates of where the charity box is located.

Voice recognition is a voice recognition module and device that recognizes input in the form of sound given via a microphone on the voice recognition module. After the sound is input, it will be converted to a digital signal which will later be processed by the ESP 32 microcontroller as a basis for controlling information and processing the results (output) as a stage for interfacing commands to be executed [4].

RESEARCH METHODS

The research method used is an experimental method, namely, designing a mosque charity box with a safety or lock in the form of a servo motor equipped with a voice recognition module as a system for opening and

closing the mosque charity box. The brains of all components in this research are Arduino ATmega328 and ESP-32. Apart from that, this tool also uses the internet of things system, namely the Telegram application, where this Telegram application will later become a medium for providing information in the form of coordinates of mosque charity boxes. This can minimize cases of theft that occur. The following is a system or flowchart for designing a mosque charity box as in Figures 1 and 2.

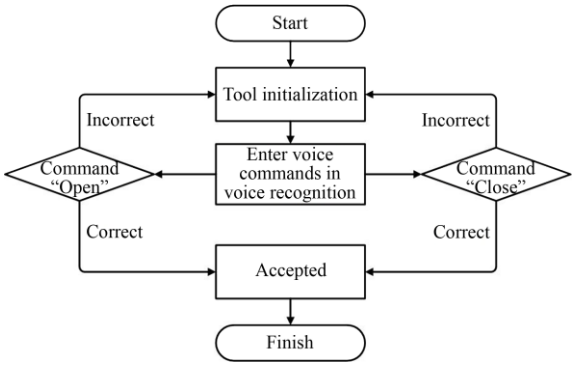

Figure 1. Flowchart of opening and closing the charity box.

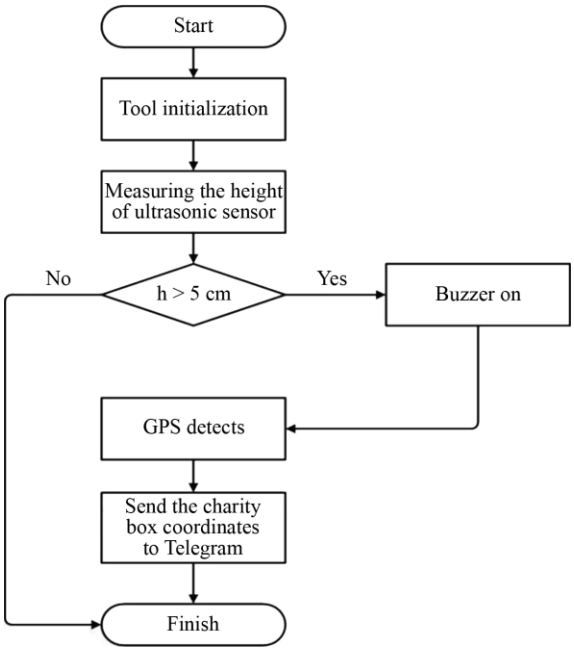

Figure 2. Telegram notification flowchart.

RESULTS AND DISCUSSION

The design of this mosque charity box uses acrylic material with dimensions of 30 cm long, 30 cm wide, and 30 cm high. Apart from that, there is a support or stand for this mosque's charity box which is 15 cm high and 30 cm wide and is made of aluminium.

Figure 3. Mosque charity box design.

This mosque charity box uses two types of microcontrollers, namely, ATmega328P and ESP-32. The sensor used is the HC-SR04 ultrasonic sensor.

Adapter Test Results

Table 1. Adapter test results.

Adapter (V_{in}) (Volt)	Stepdown output (V_{out}) (Volt)
12.67	4.94

In testing the voltage or adapter, the input voltage on the adapter (V_{in}) which was tested with a multimeter was 12.67 V and the output voltage (V_{out}) after going through the stepdown was 4.94 V. Stepdown here functions to reduce the output voltage or output from the power supply, before going through the stepdown, the output value is 5 V. The test results mean that the resulting voltage is safe to use and stable for all tool component systems and does not damage the tool components.

Voice Recognition Test Results

Based on the table above, it can be concluded that the voice that has been input to

the system in the voice recognition module can open and close the charity box with an index or symbol in programming marked with 0 and 1 for BKM 1 users, and an index of 3, 4 for BKM 2 users. Meanwhile, voice those not entered into the system will be rejected or will not be able to open the mosque charity box.

The system for opening and closing mosque charity boxes uses sound indicators recorded by the voice recognition module. Only registered voices can open and close the mosque's charity box. The working system is that when the quote display has finished running, the user says the keyword "Open" right into the voice recognition mic, when the keyword is pronounced it is required to be in silence. So that the module can process sound properly, if sound has been detected then the lid of the charity box will open. Meanwhile, the closing process is not much different from when you want to open the lid of the charity box, namely by saying the keyword "Close" if successful, it will immediately close.

Table 2. Voice recognition test results.

User	Command	Result	Index
BKM 1	"Open"	Accepted	0
	"Close"	Accepted	1
BKM 2	"Open"	Accepted	3
	"Close"	Accepted	4
Foreigners	"Open"	Rejected	-
	"Close"	Rejected	-

GPS Module Test Results

In Table 3 it can be seen that the location of the latitude point on Google Maps is 3.492006, while the latitude point on the Neo-6M GPS module is 3.491760. Then the longitude points of the mosque charity box on Google Maps and the GPS-Neo 6M module are 98.587856 and 98.587943 respectively. Both have quite accurate accuracy with a distance difference of approximately 3 meters.

Table 3. Google Maps coordinates and neo-6M GPS module.

Maps		GPS module		S
Latitude	Longitude	Latitude	Longitude	(m)
3.492006	98.587856	3.491760	98.587943	± 3

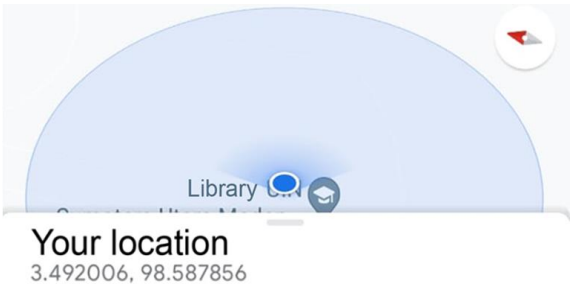

Figure 4. Coordinate points on Google Maps.

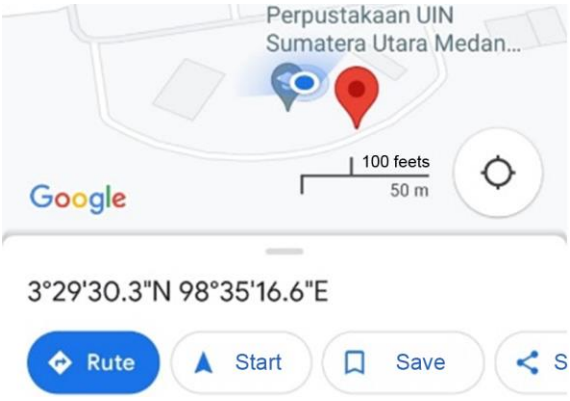

Figure 5. Coordinate points on GPS.

Servo Motor test results

In this research, a servo motor was used to open and close the charity box door. If voice command is successful, the servo motor will open 180º. The same thing also applies when you want to close the mosque's charity box, namely saying the exact command word into mic of voice recognition module. If successful, the servo motor will close and move 90º.

Table 4. Servo motor testing.

Servo location	Open door (º)	Close door (º)
Front	180	90
Behind	90	180

Telegram Test Results

The way it works is that if there is movement or shifting of the charity box as high

as 5 cm, the ultrasonic sensor will detect it and the GPS will automatically send information or notifications to Telegram repeatedly or what could be called spam. At the same time, the buzzer will also ring as a form of early warning alarm.

Figure 6. Telegram notification test result.

CONCLUSION

Mosque charity box security using Voice Recognition works in a way where the system will recognize the voice and commands that have been set in the program, the voice that has been input into the program will be detected and can open and close the door of the mosque charity box and vice versa if the voice is not recognized or not. registered then cannot open the mosque charity box. The Neo-6m GPS module which has been installed in the mosque's charity box will automatically store information regarding coordinate points, and if movement occurs, the Wi-Fi system on the ESP-32 will automatically send the longitude and latitude points to the Telegram application continuously or spam. Ultrasonic sensors play an important role in detecting theft because if the charity box moves at a height of more than 5 cm from a distance, the ultrasonic sensor detects it and the buzzer will sound as a form of early warning alarm, then send a notification to Telegram.

REFERENCES

1. Pambudi, B. C. & Vidyastari, R. I. (2020). Pengaman kotak amal Masjid dilengkapi GPS dan SMS gateway. *SinarFe7*, **3**(1), 1.
2. Putra, B. M. & Almasri. (2023). Sistem keamanan kotak amal uang dengan terintegrasi telegram berbasis mikrokontroler ESP32. *Jurnal Pendidikan Tambusai*, **6**(2), 16834–16844.
3. Napitupulu, F. & Ekaputri, C. (2017). Desain dan implementasi sistem keamanan sepeda motor berbasis mikrokontroler. *eProceedings of Engineering*, **4**(2), 1449.
4. Rosiska, E. (2021). Rancang bangun kotak penyimpanan uang dengan voice recognition berbasis mikrokontroler. *Computer and Science Industrial Engineering (COMASIE)*, **5**(3), 16–24.
5. Yudhanto, Y. & Azis, A. (2019). *Pengantar teknologi internet of things (IoT)*. Surakarta: UNS Press.
6. Qalbi, N. I., Purnama, C. W., Dwi, N. I., Kaswar, A. B. & Parenreng, J. M. (2020). Rancang bangun kotak amal cerdas sebagai solusi ketidak efisienan pendistribusi kotak amal di Masjid. *Jurnal Media Elektrik*, **17**(2), 25–32.
7. Santoso, H. (2015). *Panduan praktis Arduino untuk pemula*. Malang: Elang Sakti.
8. Santoso, H. (2017). *Monster Arduino 2 panduan praktis Arduino untuk pemula*. Malang: Elang Sakti.
9. Sendari, S., Wirawan, I. M. & Nasrulloh, M. (2021). *Sensor tranduser*. Malang: Ahlimedia Press.
10. Suhaeb, S., Djawad, Y. A., Jaya, H., Ridwansyah, S. & Risal, A. (2017). *Mikrokontroler dan interface*. Makassar: UNM.

IPC

Indonesian Physics Communication

Department of Physics, Universitas Riau, Pekanbaru, Indonesia
p-ISSN 1412-2960 | e-ISSN 2579-521X

Vol. 21 | No. 2
July 2024

Web: https://kfi.ejournal.unri.ac.id
E-mail: kfi@ejournal.unri.ac.id

Literature study of the influence of exposure factors on receiving radiation doses in radiographic examinations

Novia Anita
Department of Physics, Matana University, Tangerang 15810, Indonesia

Corresponding author: novia.anita@student.matanauniversity.ac.id

ABSTRACT

High tube voltage with reduced tube current and exposure time can reduce the dose received by the patient. Based on the principle of optimizing radiation protection and safety, efforts are needed to minimize patient doses in such a way that it still allows for obtaining the necessary diagnostic information. The aim of this study is to investigate whether high tube voltage and lower exposure time can minimize the radiation dose received by patients. This study used a literature review method as the basis for research planning. Literature review involves searching and analyzing various sources of information such as books, journals, and relevant publications to understand the research topic. The research findings indicate that high tube voltage and lower exposure time can minimize the radiation dose received by patients. Therefore, understanding the role of technical factors in radiation dose settings is crucial for medical operators performing X-ray examinations. By selecting the appropriate kVp and mAs settings, it is possible to ensure minimal exposure dose.

Keywords: Dose; literature review; kVp; mAs; X-rays

Received 24-04-2024 | Revised 29-05-2024 | Accepted 20-06-2024 | Published 25-07-2024

INTRODUCTION

X-rays are a type of electromagnetic radiation similar to visible light. However, X-rays have higher energy and can penetrate most objects, including the human body. The use of X-rays in the medical field is to create images of structures and tissues in the body. When X-rays pass through the body and reach the detector on the other side, a “shadow” image of the objects inside the body is formed [1].

In diagnostic procedures, good quality is essential. Exposure factors can influence the quality of radiography. Exposure factor settings must be carried out carefully to produce optimal-quality radiographs and ensure that the patient receives the smallest possible radiation dose, in line with the ALARA (as low as reasonably achievable) principle. The use of radiation sources is carried out by paying attention to minimizing the radiation dose received by patients, medical workers, and the general public as much as possible. The exposure factor consists of tube current (mA), tube voltage (kV), and exposure duration (s). Tube voltage is one of the important factors for X-ray tubes which regulates the amount of energy emitted and controls the quality of the beam, the tube current. The tube current regulates the total number of electrons that can pass through the target, producing X-rays with the energy and intensity used to penetrate specific organs. Meanwhile, the duration of exposure is determined by the exposure time, thus influencing the number of X-rays produced [2].

Radio diagnostic examination is a diagnostic process that uses X-ray technology or other ionizing radiation to produce an internal image of the human body. Its main purpose is to detect, diagnose, and monitor medical conditions or injuries in the body. To improve the optimization of radiation dose in patients undergoing radio diagnostic examinations, it is essential to have detailed knowledge of the dose the patient receives during the procedure. This ensures that radiation protection is met without compromising the image quality required for diagnosis. In contrast to the doses received by radiation workers and the public, medical

radiation doses cannot have a set limit value because they must be adjusted to specific diagnostic needs. Thus, protecting patients from excessive doses can be done by limiting radiation doses as a guide used for radio diagnostic techniques.

Thus, it is important to pay attention to the radiation dose received by the patient during diagnostic imaging procedures, both in terms of the technique to be used and in terms of equipment. The total radiation dose received can be a topic of interest for radiation dosimetry. Because it can indicate a potential risk of biological tissue damage to the patient. The biological impacts of radiation are categorized into stochastic and deterministic effects. As regulated in Regulation Number 8 of 2011 by the Head of the Nuclear Energy Regulatory Agency, the radiation dose received by the public must not exceed 1 mSv per year. The guideline value for skin surface radiation dose per radiograph on PA projection chest x-ray examination for patients is 0.4 mGy. This study aims to determine whether a lower exposure time with a high tube voltage can minimize the radiation dose received by the patient.

RESEARCH METHODS

The method used in this research is the literature study method which is used as a basis for planning in research. Literature studies involve searching and analyzing various sources of information such as journals, publications, and related books to understand the research topic. The goal is to introduce new knowledge on a topic and increase researchers' understanding of the topic. In this case, researchers analyzed scientific papers published in national journals and published between 2014 and 2023 to support the research being carried out [4]. The steps in carrying out this research were carried out as follows [5], determining the research topic, collect relevant information, determine the research focus, collect data sources, present the collected data, and prepare reports.

This research uses a data analysis method that refers to the approaches of Krippendorff (1993) and Sabarguna (2005) [6,7]. This approach involves four steps, namely the process of selecting, comparing, combining, and sorting data to find relevant information.

RESULTS AND DISCUSSION

Based on the results of a literature review from several journals, it was found that the X-ray tube voltage was between 60-120 kVp. Increasing the tube voltage produces more electrons from the filament (cathode); as a result, there is an increase in the production of X-rays due to greater interaction between the electrons and the anode of the X-ray tube. When the kVp value is increased in technical factors, this results in an increase in the X-ray energy produced. High voltage increases the number of electrons in the X-ray tube around the cathode and can cause penetration into the patient's body. In addition, mAs is a measure of the radiation produced over a certain period. Data obtained from several journals are:

Table 1. Results of skin surface radiation dose measurements in postero anterior projection thorax examination using high tube voltage [2].

Exposure factor				TLD	Radiation dose (mGy)
kV	mA	Ms	mAs		
100	100	20	2	86	0.029
100	100	8	0.8	88	0.023
100	100	6	0.6	87	0.006
100	100	8	0.8	89	0.023

Based on the research journal in Table 1, it is known that the use of a higher kV in radiographic examinations, such as 100 kV with 2 mAs, produces a radiation dose of 0.029 mGy, proven safe and by the guidelines in Regulation Number 8 of 2011 by the Head of the Nuclear Energy Regulatory Agency. This is because high kV produces greater X-ray penetrating power, thus allowing the use of lower radiation doses to achieve optimal results. The use of high kV is in line with the ALARA principle which prioritizes the use of the minimum possible radiation dose [2].

Table 2. Estimated radiation dose values [8].

Sample	kVp	mAs	Radiation dose
1	55	8	0.194
2	58.5	8	0.225
3	60	10	0.298
4	60	12.5	0.373
5	70	3.2	0.131
6	121	0.9	0.087
7	121	1	0.097
8	125	1	0.101
9	125	0.9	0.091

From the data presented in Table 2, it is evident that radiography number 9 shows the lowest estimated radiation dose of 0.091 mGy, while radiography number 4 shows the highest estimated radiation dose of 0.373 mGy. The total radiation dose received by the patient is directly influenced by various exposure factors, with an important emphasis on increasing the mAs value which is an indicator of the amount of radiation produced, so that the higher the value, the greater the radiation dose received by the patient. From this research, it appears that the results of setting X-ray exposure parameters such as lower exposure time and higher tube voltage can minimize the radiation dose received by the patient by the guidelines of Regulation Number 8 of 2011 by the Head of the Nuclear Energy Regulatory Agency [3-4].

Table 3. Ovarian dose acceptance at low kV and high kV [9].

No	Low kV		High kV	
	kV	Ovaries (mSv)	kV	Ovaries (mSv)
1	66	1.63664 ± 0.03412	100	0.67662 ± 0.01504
2	68	1.50899 ± 0.02524	102	0.65728 ± 0.03177
3	70	1.49071 ± 0.01054	104	0.62369 ± 0.04854
4	72	1.45497 ± 0.04186	106	0.53602 ± 0.01100
5	74	1.25449 ± 0.02957	108	0.52863 ± 0.02031
6	66	1.60063 ± 0.02003	100	0.62483 ± 0.03443
7	68	1.51047 ± 0.00529	102	0.64397 ± 0.02261
8	70	1.48841 ± 0.02386	104	0.60195 ± 0.00416
9	72	1.35912 ± 0.01222	106	0.55765 ± 0.01069
10	74	1.35573 ± 0.03430	108	0.54213 ± 0.01017
Average		1.46602 ± 0.02370		0.59928 ± 0.02087

In Table 3, each phantom model is used for two exposures, using a high kV technique and a low kV technique. For the low kV technique, the exposure factor setting uses tube voltage and tube current at certain values (68 kV 22 mAs, 74 kV 16 mAs, 66 kV 25 mAs, and 72 kV 18 mAs) which are usually used in routine abdominal examinations in clinics. The goal of this setup is to produce abdominal radiographs that meet good quality criteria. Meanwhile, for the high kV technique, the tube current and tube voltage are set at higher values (102 kV 4.4 mAs, 108 kV 3.6 mAs, 100 kV 5 mAs, 106 kV 3.8 mAs, and 104 kV 4.0 mAs) [5].

The results of measuring the dose absorbed by the reproductive organs, measured using a TLD dosimeter, are reported in mSv. Based on Table 3, on abdominal examination with AP projection, the radiation dose received by the ovaries at the high kV setting is 0.599277 ± 0.02087 mSv, and at the low kV setting is 1.466017 ± 0.02370 mSv. In the paired t-test there was a significant difference in the results in the dose received by the ovaries for the high kV and low kV settings, with a p-value <0.001 at the 95% significance level. The average dose difference was 0.86673 (95% CI: 0.81295 – 0.92051), indicating that the number of radiation doses received by patients in the low kV setting resulted in a higher dose than the high kV setting [5].

For abdominal examination with AP projection and using low kV techniques (66 – 74 kV), on the surface of the ovarian skin, the average absorbed dose received is 1.46602 mSv. Meanwhile, with the use of high kV techniques, the dose received by the ovaries is 0.59928 mSv. According to Statkiwieckz, the permitted dose limit is by the guidelines of Regulation Number 4 of 2014 by the Head of

the Nuclear Energy Regulatory Agency. The ovarian dose for abdominal examination is a maximum of 2 mSv. Therefore, the dose received in both techniques does not exceed the established dose limit [5]. Previous studies have shown that the use of high kV techniques tends to produce lower radiation doses to the ovarian skin surface compared with the use of low kV techniques. The effects caused by the radiation dose received by the body can be non-stochastic or stochastic. Therefore, choosing the right exposure factor is very important to minimize the possibility of stochastic effects and reduce the risk of non-stochastic effects [5].

Tube voltage (kV) also plays an important role in determining the level of radiation dose obtained. There is a negative correlation between kV and the dose obtained by an individual. As the applied tube voltage (kV) increases, the amount of radiation dose received by the patient decreases. Therefore, increasing the kV value can be used to reduce the radiation dose. X-rays are produced with increased penetration capacity, allowing more X-rays to be transmitted while minimizing the dose absorbed by the body [10,11]. Many factors influence radiation exposure during X-ray examinations, and medical operators need to be aware of the role these factors play in patient safety. Repeated exposure time may increase the risk of radiation, therefore, it is important to reduce exposure time. The use of low mAs and high kVp can reduce the radiation dose absorbed by the patient. Adjustment of kVp and mAs is the main technical factor that can be done to protect patients from excess radiation exposure. Optimal kVp determination ensures adequate penetrating power and exposure, according to photon energy and tissue absorption [6].

CONCLUSION

Based on a literature review from three journals, it was concluded that setting a high kVp and a lower mAs can reduce the radiation dose. Technical factors such as kVp and mAs are important parameters that can be adjusted to protect patients from excessive radiation exposure during X-ray examinations. Thus, understanding the role of technical factors in setting radiation doses is very important for medical operators performing X-ray examinations. By selecting the correct kVp and mAs settings, a minimal exposure dose can be provided.

REFERENCES

1. National Institute of Biomedical Imaging and Bioengineering. (2022). X-Rays. nibib.nih.gov/science-education/science-topics/x-rays, diakses pada 12 Maret 2024.
2. Darmini, D., *et al*. (2015). Analisa penerimaan dosis radiasi permukaan kulit. *JImeD*, **1**(1), 44–48.
3. Bapeten. (2011). *Keselamatan radiasi dalam penggunaan pesawat sinar-X radiologi diagnostik dan intervensional*.
4. Asbar, R. F. & Witarsa, R. (2020). Kajian literatur tentang penerapan pembelajaran terpadu di sekolah dasar. *JRPP*, **3**(2), 225.
5. Kulthau, C. C. (2002). *Teaching the library research*. USA: Scarecrow Press.
6. Krippendoff, K. (1993). *Analisis isi: Pengantar teori dan metodologi*. Jakarta: Citra Niaga Rajawali Press.
7. Sabarguna, B. S. (2005). *Analisis data padapenelitian kualitatif*. Jakarta: UI Press.
8. Asriningrum, S., *et al*. (2021). Faktor eksposi terhadap kualitas citra radiografi dan dosis pasien. *JImeD*, **7**(1), 15–18.
9. Indrati, R., *et al*. (2017). *Analisa penerimaan dosis serap organ reproduksi pada pemeriksaan radiografi abdomen*.
10. Bapeten. (2014). *Perizinan praktik radiologi kedokteran dan rekayasa nuklir*.
11. Hassan, F. F. (2020). Assessment of X-ray tube technical factors. *Disease and Diagnosis*, **9**(4), 144.

IPC

Indonesian Physics Communication

Department of Physics, Universitas Riau, Pekanbaru, Indonesia
p-ISSN 1412-2960 | e-ISSN 2579-521X

Vol. 21 | No. 2
July 2024

Web: https://kfi.ejournal.unri.ac.id
E-mail: kfi@ejournal.unri.ac.id

Production of activated charcoal from sugarcane bagasse using physical activation

Mella Yolanda Alfika*, Ety Jumiati, Miftahul Husnah
Department of Physics, Universitas Islam Negeri Sumatera Utara, Deli Serdang 20353, Indonesia

*Corresponding author: mellayolanda0605@gmail.com

ABSTRACT

Activated carbon is a material containing 85% – 95% carbon elements and is a porous solid. This activated carbon is the result of heating materials containing carbon at high temperatures but not oxidized. In this study, the material used is sugarcane bagasse, and its activator is NaOH. The purpose of this research is to examine the production of Activated Carbon from Sugarcane Bagasse with different concentrations of NaOH activator, analyze the moisture content, ash content, volatile matter content, and fixed carbon content. Carbonization is carried out using a furnace at a temperature of 500°C for 1 hour. Carbon activation is done using NaOH solution with concentrations of 0.3%, 0.5%, and 0.7%. Irradiation is done using a microwave with a power of 630 Watts for 20 minutes. The results of this study indicate that the NaOH concentration affects some characteristics of the activated charcoal produced from sugarcane bagasse. A NaOH concentration of 0.7% produces activated charcoal with the best characteristics, with a moisture content of 3.1%, volatile matter content of 20.4%, total ash content of 5.9%, and carbon content of 62.2%.

Keywords: Activated charcoal; activator; concentration; NaOH; sugarcane bagasse

Received 27-04-2024 | Revised 30-05-2024 | Accepted 22-06-2024 | Published 26-07-2024

INTRODUCTION

Bagasse is one of the organic wastes produced from the processing of sugar cane into sugar. This waste generally contains a large amount of organic matter such as cellulose, lignin, and hemicellulose, as well as other compounds that can be used for various purposes. However, bagasse can also be a source of environmental problems if not managed properly, because it can pollute water and soil and become a source of greenhouse gas emissions [1].

One method that can be used to manage bagasse is by carrying out physical activation. Physical activation is a processing process that uses heat or mechanical energy to change the physical and chemical properties of a material. In the context of bagasse processing, physical activation can increase the porosity and surface area of bagasse, thereby increasing its ability to absorb certain substances, such as heavy metals in wastewater or dyes in the textile industry [2].

The physical activation process on bagasse generally involves heating using high temperatures or the use of mechanical energy, such as grinding or crushing. This can cause cell rupture in the bagasse and increase accessibility to the pores in the bagasse structure. As a result, the absorption capacity and adsorption ability of bagasse can be significantly increased [1].

In addition, physical activation can also increase the regeneration or reuse of bagasse after the absorption process is complete. Thus, the use of physical activation in bagasse management can be an effective and environmentally friendly solution in reducing the negative impact of this waste on the environment. By utilizing physical activation technology, it is hoped that bagasse can be managed more efficiently and has the potential to become a value-added raw material in various industrial applications, such as wastewater treatment, alternative fuel production, or as a raw material in the

production of environmentally friendly composites and construction materials [3].

RESEARCH METHODS

Preparation of Activated Carbon from Sugarcane Bagasse

The preparation of activated carbon from sugarcane bagasse waste is done by cutting the bagasse to a size of ± 1 – 2 cm, then air-dried for 4 days. After the bagasse is dry, the carbonization process is carried out which aims to convert the bagasse into carbon. Where carbonization is carried out at a temperature of 300°C for 1 hour. This temperature is the optimum temperature in the bagasse carbonization process, then the carbonized bagasse charcoal is ground using a mortar and pestle and then sieved using a 100 mesh sieve.

The activation process uses a chemical activator, namely NaOH with different concentrations and different charcoal temperatures, to see the best-activated carbon results from changes in temperature and concentration factors. Through this activation process, carbon will have a higher absorption capacity because the dirt that covers the carbon pores is released (evaporated) as the activation temperature increases.

RESULTS AND DISCUSSION

Relationship of Water Content to NaOH Concentration

The determination of water content aims to determine the hygroscopic properties of activated carbon [1]. Activated carbon has hygroscopic properties so that it easily absorbs water vapor from the air. The water content of activated carbon is expected to have a low value because high water content can reduce the absorption capacity of activated carbon to gas or gas liquids [2]. Activated carbon can absorb water vapor in very large amounts, this very hygroscopic property is often proposed that activated carbon is a material that is very suitable to be used as an adsorbent, the water content of all NaOH-activated activated carbon meets the requirements of the Indonesian national standard which is less than 15% [3].

The existence of an activator agent in water content is a dehydrating agent [4]. How it works as a binder of water molecules contained in the raw material to enlarge the pores of activated carbon and expand the absorption surface [5]. The low water content of activated carbon indicates the success of the activator agent in binding water molecules contained in the material and the release of free water and bound water contained in the raw material during the carbonation process [2].

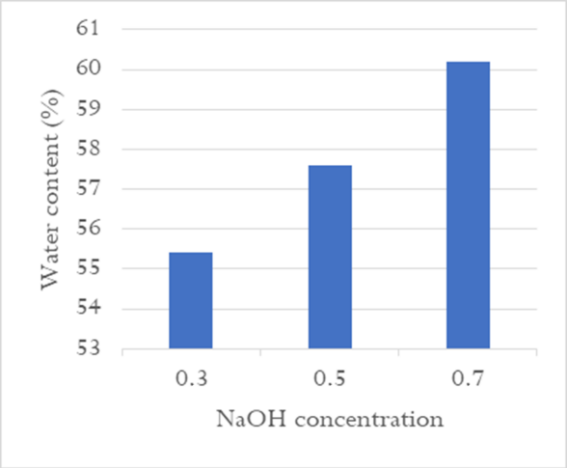

Figure 1. Water content value graph.

Figure 1 shows that the higher the concentration of the activator, the lower the water content tends to be. At a concentration of 0.3%, the water content reaches 4.2%. This value decreases further at a concentration of 0.5%, which is 3.7%, and at a concentration of 0.7% it is smaller, namely 3.1%. Soaking with an activating agent is carried out to reduce the tar content in carbon, as a result, the higher the concentration of the activator, the tar content will decrease but the surface of the activated carbon will also be wider, causing the water content in the carbon pores to be released. The quality requirements for activated carbon for water content are a maximum of 15% (SNI 06-3730-1995), so the water content results obtained in this study have met the requirements [3].

Relationship of Ash Content to NaOH Concentration

The purpose of determining the ash content is to determine the metal oxide content in activated carbon. Ash is a metal oxide in carbon consisting of minerals that cannot evaporate (nonvolatile) during carbonation. The ash content greatly affects the quality of activated carbon [1]. The presence of excess ash will clog the pores so that the surface area of the carbon is reduced [6,7]. The varying relationship between the high and low ash content in each activator is likely caused by the reaction that occurs between the type of activator and the environment. In the event of a basic NaOH activator, the reaction is less formed. It is evident from the value obtained which is lower than the acidic activator agent. While acidic compounds will react with groups containing oxygen so that the ash content produced is higher than the basic activator.

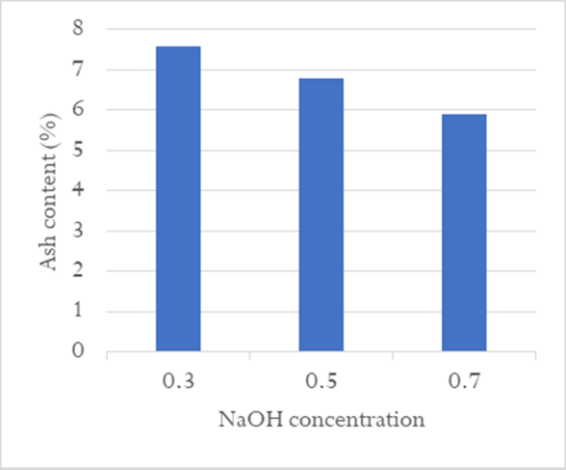

Figure 2. Ash content value graph.

Figure 2 shows that the increasing concentration tends to decrease the ash content value. The ash content values at different NaOH variations in samples of 0.3%, 0.5%, and 0.7% have respective values of 7.6%, 6.8%, and 5.9%. The lowest ash content value at a concentration of 0.7% is 5.9%, while the highest ash content value obtained at a concentration of 0.3% is 7.6%. This is because the higher concentration of activator can expand the surface of bagasse-activated carbon. During pore formation, in the activation process, crystals are burned which will become ash, so the more pores are formed, the more ash is produced.

Relationship of Volatile Substances to NaOH Concentration

Based on the results of measuring volatile substances from bagasse activated carbon, the graph data of volatile substance content values is obtained as in Figure 3

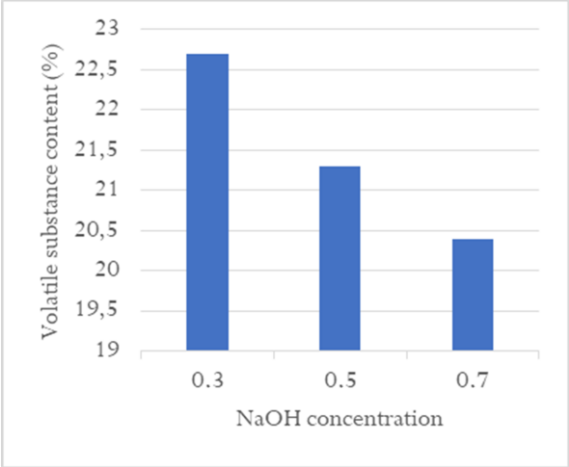

Figure 3. Volatile substance value graph.

Figure 3 shows that the higher the NaOH concentration, the more volatile substance content decreases. High volatile content indicates that the surface of activated carbon contains volatile substances originating from the interaction between carbon and water vapor. The volatile content produced by activated carbon with a concentration of 0.3% is higher than the volatile content produced at a concentration of 0.5%. The highest volatile content (22.7%) was obtained from activated carbon with a concentration of 0.3% and the lowest volatile content (20.4%) was obtained at a concentration of 0.7%. The quality requirements for activated carbon for volatile content according to SNI 06-3730-1995 are a maximum of 25%, so the volatile content at each concentration has met the quality requirements for activated carbon.

Relationship between Carbon Content and NaOH Concentration

The results obtained, the results of measuring the bound carbon content of bagasse activated carbon are shown in Figure 4. Figure 4 shows that the bound carbon content produced by activated carbon with a concentration of 0.3% is smaller than that of 0.5% and 0.7% concentrations. The amount of carbon content is highly dependent on the amount of ash content and volatile matter content. If the activated carbon has a high ash content and volatile matter content, the carbon content will be smaller, and vice versa. In the test, it can be seen that the highest carbon content was obtained from activated carbon with a concentration of 0.7% of 60.2% and the lowest carbon content was obtained at a concentration of 0.3% of 55.4%. The quality requirements for activated carbon for carbon content according to SNI 06-3730-1995 are a minimum of 65%, so the results of the bound carbon content obtained in this study have met the requirements.

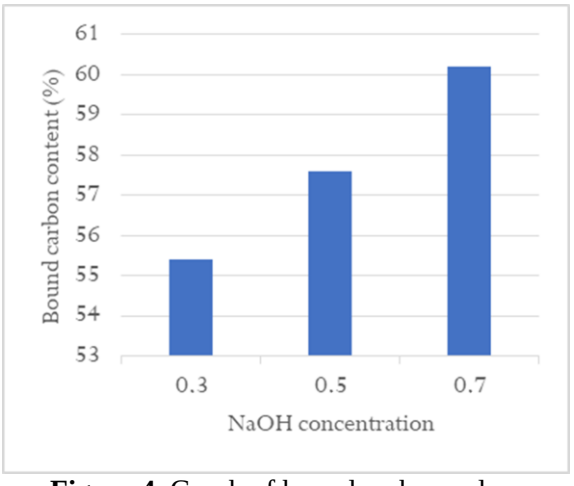

Figure 4. Graph of bound carbon value.

CONCLUSION

From the research results obtained the characteristics of activated carbon with the lowest water content of 3.1% with 0.7% NaOH activator, the lowest ash content of 5.9% with 0.7% NaOH activator, the lowest volatile matter content of 20.4% with 0.7% NaOH activator and the highest bound carbon content of 62.2% with 0.7% NaOH activator. The addition of concentration greatly affects the manufacture of activated carbon. The characteristics of the activated carbon produced are by SNI 06-3730-1995 for activated carbon. The suggestion that can be given is the need to vary the raw materials and temperature used to manufacture activated carbon.

REFERENCES

1. Turisna, T. (2011). *Perbandingan metode aktivasi fisika dan kimia pada proses pembuatan arang aktif dari ampas tebu*. Skripsi, Universitas Malikessaleh.
2. Pari, G. (1996). Pembuatan arang aktif dari serbuk gergajian sengon dengan cara kimia. *Bul. Penelitian Hasil Hutan*, **14**(8), 308–320.
3. SNI. (1995). *SNI 06-3730-1995 tentang arang aktif teknis*. Jakarta: BSN.
4. Miranti, S. T. (2012). *Pembuatan karbon aktif dari bamboo dengan metode aktivasi terkontrol menggunakan activating agent H_3PO_4 dan KOH*. Skripsi Teknik Kimia, Universitas Indonesia.
5. Prasetyo, Y. & Nasrudin, H. (2013). Determination consentration $ZnCl_2$ the making of activated corn cob carbon and decreasing surfactant. *UNESA Journal of Chemistry*, **2**(3).
6. Schröder, E., Thomauske, K., Weber, C., Hornung, A. & Tumiatti, V. (2007). Experiments on the generation of activated carbon from biomass. Journal of analytical and applied pyrolysis, **79**(1-2), 106–111.
7. Bartoňová, L. (2015). Unburned carbon from coal combustion ash: An overview. *Fuel Processing Technology*, **134**, 136.

IPC

Indonesian Physics Communication

Department of Physics, Universitas Riau, Pekanbaru, Indonesia
p-ISSN 1412-2960 | e-ISSN 2579-521X

Vol. 21 | No. 2
July 2024

Web: https://kfi.ejournal.unri.ac.id
E-mail: kfi@ejournal.unri.ac.id

Random forest algorithm for precision dose prediction in brain cancer radiotherapy

Luqyana Adha Azwat*, Prawito Prajitno, Dwi Seno Kuncoro Sihono, Dewa Ngurah Yudhi Persada

[1]Department of Physics, Universitas Indonesia, Depok 16424, Indonesia
[2]Department of Physics, MRCCC Siloam Hospitals Semanggi, South Jakarta 12930, Indonesia

*Corresponding author: luqyana.adha@ui.ac.id

ABSTRACT

Improving dose optimization during clinical planning using the treatment planning system for radiotherapy patients is crucial, yet executing this process can be time-consuming and reliant on the expertise of medical physicists. This research focuses on dose prediction employing machine learning for the planning target volume (PTV) and organ at risk (OAR) in cases of brain cancer treated with the volumetric modulated arc therapy planning technique. Utilizing DICOM planning data from brain cancer cases, this study utilizes extracted radiomic and dosiomic values as inputs and outputs for the research, employing a random forest algorithm model. Evaluation of the model reveals its effectiveness in predicting doses for PTV in brain cancer and OAR, with predicted homogeneity index and conformity index values of 0.14 ± 0.04 and 0.95 ± 0.01, respectively, compared to clinical values of 0.14 ± 0.13 and 0.94 ± 0.13. Thus, the random forest model demonstrates proficiency in predicting doses for brain cancer PTV and OAR, with an mean square error value of 0.017.

Keywords: Mean square error; OAR; PTV; p-value; random forest

Received 08-05-2024 | Revised 10-06-2024 | Accepted 24-06-2024 | Published 26-07-2024

INTRODUCTION

Brain cancer significantly impacts public health in Indonesia, with 5,964 cases reported in 2020 according to Global Burden of Cancer data [1]. Although not the most common cancer, it requires attention due to the brain's role as the central nervous system, controlling the body's movements and necessitating the protection of many healthy organs during treatment [2]. Radiotherapy, including the advanced technique volumetric modulated arc therapy (VMAT), is an effective treatment for brain cancer. VMAT delivers precise radiation doses to the tumor while minimizing damage to surrounding healthy tissue, offering benefits in speed, precision, and efficiency compared to conventional methods [3]. Proper radiation therapy planning is essential for effectiveness and minimizing damage to healthy tissue [4].

The treatment planning system designs optimal radiation plans, ensuring accurate targeting and minimal impact on healthy tissue. To enhance planning quality and efficiency, artificial intelligence technologies like knowledge based planning with machine learning, including random forest algorithms, are used for accurate dose prediction in VMAT techniques. This study will predict doses for the planned target volume (PTV) and organ at risk (OAR) using a random forest model with k-fold validation and DICOM data [5].

RESEARCH METHODS

Data and Research Tools

This study utilized 178 radiation therapy planning data in DICOM file format from brain cancer cases. The hardware used was an Asus laptop with a Ryzen 7 processor, 8 GB RAM, 500 GB SSD, and Windows 11 OS. Software utilized included3D Slicer, Python, and Microsoft Excel.

Pre-processing

Data Radiomic and dosiomic feature extraction was conducted using 3D Slicer. For dosiomic, features such as its shape were extracted, involving dose analysis foreach organ obtained from DICOM dose data. Dosiomic data included V_{95}, V_{PTV}, $D_{2\%}$, D50%, $D_{98\%}$, D_{mean}, and D_{max}. The organs involved in this study were the PTV and its OAR, the brainstem. Dosiomic data were normalized with the prescriptiondose to ensure scale consistency, then merged into a CSV format.

Build the Random Forest Model

Radiomic and dosiomic data were imported into Python for training and testing.70% of the data were used for training, and 30% for testing. The prediction model utilized radiomic features to compute dosiomic data during testing, with prediction results derived from the average value of all estimators [6].

Evaluating the Random Forest Model

Evaluation involved several steps. First, assessing error values in the validation stage to gauge the fit of the random forest model with actual clinical data, yielding the mean squared error (MSE). Subsequently, testing the planning quality using homogeneity index (HI) and conformity index (CI) parameters with the following formulas:

$$HI = \frac{D_{2\%} - D_{98\%}}{D_{50\%}} \quad (1)$$

$$CI = \frac{V_{95}}{V_{PTV}} \quad (2)$$

RESULTS AND DISCUSSION

During the pre-processing stage, radiomic and dosiomic data were obtained. Dosiomic data extracted underwent normalization against the prescription dose of each patient. This normalization process ensures data within the same value range.

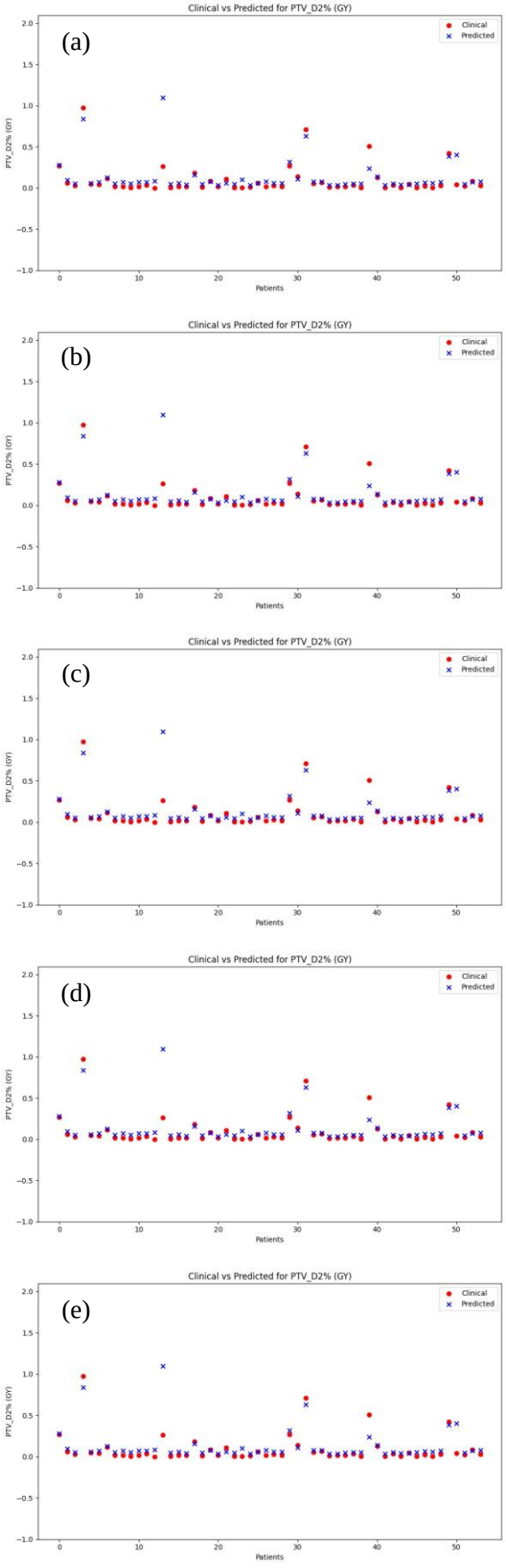

Figure 1. Clinical versus predicted for: (a) PTV $D_{2\%}$; (b)PTV $D_{50\%}$; (c) PTV $D_{98\%}$; (d) brainstem mean; and (e) brainstem max.

Normalization exclusively applied to dosiomic data, as radiomic data did not require normalization due to their association with organ shape information, necessitating consistency with the original data. Out of 124 data points, 70% were allocated for training and 30% for testing. The feature values from the machine learning training data influenced the regression outcomes in this random forest method. The results indicate clinical and predicted outcomes for PTV and OAR brainstem as follows in Figure 1.

From Figure 1, it can be observed that the overall prediction results are quite close to the clinical values, with an average MSE value of 0.0177. MSE is used to evaluate the model's performance, where a smaller MSE value indicates that the model has predictions closer to the actual values. It can be concluded that the machine learning model's performance is capable of predicting PTV and OAR organs well, resulting in an MSE error value very close to 0 [7].

In the radiation therapy planning stage, important parameters to consider are the conformity of the dose distribution with the target shape, determined by the CI value, and the homogeneity of the dose distribution within the target volume, determined by the HI value. With clinical HI and CI values of 0.14±0.13 and 0.94 ± 0.13, respectively, while the predicted values are 0.14 ± 0.04 and 0.95 ± 0.01, according to ICRU 83 recommendations [8], the HI value should be 0, and for CI, according to ICRU 62 recommendations [9], the CI value should be 1.

CONCLUSION

The Random Forest model accurately predicts dose distribution with an error value of 0.017 and shows no significant difference between clinical outcomes and predicted results. As a result, this Random Forest model can be used as a reference to streamline the radiation therapy planning process for medical physicists.

REFERENCES

1. Sung, H., Ferlay, J., Siegel, R. L., Laversanne, M., Soerjomataram, I., Jemal, A. & Bray, F. (2021). Global cancer statistics 2020: GLOBOCAN estimates of incidence and mortality worldwide for 36 cancers in 185 countries. *CA: A Cancer Journal for Clinicians*, **71**(3), 209–249.
2. Abdullah, F., Ganiem, A. R., Rasyid, A., Munir, B. & Wiratman, W. (2023). Pedoman praktik klinik neurologi 2023, Department of Neurology.
3. Verbakel, W. F., Cuijpers, J. P., Hoffmans, D., Bieker, M., Slotman, B. J. & Senan, S. (2009). Volumetric intensity-modulated arc therapy vs. conventional IMRT in head-and-neck cancer: a comparative planning and dosimetric study. *International Journal of Radiation Oncology*Biology*Physics*, **74**(1), 252–259.
4. Van Herk, M., Remeijer, P., Rasch, C. & Lebesque, J. V. (2000). The probability of correct target dosage: dose-population histograms for deriving treatment margins in radiotherapy. *International Journal of Radiation Oncology*Biology*Physics*, **47**(4), 1121–1135.
5. Savargiv, M., Masoumi, B., & Keyvanpour, M. R. (2021). *A new random forest algorithm based on learning automata*. *Computational Intelligence and Neuroscience*, **2021**(1), 5572781.
6. Purwanto, A. D., Wikantika, K., Deliar, A., & Darmawan, S. (2022). Decision tree and random forest classification algorithms for mangrove forest mapping in Sembilang National Park, Indonesia. *Remote Sensing*, **15**(1), 16.
7. Song, Y., Hu, J., Liu, Y., Hu, H., Huang, Y., Bai, S., & Yi, Z. (2020). Dose prediction using a deep neural network for accelerated planning of rectal cancer radiotherapy. *Radiotherapy and Oncology*, **149**, 111–116.
8. Menzel, H. G. (2012). The international commission on radiation units and

measurements. *Journal of the ICRU*, **12**(2), 1–2.
9. International Commission on Radiological Units. (1961). *Report of the International Commission on Radiological Units and Measurements (ICRU)*, 1959 (Vol. 78). US Department of Commerce, National Bureau of Standards.